Computational Studies of Interactions Between Vanadyl, Uranyl, and Thorium Aqua Ions with Bidentate Eudistomin Ligands of Ascidian-origin

by

Ashutosh Parimi

Thesis submitted to the Faculty of Graduate Studies

Of the University of Manitoba

In partial fulfilment as per the requirements for the

MASTER OF SCIENCE

Department of Chemistry

University of Manitoba

Winnipeg

ABSTRACT

The nuclear waste generated in nuclear power plants is reprocessed to extract useful actinide elements, especially uranium and plutonium. In recent times, interest has been growing towards N-containing ligands to facilitate extraction. More often than not, these ligands have similarities to biogenic compounds such as eudistomins, which are found in marine animals called Ascidians.

Ascidians are tunicates which adopt unusual techniques to deter predation, the three main methods are sequestration of unusual metals, high concentrations of sulphuric acid/sulphate ions in tunicate-cells, and the presence of eudistomins. Studies have shown the presence of sulphate ion/sulfuric acid plays a key role in deterring predation. In a separate study, researchers have found that eudistomins can form metal-complexes with Iron outside of the ascidian's body. Whether eudistomins play any role in the presence of sulfuric acid/sulphate ion, and/or the sequestration of the metals was never studied.

In this study, we have explored the possible interactions of eudistomins as ligands with metal-aqua ions viz., vanadyl, uranyl, and thorium ions. We have designed five model reactions and have calculated the formation energies. The model reactions were designed to resemble what might happen in the body of an ascidian, based on the information obtained from the literature.

We have adopted density function theory (DFT) using PBE-D3, BLYP, and B3LYP functionals with the ADF (PBE-D3 and BLYP) and ORCA (BLYP and B3LYP) software packages for our calculations. The formation energies of the complexes were calculated in gas phase and in solvation phase. COSMO (in ADF) and CPCM (in ORCA) were used for solvation effects. ZORA was the relativistic method adopted in this work.

From our study, based on the results, we can confirm that with respect to model reactions 1, 4, and 5, the anionic form of the ligand is capable of forming decent interactions with the metal aqua ions. The closeness of the ΔG values obtained with respect to all three aqua ions suggest that ascidians may not have a preference to a specific metal. The adoption of different methodology has resulted in similar results. To conclude this work, we are confident that eudistomins may be used as biogenic N-based ligands in the nuclear reprocessing facilities.

Table of Contents

List of Figures

List of Tables

List of Abbreviations

V	Vanadium
U	Uranium
Th	Thorium
N	Nitrogen
L	Ligand
PUREX	Plutonium and Uranium Reduction Extraction
UREX	Uranium Reduction Extraction
TRUEX	Trans-uranium Reduction Extraction
DIAMEX	Diamide Extraction
SANEX	Selective Actinide Extraction
UNEX	Universal Extraction
CEA	Commissariat à L'Énergie Atomique et aux énergies
CHNO	Carbon Hydrogen Nitrogen Oxygen
ADF	Amsterdam Density Functional
DFT	Density Functional Theory
PBE	Perdew-Burke-Ernzherof
BLYP	Becke-Lee-Yang-Par
B3LYP	Becke 3- Lee-Yang-Par
LDA	Local Density Approximation
GGA	Generalized Gradient Approximation
STO	Slater Type Orbital
GTO	Gaussian Type Orbital
ZORA	Zeroth Order Relativistic Approximation

ACKNOWLEDGEMENTS

I would like to express my sincerest possible gratitude to Dr. Georg Schreckenbach for his constant support, trust, and supervision. I cannot think of enough adjectives or words of gratitude to express how valuable the conversations are. I unquestionably thank him from the bottom of my heart.

The advisory committee, Dr. Rebecca Davis and Dr. Mazdak Khajehpour, have consistently supported me via their respective criticism and valuable suggestions. I am absolutely grateful for that.

Dr. Ali Kerrache and Dr. Grigory Shamov are the two people without whom I would not have been able to complete my work. Their prompt response to every technical trouble I had was incredible and I am very much thankful to them.

I cannot forget the fruitful discussions I had with Dr. Marcel Jaspers, Dr. Mario Bieringer, Dr. Sean McKenna, and Dr. Joe O'Neil. Their suggestions and discussions have helped me very much and I would like to acknowledge it as well.

The group members, Xiaobin Zhang, Yang 'Rico' Gao, Cen Li, and Varathan Elumalai have been ever present during the course of this project and have consistently aided me with their criticism and suggestions. The newer group members and other 'computational group' members have also provided me with their words of advice during the 'group meetings'. I am very much grateful to each and everyone.

Dr. James Xidos has consistently helped me with his thoughts, regardless of the 'odd' timings. I respect his words and I am grateful to him.

“*Dedicated to the frontline workers, families, and the dead who have been affected by the COVID-19 pandemic around the world”*

CHAPTER-1

INTRODUCTION

1.1. General Introduction

Nuclear power-based applications use nuclear fuel to generate electricity, via uranium (and plutonium resources as well in few countries) in nuclear power plants. Fissile isotopes are subjected to nuclear fission, and the generated thermal energy is harnessed to produce electricity. A neutron, when made to hit the nucleus of a fissile material, would split the nucleus into two daughter nuclei in a nuclear fission event. This process generates heat, which is used to run steam-turbines, which in turn convert thermal output to electrical energy via mechanical work. It is estimated that currently around 10% of global electricity generation is done via nuclear power.[1] Nuclear power is considered as one of the most efficient and non-carbon-emitting sources of energy, ergo, one for the modern-day world.

Uranium is one of the main sources for nuclear power as it is one of the reasonably abundant materials. Canada has the joint 3rd largest uranium reserves along with Russia, only less than those of Australia and Kazakhstan (Figure 1.1).[2] It is estimated that uranium is also present in sea water at a concentration of 3µg/l, which amounts to 4.4 billion tons of uranium.[3] Nuclear fuel that is being used often generates waste. This is called nuclear waste and is radioactive, and its disposal requires high level safety measures. Nuclear waste contains unused fuel, and some important transuranic elements like Americium which are of scientific interest in order to explore the physical and chemical properties of the heavy elements.[4] Separation of actinides from nuclear waste has been a priority to recover the potentially useful metals, mainly uranium and other actinides.

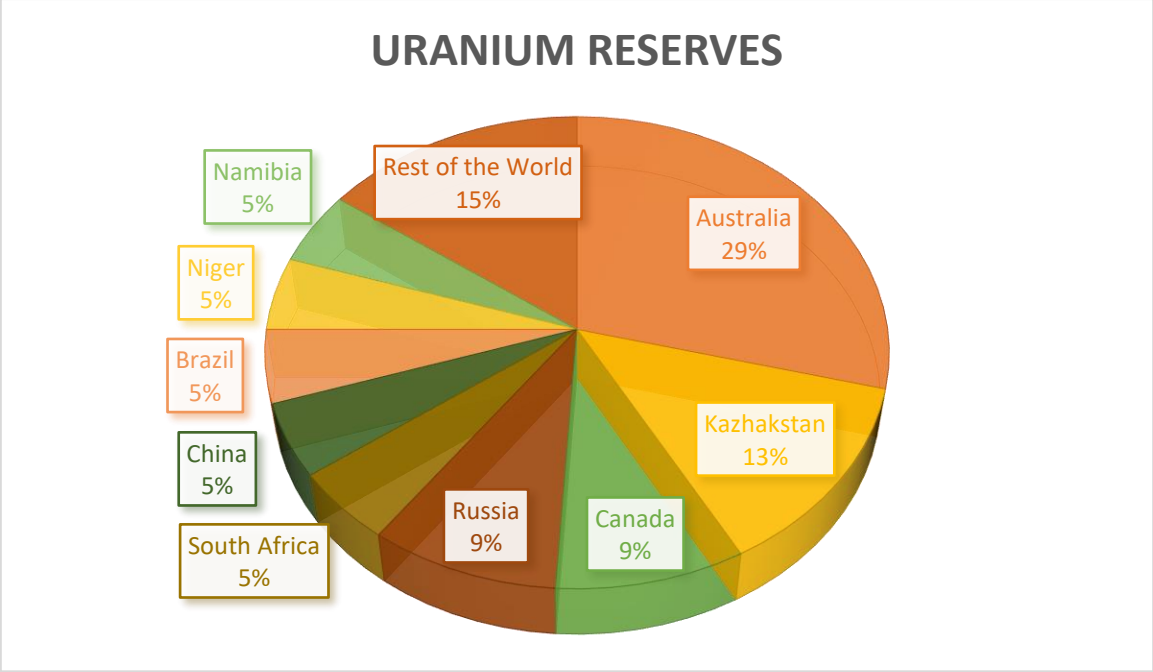

Figure. 1.1 Percentage of Uranium Reserves across the globe

1.2. Nuclear Reprocessing

Nuclear reprocessing is the act of separating the important materials from the nuclear waste. Spent nuclear fuel often has valuable uranium, plutonium, and other minor actinides (composition of spent nuclear fuel given in Figure 1.2)[4], which could be useful for various purposes, one of them being the exploration of minor actinide chemistry from a purely scientific enthusiast perspective. The first large-scale nuclear reactors were built during the Second World War. The main reason was to produce plutonium for nuclear weapons. Therefore, the extraction of plutonium was a priority. The bismuth-phosphate-based extraction process was operated on a large scale at the Hanford project in the later parts of 1944. While it was a successful procedure to recover plutonium, the procedure was unable in recovering uranium. In 1947, American chemists Herbert H. Anderson and Larned B. Asprey have developed the Plutonium Uranium Reduction Extraction (PUREX) process as a part of the Manhattan project under Glenn T. Seaborg.[5] This is a liquid-liquid extraction process that is currently being used to reprocess spent nuclear fuel to extract uranium and plutonium, independently. Modifications of PUREX, include processes such as UREX, TRUEX, DIAMEX, SANEX, and UNEX.[6]

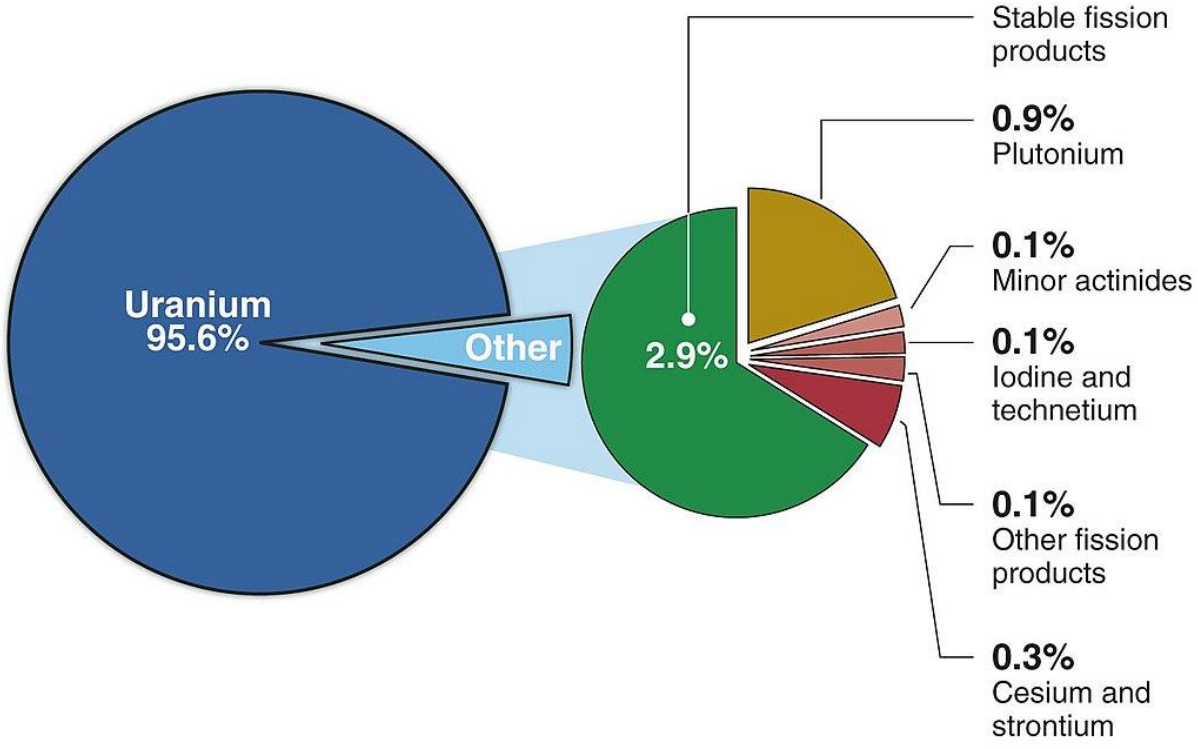

Figure 1.2 Composition of spent nuclear fuel[7]

In UREX (Uranium Reduction Extraction), the priority is to extract uranium from high level nuclear waste. The TRUEX (Transuranic Extraction) process is designed to remove transuranic metals, mainly americium and curium, from the nuclear waste. DIAMEX (Diamide Extraction) is an alternative to TRUEX, and this process involves using malondiamide. This process has the advantage of avoiding the formation of organic waste which contain elements other than CHNO, i.e., it is an environmental-friendly method. DIAMEX is currently being worked on by the French organisation, Commissariat à L'Énergie Atomique et aux énergies alternatives (CEA).

Management of the trivalent minor actinides requires separation from lanthanides. One such method is SANEX (Selective Actinide Extraction), which focuses on the separation of lanthanides from actinides. The very close resemblance in the chemistry of lanthanides and actinides proves to be a challenging task in the separation process. Currently, research is being done to utilize organic ligands for this separation. UNEX (Universal Extraction) process developed in Russia and Czechia is designed to completely remove highly troublesome radioisotopes such as strontium and caesium from the raffinate after the extraction of uranium and plutonium from the nuclear waste. This process as well, adopts organic compounds for the separation.

Separation of trivalent actinides from lanthanides in a very problematic challenge in nuclear reprocessing. Trivalent lanthanides and actinides exhibit similar chemical behaviour such as the exhibition of +3 oxidation state, ability to form complexes with similar types of ligands, comparable ionic radii, etc. Regardless of this, many soft donor ligands have shown preference to actinides over lanthanides when binding, possibly due to the greater availability of 5f orbitals in comparison to the 4f orbitals of lanthanides.[8,9] This a crucial and critical factor, as the bonding differences in actinide complexes and lanthanide complexes could help us in understanding the chemistry of actinides, as well as help in nuclear reprocessing. Recent studies have suggested the potential of N-donor and/or N-O donor ligands, and their role in the separation of such useful metals from the waste.[9–14] N-donor ligands are currently being investigated by various research groups in the actinide community to explore their potential in the separation of actinides. The nitrogen atom's lone pair provides an opportunity for the 5f orbitals in the actinides to bind, thereby, helping with the extraction of the actinides.

Terpy (2,2':6',2"-terpyridine), first synthesised in the 1930s, has been introduced in the extraction process for the separation of lanthanides and actinides in 1970s. Its heterocyclic trident N-donor structure has proven to be the basis for many extraction ligands including BTP (2,6-bis(1,2,4-triazine-3-yl)pyridine) and BTBP (6,6'-bis(1,2,4-triazine-3-yl)-[2,2']bipyridinyl). In acidic conditions, i.e., when the pH is low, extraction ligands need to have lower proton affinity. TPTZ (2,4,6-tripyridil-1,3,5-triazine) is one such molecule which is used as an extraction ligand. Apart from BTP (Figure 1.3), BTBP, TPTZ (Figure 1.4), and Terpy (Figure 1.5),there are various other ligands as well which can act as extraction ligands.[14]

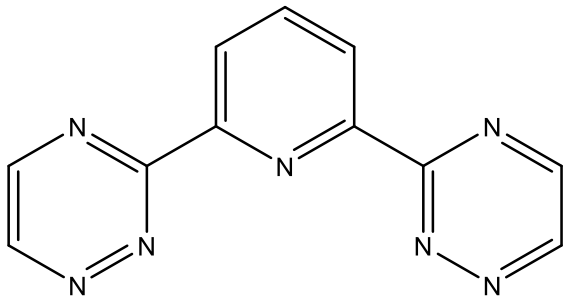

Figure. 1.3 2,6-bis(1,2,4-triazine-3-yl)pyridine (BTP)

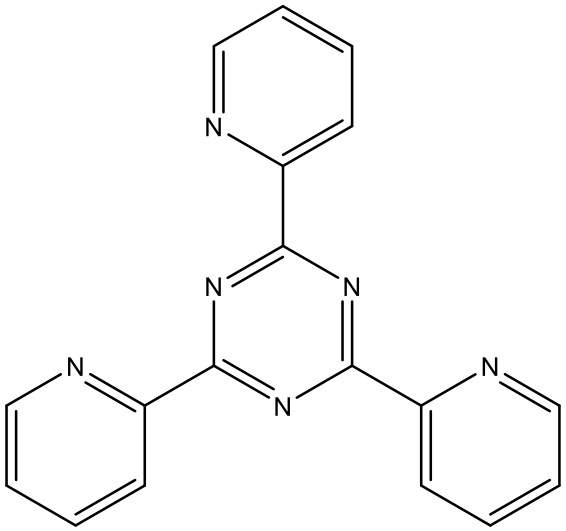

Figure. 1.4 2,4,6-tripyridil-1,3,5-triazine (TPTZ)

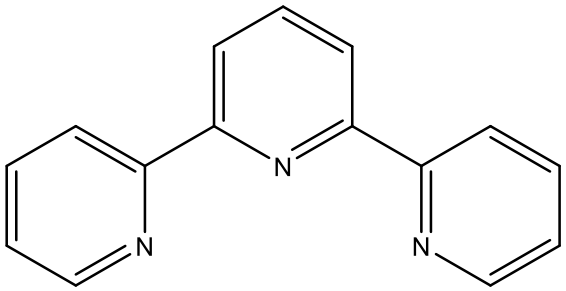

Figure. 1.5 2,2':6',2"-terpyridine (Terpy)

While a significant amount of effort is put into the design and the synthesis of these ligands, molecules resembling the ligands can be obtained from the nature. A very interesting fact is that more often than not, these ligands are akin to biological compounds which are naturally found in various plants, marine, and terrestrial organisms.[15,16] These molecules operate and are stable in similar conditions (as extractant ligands) such as temperature, pH, etc.; and have the ability to be soft-donors, and can contribute to the x-dentate part in ligand-metal complexes. One such set of molecules are eudistomins, alkaloids of marine origin. These compounds are isolated from ascidians.

1.3. Eudistomins

Ascidians (Figure 1.6), commonly knowns as sea-squirts or tunicates, are marine organisms of kingdom *Animalia*, which belong to the phylum *Chordata*, subphylum *Tunicata*.[17] These

animals supposedly have been on earth since the Ediacaran period (635 to 541 million years ago), with studies strongly suggesting their presence since the Jurassic times (201.3 to 145 million years ago).[18–22] These animals are found all around the world in marine environment. Despite their evolution and presence in the modern-day world, which emphasizes on their 'adaption to change', there is a lack of proper fossil evidence as these animals are soft and sessile after their larval phase. For this reason, as a part of their 'adaption to change', it is believed that they have adopted various techniques to void predation.

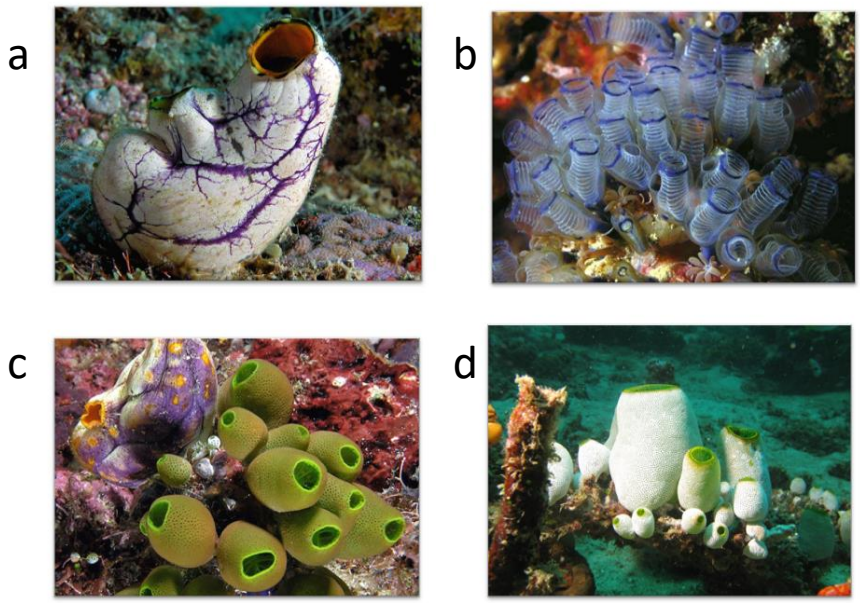

Figure 1.6 Ascidians [(a) *Polycarpa aurata* (b) *Clavelina moluccensis,* (c) *Atriolum robustum*, (d) *Didemnum molle*] [Images from wikipedia.org. *Polycarpa aurata*, *Clavelina moluccensis*, and *Atriolum robustum* are of CC BY-SA 3.0. *Didemnum molle* has CC BY 2.0 license]

One such adaption is believed to be the sequestration of unusual metals.[23] Studies have pointed to the presence of metals, especially vanadium, iron, zinc, nickel, lithium, etc., in the bio-system of ascidians.[24] Significantly enriched concentrations of uranium are also observed in these animals. The biological significance of the enrichment and its role in voiding predation is yet to be investigated in detail. Eudistomins, secondary metabolites, derivates of ß-carboline (Figure 1.8), are alkaloids found in ascidians.[25,26] While their role to void predation remains a topic that needs deeper study, these compounds have a huge pharmacological significance.[27–31] In some plants, insects, etc., usually alkaloids have a role in their chemical defence[32,33], which might be the same in the case of ascidians. Various studies also point to the presence of sulphate

ion and/or sulphuric acid in the cells of ascidians.[34–36] The presence of acidic cells is supposedly an effective way to deter potential predators.[37] Whether all three factors (sequestration of metals, presence of alkaloids, and presence of sulphuric acid/sulphate ions) are needed, or only the presence of acidity does the job, remains a question to biologists. One study suggests that the role of sulphuric acid and/or sulphate ion is to act as an effective weapon in the arsenal of ascidians to defend against predators.[37] If the formation of sulphate ion/sulfuric acid is a priority, then there may not be a preference for a particular metal sulphate; assuming the metals are sequestered in the form of metal sulphate (given that sulphates are second most abundant salts after chlorides in the ocean[38]) for making the necessary amount of sulphuric acid. This could be one of the reasons why ascidians manage to sequester various unusual metals and eudistomins might have a role in this operation, which could be the formation of complexes with these metals and leaving out the sulphate part.

Eudistomins are tryptophan (Figure 1.9) derived secondary metabolites, with a ß-carboline backbone structure.[15] While the majority of these compounds have been isolated from tunicates of the genus *Eudistoma* (Figure 1.7),[28,39,40] there are other sources as well, such as the genera *Ritterella*,[26] *Pseudodistoma*,[41] *Didemnum*,[42] *Synoicum*,[43] and *Lissoclinum*.[44] Most of the compounds are observed to be either hydroxylated and/or brominated. Other substituents such as pyrrole, pyrroline, indole rings, amines, thiomethyl, and/or thiomethyl alkyl residues are observed as well. Most of these compounds are related to biosynthesis, i.e., coupling of tryptophan with a second amino acid.[15] For instance, Eudistomin G may be considered to be a derivate of tryptophan and glutamine,[28] and Eudistomidins B and C are supposedly derivates of tryptophan and unusual amino acids p-methylphenyl-L-alanine and S-methyl-D-cysteine, respectively.[45] *In vivo* studies with *Eudistoma olivaceum* confirmed that tryptophan is a primary precursor of eudistomin I.[46] The pharmacological importance of eudistomins is an intriguing topic. These compounds exhibit a wide variety of bio-activity, and demonstrate a broad spectrum of pharmacological properties including sedative, anxiolytic, hypnotic, anticonvulsant, antitumour, antiviral, antiparasitic, and antimicrobial activities.[27]

Figure 1.7 *Eudistoma reginum,* a species in the genus *Eudistoma* (image from wikipedia.org. CC BY-SA 2.0)

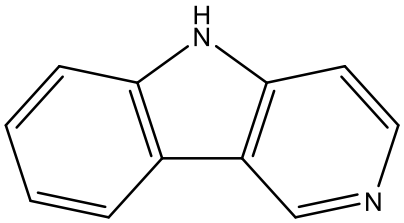

Figure 1.8 ß-carboline backbone structure

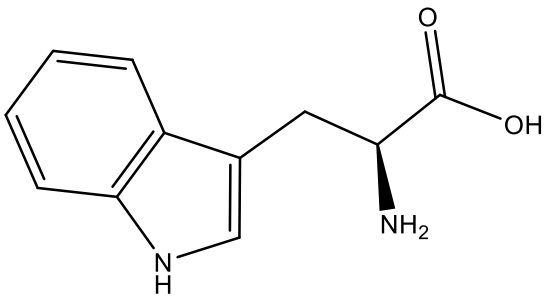

Figure 1.9 Tryptophan, an α-amino acid, proven to be the precursor of various eudistomins

1.4. Metal complexation in Ascidians

As the majority of the metals that ascidians sequester have the capability to form complexes with ligands, and as eudistomins resemble N-donor organic ligands, and as they supposedly have a similar reason to exist in the bio-system of the tunicates, i.e., to deter predation, we hypothesize that there might be an organometallic type complexation. A non-covalently bound

iron complex in the lipophilic extract of *Eudistoma gilboviride* has been identified and reported by Wright *et al*.[47] *Eudistoma gilboviride* is known to produce eudistomins G, H, and I (Figure 1.10). Analysis in their work has shown very high amounts of lipophilic iron complex in the extract of the animal. Upon further investigation, they have observed 2:1 ligand/metal complexes. They concluded their study by suggesting that eudistomin/metal complexes might have a physiological role in the sequestration of these metals.

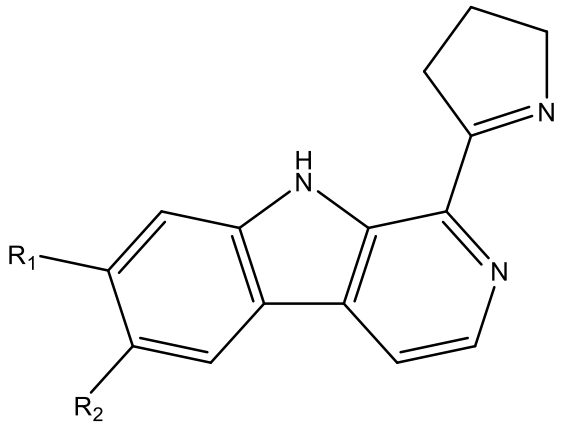

Figure 1.10 Eudistomins G, H, & I [Eudistomin G— R_1 = Br, R_2 = H | Eudistomin H— R_1 = H, R_2 = Br | Eudistomin I— R_1 = R_2 = H]

Vanadium is often the most discussed metal in tunicates.[48] The sequestration of vanadium has been studied in detail by various groups.[23,24,36,49–51] In the tunicate tissues, vanadium complexed with sulphate and chelated with amino groups of a protein called haemovanadin is observed.[34,52] Haemovanadin was assumed to be a pigment and an oxygen carrier. But it does not necessarily add 'green' colour to blood, and certainly doesn't help in carrying the oxygen in tunicates.[53] This complicates the understanding of the biological significance of vanadium in ascidians further, because if vanadium doesn't help in the voiding of predators, isn't significant in oxygen carrying, doesn't significantly help in the pigmentation of the blood, what exactly is the role of vanadium and/or other metals in these animals? Why do they sequester these metals? That is a question which needs a thorough investigation by biologists. Another class of proteins which are bound to vanadium, known as Vanabins were identified in cells called 'vanadocytes' in ascidians.[34,54–56,57] High concentrations of vanadium (10^7 higher than that of sea water concentration) are found in these vanadocytes. These cells also contain high concentrations of sulphuric acid and have a pH ranging from 1.5 to 2.0. But the role of vanabins is more like that of a vanadium-transfer protein. The actual significance of vanadium remains

an enigma. Regardless of the role of vanadium, it is evident that organometallic complexes exist in the bio-system of ascidians. Do vanadocytes also host other sequestered metals? Can vanabin also bind with other metals? Only a biochemist can provide an evidence.

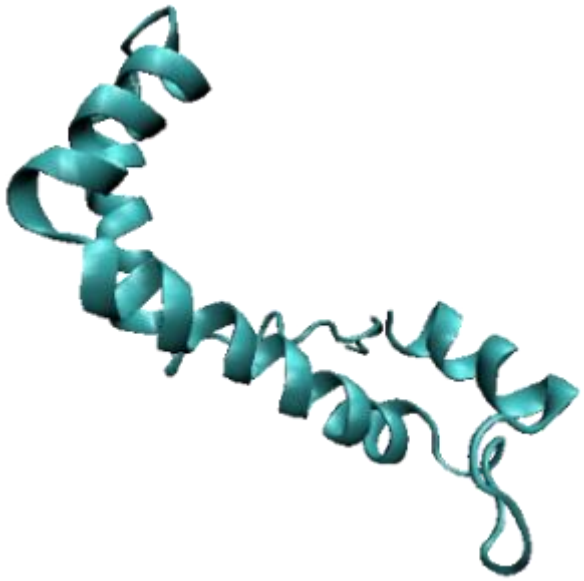

Figure 1.11 Vanabin2 from *Ascisia sydneiensis* var. samea (image from wikipedia.org. CC BY-SA 2.5)

1.5. Objective and Approach

The goal of this research work is to Figure out if there could be valid interactions between eudistomins and aqueous ions of metals that could help in the enrichment of the metals in the bio-system of ascidians, also helping the formation of sulphate/sulfuric acid. We hypothesize that metal-sulphates would react with the eudistomins and would result in the complexation of the metals with eudistomins and the formation of sulphate ion/sulfuric acid, which could be the reason for the enrichment of the metals. We have designed model reactions and have used quantum mechanical tools to test our hypothesis. The model reactions used for our computational experiments are very much simplified compared to the actual and complicated experimental situation in the bio environment of the ascidians. The challenge in designing such models is to capture the experimental situation by maintaining the simplistic approach. This type of approach was previously adopted in literature.[58–60]

In this problem, the focus is on the interactions of eudistomins and aqueous metal ions. As vanadium is a well-studied metal with respect to ascidians, it is one of the choices. As uranium

is the second most earth-abundant actinide, and as its recovery is a priority in nuclear reprocessing which is the primary application of this study, i.e., the usage of eudistomins as extraction ligands, it is one of our choices. Thorium, as it is the most earth-abundant actinide (second most in the ocean waters)[61], it is fairly possible that in a marine setting, thorium can interact with eudistomins if an ascidian picks it up. So, for this reason, vanadium, uranium, and thorium have been chosen as the metals to be studied.

Eudistomins, as forementioned, are ß-carboline derivatives. Depending on the functional groups attached to the tricyclic skeleton, there are multiple choices. Four eudistomins which can act as bi-dentate ligands have been chosen from the literature.[15,27] Three of the four structures provide a N-N donor type ligand interaction (Debromoeudistomin-K, Eudistomidin-B, Eudistomidin-C), while one of them provides N-O type interactions (Eudistomin-W).

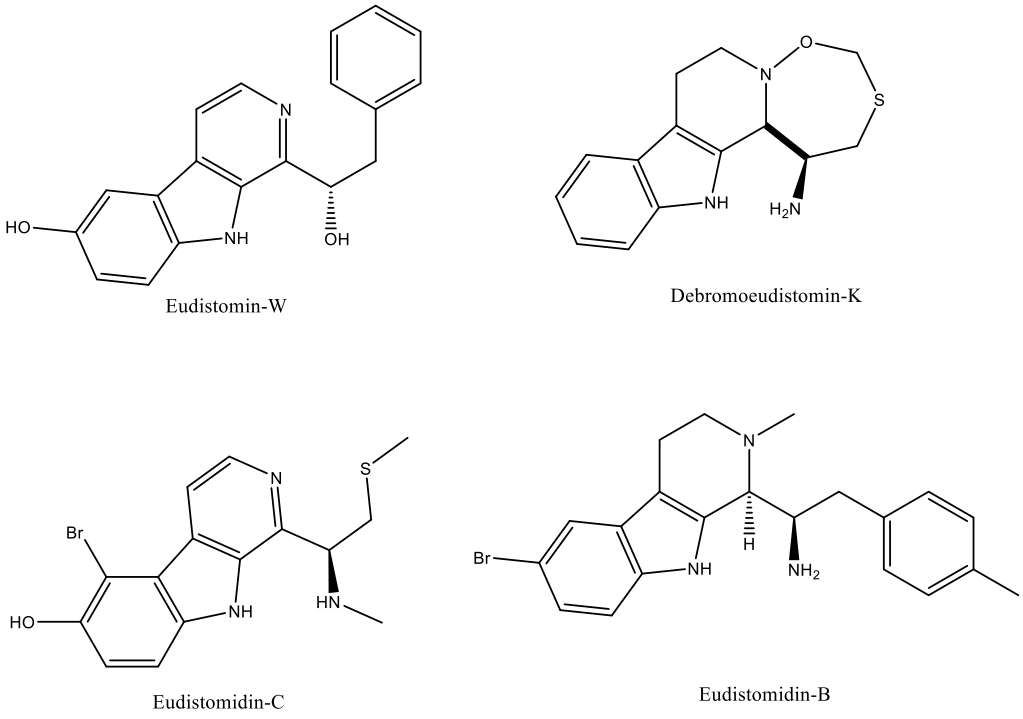

Figure 1.12 Molecular structures of the simple bi-dentate eudistomins

To replicate the marine environment, solvation phase calculations with water as the solvent was the default choice. We have modelled first solvation coordination as a part of explicit solvation to capture the interactions between the metal and water molecules, and have then considered the implicit solvation using continuum models. To design model reactions, the first factor that was taken into account was the metal aqueous ions and the number of water molecules that are in the coordination sphere. Vanadyl ion (VO^{2+}) with four or five water molecules is the most likely form of its aqueous ion.[62] Uranyl ion (UO_2^{2+}) with five water

molecules in the equatorial plane is the aqueous ion that has been chosen for this work.[63] Thorium tetra-positive ion (Th^{4+}) with nine water molecules is the aqueous ion that has been adopted for the calculations.[64] As forementioned, typically ascidians' cells are highly acidic with a pH at around 1.8-2.0.[35,65] Also, the presence of sulphuric acid and/or sulphate ions is reported in multiple studies. At pH ranging from 1.5 to 2.0, sulphuric acid mainly exists as HSO_4^- ion. However, as sulphate ion (SO_4^{2-}) was also mentioned in the literature[34]. This ion was also taken into account. This means, on the product side of the reaction, there needs to be a HSO_4^-/SO_4^{2-} ion(s) or sulphuric acid.

With the details mentioned above, five model reactions are designed as follows. (The equations here are given only as introduction, detailed equations will be discussed in the subsequent chapters.) In reaction 1, the cation and anion combine to form the complex and water, akin to a salt-type reaction. In the reaction 2, cation reacts with the neutral ligand, and forms the complex. The charge in this reaction is transferred to the hydronium ions. In reaction 3, the metal-sulphate reacts with the neutral eudistomin ligand to form complex and sulphuric acid. In reaction 4, the metal-sulphate reacts with the ligand anion, forming the complex. The charge in this reaction is transferred to the sulphate anion. In reaction 5, the metal-sulphate reacts with the ligand anion in the presence of sulfuric acid, forming the complex and transferring the charge to HSO_4^- ions.

1. Aqueous cation + Eudistomin ligand anion => Complex + n. Water
2. Aqueous cation + Neutral eudistomin ligand => Complex + n. Hydronium ion(s)
3. Sulphate + Neutral eudistomin ligand => Complex + n. Sulphuric acid
4. Sulphate + Eudistomin ligand anion => Complex + n. SO_4^{2-}
5. Sulphate + Sulphuric acid + Eudistomin ligand anion => Complex + n. HSO_4^-

With the above model reactions, the formation energies of the complexes are calculated to validate the interactions between the metals and the eudistomins.

1.6. Organization of the thesis

The aim of this thesis is to understand if valid interactions are possible between naturally occurring actinide metal aqua ions and eudistomins found in ascidians. Based on this study, we aim at determining if eudistomins can be employed as extractant ligands in nuclear reprocessing.

Chapter 1 and 2 serve as introductory chapters, the former providing a generic introduction and the latter providing an introduction to the computational methodology adopted in this work.

Chapter 3 provides details about the research work done. Vanadyl, uranyl, and thorium aqua ion interactions with Eudistomin-W, Debromoeudistomin-K, Eudistomidin-C, and Eudistomidin-B were calculated using Density Functional Theory (DFT) methods PBE-D3, BLYP, and B3LYP using Amsterdam Density Functional (ADF) and ORCA software applications with the usage of relativistic and solvation effects, and the related data are presented and discussed.

Chapter 4 provides the concluding remarks and future direction of this study.

CHAPTER-2

COMPUTATIONAL METHODS

Theoretical chemistry is a branch of chemistry that focuses on developing mathematically constructed equations which are built on the laws of physics to study chemical properties. Computational chemistry is the branch where the focus is on the application of theoretical methods to simulate, study, and solve various types of chemical problems. The first attempts to solve chemical problems using theoretical methods date back to 1927, using Valence Bond Theory. With the development of sufficient computer technologies in 1940s, in the early 1950s, the first semi empirical atomic orbital calculations were performed. By the mid 1970s, Hartree-Fock and ab initio methods were well established to solve poly atomic molecular chemical problems.[66–69] Density Functional Theory (DFT) was popular among solid state physicists by the 1970s, and its use among chemists has become popular by the 1990s chiefly due to the development of better functionals. Today, DFT methods can be surmised as the 'heart' of modern-day computational chemistry. Computational chemists have been recipients of the Nobel Prize, conspicuously in 1998 and 2013. Walter Kohn and John Pople have been awarded the Nobel Prize for their works "Development of the Density-Functional-Theory" and "Development of computational methods in quantum chemistry" in 1998.[70] Martin Karplus, Michael Levitt, and Arieh Warshel have been awarded the Nobel Prize in 2013 for "Development of multiscale models for complex chemical systems".[71]

More often than not, computational chemistry serves as the "theoretical lab" for various chemical problems. Where experiments are either difficult to perform, need to find a 'starting point', need a 'double-check', simply cannot explain certain results, or need a 'design' for a novel molecule; computational chemistry is the go-to-tool. How accurate are the results obtained from the computational chemistry tools? This depends on the level of theory used, conditions assumed, and approximations made. The best computational choice is always computationally expensive, i.e., it requires a large amount of computational 'power'. The 'cheapest' computational method is, more often than not, not so accurate, ergo, gives dross. The cliché 'one needs to find balance' fits perfectly for the computational problems as well.

As atoms have nuclei and electrons, most computational methods are built on the basis of quantum mechanics, and they attempt to solve the non-relativistic Schrödinger equation, with

relativistic corrections added (where applicable). Solving the fully relativistic Dirac equation is an ongoing and active area of research in computational chemistry. There are a number of approximate methods which give the 'right balance' betwixt accuracy and computational cost.

2.1. Schrödinger's Equation

The contents in the section are adopted from the works of Schrödinger, Cramer, and Jensen.[72–74]

Schrödinger's equation is arguably one of the greatest modern-day scientific discoveries. Dissimilar to classical mechanics, quantum mechanical problems are not deterministic, but are probabilistic. Quantum mechanical calculations would allow us to 'know' the probability of a quantum particle at a certain place, at a certain time. The probability function **P**(r,t) [where r = position, t = time] is given as the square of the wave function, **Ψ** (r,t) (see eq. 2.1.1).

$$P(r,t) = |\Psi|^2(r,t) \qquad \text{(eq. 2.1.1)}$$

The wave function can be obtained by solving the Schrödinger wave equation, which can be given in a simple form (eq. 2.1.2). [This shows the time independent Schrödinger wave equation]

$$\hat{H}\Psi(r,t) = E\Psi(r,t) \qquad \text{(eq. 2.1.2)}$$

Where, $\hat{H}$ is the Hamiltonian operator

E is the energy of the system.

In linear algebraic terms, the wavefunction is an eigenfunction of the Hamiltonian operator with the corresponding eigenvalue(s) E.

In its general form, the time-dependant Schrödinger equation can be given as follows (eq. 2.1.3).

$$\hat{H}\left|\Psi(r,t)\right\rangle = i\hbar\frac{d}{dt}\left|\Psi(r,t)\right\rangle \quad \text{(eq. 2.1.3)}$$

Where, i is the imaginary unit, and ħ is the reduced Planck's constant.

For a molecular system, the Hamiltonian has five contributors (eq. 2.14).

$$\hat{H} = -\sum_i \frac{\hbar^2}{2m_e}\nabla_i^2 - \sum_k \frac{\hbar^2}{2m_k}\nabla_k^2 - \sum_i \sum_k \frac{e^2 Z_k}{r_{ik}} + \sum_{i<j} \frac{e^2}{r_{ij}} + \sum_{k<l} \frac{e^2 Z_k Z_l}{r_{kl}} \quad \text{(eq. 2.1.4)}$$

Where i and j correspond to electrons, k and l to nuclei, m_e is the mass of an electron, m_k is the mass of the nucleus, e is the charge on the electron, Z is the atomic number, and r is the distance between the respective particles [the units are atomic units (a.u)].

The equation (eq. 2.1.4) has five terms. The first term is the kinetic energy term for each electron in the molecular system. The second term corresponds to the kinetic energy of each nucleus in the system. The third term relates to the total electron-nucleus Coulomb attraction in the molecule. The fourth term is the potential energy from the electron-electron repulsions. The fifth term is the potential energy from nucleus-nucleus repulsions.

2.2. Born-Oppenheimer Approximation

In a many-body system like that of a molecule, it is always arduous to obtain proper wave functions, mainly because of the complexity in the Hamiltonian operator. For this reason, to simplify the problem, one can take the aid of the Born-Oppenheimer approximation.[75,76] In this approximation, the nuclei and the electrons are treated separately, mainly because the nuclei are massive, move much slower in comparison to the electrons, and are nearly fixed with respect to the electron-motion. This can mean that one can compute electronic energies for fixed nuclear positions. The kinetic energy term of the nucleus can be eliminated and the nucleus-nucleus potential energy term is constant for a fixed geometry. Therefore, the Schrödinger equation can be given as (eq. 2.2).

$$(\hat{H}_{el} + V_N)\Psi_{el}(q_i; q_k) = E_{el}\Psi_{el}(q_i; q_k) \quad \text{(eq. 2.2)}$$

The subscript ‘el’ emphasizes that the Born-Oppenheimer approximation is considered for the equation. V_N is the nucleus-nucleus potential energy term. q_i and q_k are independent variables (electron and nucleus coordinates respectively)

Born-Oppenheimer approximation is fairly accurate for most of the cases, with exceptions. The Schrödinger equation cannot be solved except for hydrogen atom and H_2^+ molecule. The detailed discussion of this topic is beyond the scope of this study.

The contents in the section are adopted from the works of Cramer, Jensen, and Born & Oppenheimer.[73,74,77]

2.3. Variational Method

The contents in the section are adopted from the works of Cramer, and Jensen.[73,74]

Variational method is one of the ways to find approximations to the least energy eigen state, i.e., the ground state, to evaluate the wavefunctions, that of molecular orbitals in a molecular system.[78] A trial function is chosen, that obeys the boundary conditions of the molecular system, which depends on adjustable variational parameters. By adjusting the variational parameters, one can find the least energy trial function. The energy and the wavefunction of the resulting trial function are variational approximations to the exact wavefunction and energy. The ground state energy of the exact function is always lower than that of the trial function, as given by the variational principle (eq. 2.3)

$$E(\Psi) = \frac{<\Psi|\hat{H}|\Psi>}{<\Psi|\Psi>} \geq E_0 \qquad \text{(eq. 2.3)}$$

Where E(Ψ) is the trial function and E_0 is the exact ground state energy.

2.4. Perturbation Theory

The contents in the section are adopted from the works of Cramer, and Jensen.[73,74]

Perturbation theory, as the word suggests, adds perturbation to the existing Schrödinger's equation (eq. 2.4.1).

$$(\hat{H}^0 + \hat{H}^1)(\Psi^0 + \Psi^1) = (E^0 + E^1)(\Psi^0 + \Psi^1) \qquad \text{(eq. 2.4.1)}$$

Where the superscript '0' denotes existing states, and '1' denotes the perturbation.

One can eliminate $\hat{H}^0\Psi^0$ and $E^0\Psi^0$ terms as they are zero-order terms. Similarly, $\hat{H}^1\Psi^1$ and $E^1\Psi^1$ terms correspond to second order terms. The first order perturbation can be given as (eq. 2.4.2).

$$\hat{H}^0\Psi^1 + \hat{H}^1\Psi^0 = E^0\Psi^1 + E^1\Psi^0 \qquad \text{(eq. 2.4.2)}$$

To obtain the first order correction to the energy, the above equation can be multiplied by Ψ^{0*} and integrated on both sides. This leaves us with (eq. 2.4.3).

$$E^1 = \int \Psi^{0*}\hat{H}^1\Psi^0 d\tau \qquad \text{(eq. 2.4.3)}$$

This way, the perturbation allows us to improve an existing zeroth order energy. The higher order terms can be obtained via similar method.

2.5. Basis Sets

A basis set is a collection of mathematical functions that are used to construct a wave function. The expansion of an unknown function such as a molecular orbital in a set of known functions would not be an approximation if the basis set is complete. However, this requires an infinite number of functions in most of the cases, which is an impossible task. A small number of basis functions leads to a poor representation of the orbitals, while a larger basis set would test the computational cost. The 'balance' plays a key role while selecting the basis sets. Modern day computational chemistry offers mainly two flavours of basis sets, one with Slater Type Orbitals (STOs)[79], and the other being Gaussian Type Orbitals (GTOs).[80]

Slater type orbitals, named after John. C. Slater, who introduced them in 1930, have the functional form shown in (eq. 2.5.1).

$$\chi_{\zeta,n,l,m}(r,\theta,\varphi) = NY_{l,m}(\theta,\varphi)r^{n-1}e^{-\zeta r} \qquad \text{(eq. 2.5.1)}$$

Where, n is the principle quantum number of the valence orbitals, ζ is the exponent which depends on the atomic number and can be chosen based on the rules developed by Slater, N is the normalization constant, $Y_{l,m}(\theta,\varphi)$ are spherical harmonic functions, where l and m are angular quantum numbers , and the spherical coordinates are given by (r,θ,φ).

The shape of the atomic orbitals is well-defined by STOs. The accuracy that can be achieved via STOs is of high level, as they are exhibiting exponential decay at a long range. The modelling of the density, especially around the nucleus is accurate, ergo, less functions are required to obtain a good fit. Despite this, STOs are not computation friendly, and cost a good amount of computational time.

GTOs, the other flavour of basis sets, are fairly quick in comparison to STOs. This is because they have e^{-r^2} dependence, unlike STOs, as shown in (eq. 2.5.2). As a consequence, the relevant integrals can be evaluated analytically.

$$\chi_{\zeta,n,l,m}(r,\theta,\varphi) = NY_{l,m}(\theta,\varphi)r^{2n-2-l}e^{-\zeta r^2} \qquad \text{(eq.2.5.2)}$$

While GTOs are definitely quicker, they do not define the atomic orbitals properly. This drawback allows the loss of accuracy. Figure 2.5 compares STOs and GTOs to s-type orbitals. From the image, one can clearly see that STOs define the orbitals more accurately.

Usually, as there are different levels of basis sets, viz. SZ (single zeta), DZ (double zeta), TZ (triple zeta), and so on; to get a better accuracy, the usage of high level basis sets is always advantageous. For instance, a TZ basis set would have three basis functions per occupied molecular orbital, and this can help with the accuracy. The addition of polarization functions and diffuse functions would allow 'flexibility' to the basis functions, ergo, improving with the accuracy. However, basis sets should be chosen based on the level of theory, as few methods like Hartree Fock would tend to give semi-accurate results beyond TZ basis sets. The contents in the section are adopted from the works of Cramer, and Jensen.[73,74]

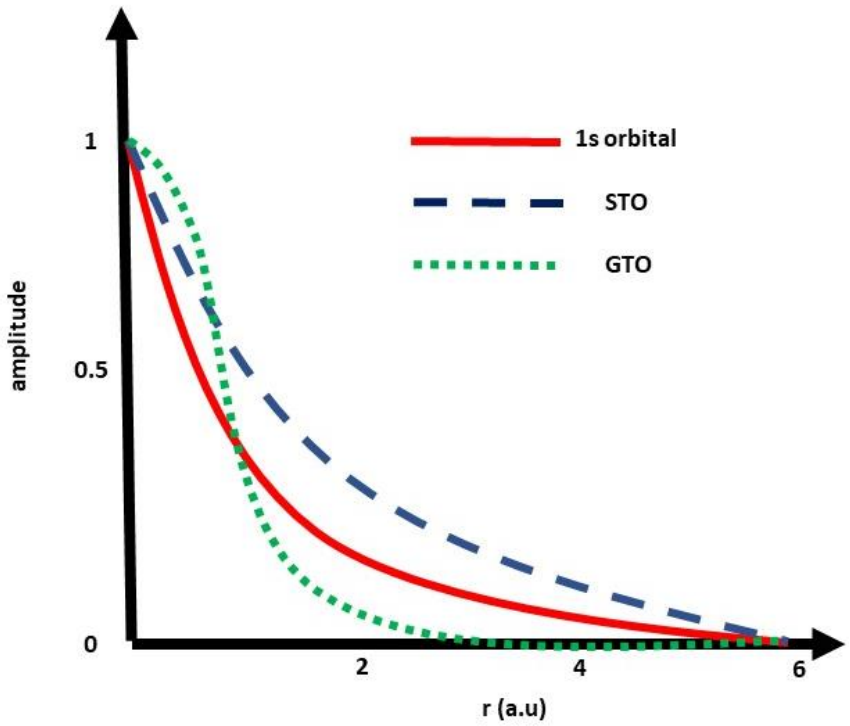

Figure 2.1 Schematic comparison of STOs and GTOs to 1s atomic orbital

2.6. Hartree-Fock Method

The contents in the section are adopted from the works of Cramer, Jensen, Hartree, Slater, and Gaunt.[73,74,81–83]

The development of the Hartree-Fock (HF) method is one of the greatest events in the history of quantum chemistry. Despite its drawbacks, it has defined an era. So much so that an entire

class of the modern-day computational approaches are termed as 'Post-HF' methods. The Hartree-Fock method adopts the Born-Oppenheimer approximation for a system with 2N electrons and M nuclei. The Hartree-Fock wave function is commonly represented by a Slater determinant (shown in eq. 2.6.1).

$$\Psi(1,2,\ldots.N) = \frac{1}{\sqrt{(2N)!}}\begin{vmatrix} \Psi_1\alpha(1) & \Psi_1ß(1) & \cdots & \Psi_N\alpha(1) & \Psi_Nß(1) \\ \Psi_1\alpha(2) & \Psi_1ß(2) & \cdots & \Psi_N\alpha(2) & \Psi_Nß(2) \\ \vdots & \vdots & \ddots & \vdots & \vdots \\ \vdots & \vdots & \ldots & \vdots & \vdots \\ \Psi_1\alpha(2N) & \Psi_1ß(2N) & \cdots & \Psi_N\alpha(2N) & \Psi_Nß(2N) \end{vmatrix} \qquad \text{(eq.2.6.1)}$$

The energy is given by (eq. 2.6.2).

$$E_{ele} = < \Psi^*(1,2,\ldots.2N)|\widehat{H}|\Psi(1,2,\ldots.2N) > \qquad \text{(eq.2.6.2)}$$

The above equation (eq. 2.6.2) can also be written as (eq.2.6.3).

$$E_{ele} = 2\sum_{j=1}^{N} I_j + \sum_{i=1}^{N}\sum_{j=1}^{N}(2J_{ij} - K_{ij}) \qquad \text{(eq.2.6.3)}$$

Where,

$$I_j = \int dr_j \Psi_j^*(r_j)(\frac{-1}{2}\nabla_j^2 - \sum_N^M \frac{Z_A}{r_{jA}})\Psi_j(r_j) \qquad \text{(eq.2.6.4)}$$

$$J_{ij} = \iint dr_1 dr_2 \Psi_i^*(r_1)\Psi_j^*(r_2)\frac{1}{r_{12}}\Psi_i(r_1)\Psi_j(r_2) \qquad \text{(eq.2.6.5)}$$

$$K_{ij} = \iint dr_1 dr_2 \Psi_i^*(r_1)\Psi_j^*(r_2)\frac{1}{r_{12}}\Psi_i(r_2)\Psi_j(r_1) \qquad \text{(eq.2.6.6)}$$

After the application of the variational principle to the energy expression in (eq.2.6.3), the spatial orbitals that are at minima of the energy E, would satisfy the equation (eq.2.6.7).

$$\hat{F}(r_1)\Psi_i(r_1) = \varepsilon_i\Psi_i(r_1) \qquad i = 1,2,\ldots.N \qquad \text{(eq.2.6.7)}$$

Where $\hat{F}(r_1)$ is the Fock operator

$$\hat{F}(r_1) = \hat{f}(r_1) + \sum_{j=1}^{N}[2\hat{J}_j(r_1) - \hat{K}_j(r_1)] \qquad \text{(eq.2.6.8)}$$

Where,

$$\hat{f}(r_1) = \frac{-1}{2}\nabla_1^2 - \sum_A \frac{Z_A}{r_{1A}} \qquad \text{(eq.2.6.9)}$$

$\hat{J}_j(r_1)$ is the Coulomb operator

$$\hat{J}_j(r_1)\Psi_i(r_1) = \Psi_i(r_1)\int dr_2 \Psi_j^*(r_1)\frac{1}{r_{12}}\Psi_j(r_2) \qquad \text{(eq.2.6.10)}$$

$\hat{K}_j(r_1)$ is the exchange operator

$$\hat{K}_j(r_1)\Psi_i(r_1) = \Psi_j(r_1)\int dr_2 \Psi_j^*(r_2)\frac{1}{r_{12}}\Psi_i(r_2) \qquad \text{(eq.2.6.11)}$$

An expression for the energy of the i[th] molecular orbital can be obtained by multiplying (eq.2.6.7) from the left by $\Psi_i^*(r_1)$ and integrating with r_1

$$\varepsilon_i = \int dr_1 \Psi_i^*(r_1)\hat{F}(r_1)\Psi_i(r_1) \qquad \text{(eq.2.6.12)}$$

Using the Fock operator, (eq.2.6.12) becomes,

$$\varepsilon_i = I_j \sum_{j=1}^{N}[2J_{ij} - K_{ij}] \qquad \text{(eq.2.6.13)}$$

Comparing (eq.2.6.13) and (2.6.3) would give,

$$E = \sum_{i=1}^{N}[I_i + \varepsilon_j] \qquad \text{(eq. 2.6.14)}$$

Molecular orbitals could be concocted as the linear combinations of basis functions, as developed by Clemens Roothaan.[73,74,84,85]

$$\Psi = \sum_{v=1}^{K}[c_v\phi_v] \qquad \text{(eq.2.6.15)}$$

The Hartree-Fock-Roothaan equations are given by

$$\sum_v[F_{\mu v}c_v] = \varepsilon\sum_v[S_{\mu v}c_v] \qquad \mu = 1,2,3,\ldots\ldots K \qquad \text{(eq.2.6.16)}$$

Where, $F_{\mu v}$ accounts for the Fock matrix elements and $S_{\mu v}$ for the overlap matrix elements.

$$F_{\mu v} = \int dr_1 \phi_\mu^*(r_1)\hat{F}(r_1)\phi_v(r_1) \qquad \text{(eq.2.6.17)}$$

$$S_{\mu v} = \int dr_1 \phi_\mu^*(r_1)\phi_v(r_1) \qquad \text{(eq.2.6.18)}$$

The equation (eq.2.6.16) can be given in matrix notion as,

$$Fc = \varepsilon Sc \qquad \text{(eq.2.6.19)}$$

Where, F and S are (K x K) matrices and, c is a (K x 1) column vector.

The equation (eq.2.6.19) could be solved via self-consistent procedure called Self-Consistent-Field method (SCF method).[73,74,82,86] Despite its greatness, HF method, as forementioned has its drawbacks, and is prone to inconsistencies in delivering proper results that can be validated by experimental results. These hindrances are addressed in most of the post-HF methods.

2.7. Density Functional Theory

The contents in the section are adopted from the works of Cramer, and Jensen.[73,74]

Often regarded as the best way of addressing quantum chemical problems, Density Functional Theory (DFT) is one of the extensively used ways to solve the electronic structure of many-body system problems pertaining to atoms, molecules, condensed phase systems, etc. Most computational works often have DFT as their go-to method, such is the accuracy as well as popularity.[73,74,87–92]

The basis or the theoretical foundation of DFT was developed by Walter Kohn and Pierre Hohenberg by two theorems known as Hohenberg-Kohn theorems, or HK theorems.[93] The first theorem points that the external potential [V(r)] is a unique functional of the electron density [ρ(r)], as shown in equation (eq.2.7.1). This means that the ground state density of a system is determined uniquely by the potential and therefore the other properties of the same system can be determined as well. The second theorem states that if the input density is the true ground state density of a system, then the functional that delivers the ground state energy of the system gives the lowest energy of the same system, which means that the ground state energy E_0 can be obtained variationally (eq.2.7.2).

$$E[\rho(r)] = \int \rho(r)V(r)\, dr + F[\rho(r)] \qquad \text{(eq.2.7.1)}$$

where $F[\rho(r)]$ is the universal functional of the electron density $\rho(r)$

$$E[\rho(r)] = \int \rho(r)V(r)\, dr + F[\rho(r)] \geq E0 \qquad \text{(eq.2.7.2)}$$

2.7.1. Kohn-Sham Theory

The contents in the section are adopted from the works of Jensen, and Kohn & Sham.[74,94]

While there have been orbital-free DFT models, most of them have resulted in a poor representation of the kinetic energy. Kohn-Sham (KS) theory was developed in a way, where it splits the kinetic energy into two parts, the first term can be calculated exactly and the second term is a correction term. In the first term, the kinetic energy of a fictious system made of non-interacting electrons is calculated exactly, while in the second term the corrections to the kinetic energy and the electron-electron repulsion energy are taken into account. The Kohn-Sham model resembles the Hartree-Fock model by sharing identical formulations.

If λ=0 represents a fictious system, and λ=1 represents a real system, with $0 \leq \lambda \leq 1$, the Hamiltonian can assume the form as shown in (eq.2.7.3)

$$H_\lambda = T + V_{ext}(\lambda) + \lambda V_{ext} \qquad \text{(eq.2.7.3)}$$

For λ=0, the electrons are non-interacting, and the exact solution to the Schrödinger equation is given as a Slater determinant composed of MOs ϕ_i, and the kinetic energy is given as (eq.2.7.4)

$$T_S = \sum_{i=1}^{N_{ele}} \langle \phi_i | \frac{-1}{2} \nabla^2 | \varphi_i \rangle \qquad \text{(eq.2.7.4)}$$

The λ=1 case is of the interacting electrons, and could be only approximated to the real kinetic energy.

Another possible way to obtain justification to the use of (eq.2.7.4) to calculate the kinetic energy is by referring to the natural orbitals, i.e., the eigenvectors of the density matrix. The exact kinetic energy can be obtained from the natural orbitals (NO) arising from the exact density matrix.

$$T[\rho_{exact}] = \sum_{i=1}^{\infty} n_i \langle \phi_i^{NO} | \frac{-1}{2} \nabla^2 | \phi_i^{NO} \rangle \qquad \text{(eq.2.7.5)}$$

$$[\rho_{exact}] = \sum_{i=1}^{\infty} n_i |\phi_j^{NO}|^2 \qquad \text{(eq.2.7.6)}$$

$$N_{elec} = \sum_{i=1}^{\infty} n_i \qquad \text{(eq.2.7.7)}$$

As the occupancy number of a natural orbital n_i will be between 0 and 1, corresponding to the number of electrons in the orbital, representation of the exact density would require an infinite number of natural orbitals. Since the exact density is not known, an approximate density can be given as a set of auxiliary one-electron functions, i.e., orbitals.

$$\left[\rho_{approx}\right] = \sum_{i=1}^{N_{elec}} |\phi_i|^2 \qquad \text{(eq.2.7.8)}$$

Kohn-Sham theory calculates the kinetic energy under the assumption of non-interacting electrons, similar to HF orbitals in wave mechanics. The difference between the exact kinetic energy and that which is calculated by the assumption of non-interacting orbitals is small. The remaining kinetic energy is adsorbed into an exchange-correlation term, and a generic DFT energy expression can be given by (eq.2.7.9).

$$E_{DFT}[\rho] = T_S[\rho] + V[\rho] + E_{XC}[\rho] \qquad \text{(eq.2.7.9)}$$

Where ρ is the electron density

T_S is the kinetic energy obtained from the Slater determinant of the hypothetical system,

V is the classical potential energy term,

and E_{XC} is the exchange-correlation term.

The exchange-correlation term is the element which makes various approximate DFT methods to be different from each other. The complete solution to the Schrödinger equation can be obtained if one can obtain the exact value to the exchange-correlation problem. Few techniques to tackle this problem are Local Density Approximation (LDA), Generalized Gradient Approximation (GGA), Meta-GGA, Hyper-GGA or Hybrid functionals, and Generalized Random Phase Approximation (GRPA) methods. The addition of dispersion corrections to the existing DFT methods would result in the betterment of the results.[95–97] One such popular correction is D3 as given by Grimme et al[98]. It is known to provide improved results and is widely used among the computational chemists.

$$E_{\text{DFT-dispersion corrected}} = E_{\text{DFT}} + E_{\text{dispersion correction}} \qquad \text{(eq.2.7.10)}$$

2.7.2. Local Density Approximation (LDA)

The contents in the section are adopted from the work of Jensen.[74]

In LDA, it is assumed that the density can be treated as a uniform electron gas locally, or equivalently that the density is a slowly varying function. The exchange correlation term for spin-unpolarized system by LDA is given by,

$$E_{XC}^{LDA}[\rho(r)] = \int \rho(r)\, \varepsilon_{XC}\big(\rho(r)\big)\, dr \qquad \text{(eq.2.7.11)}$$

Where ρ(r) is the local value of the electron density at any position r

ε_{XC} is the exchange correlation energy per particle of the homogenous electron gas (HEG) of charge density ρ

2.7.3. Generalized Gradient Approximation (GGA)

The contents in the section are adopted from the work of Jensen.[74]

An improvement to the LDA approach, GGA also accounts for the electron density gradient.

$$E_{XC}^{GGA}[\rho(r)] = E_{XC}^{LDA}[\rho(r)] + \Delta E_{XC}\left[\frac{|\nabla\rho(r)}{\rho^{\frac{4}{3}}r}\right] \qquad \text{(eq.2.7.12)}$$

2.7.4. Meta-GGA

The contents in the section are adopted from the work of Jensen.[74]

In Meta-GGA, the exchange correlation functional depends on second order terms, with the Laplacian being the second order term. The calculation of orbital kinetic energy density is numerically more stable than the calculation of the Laplacian of the density. The functional can be taken to depend on the orbital kinetic energy density τ.

$$\tau(r) = \frac{1}{2}\sum_{i}^{occupied} |\nabla\phi_i(r)|^2 \qquad \text{(eq.2.7.13)}$$

2.7.5. Hybrid functionals

The contents in the section are adopted from the work of Jensen.[74]

Hybrid theory, as the name suggests, is about linking two different levels of theory to make a hybrid. Also known as Hyper-GGA method, this method focuses on linking exchange correlation energy and the corresponding potential connecting the non-interacting reference and the actual system. The equation, known as Adiabatic Connection Formula (ACF), helps in integrating over the parameter λ, which "turns on" the electron-electron interaction. Usually, the hybrid functionals have x% of HF exchange energy, y% of GGA functional exchange energy along with the correlation energy. An example, PBE0[99] is given in the (eq.2.7.15)

$$E_{XC} = \int_0^1 \langle\Psi(\lambda)|V_{XC}(\lambda)|\Psi(\lambda)\rangle\, d\lambda \qquad \text{(eq.2.7.14)}$$

Exchange-Correlation energy of PBE0 = 25% HF exchange energy + 75% PBE exchange energy + 100% PBE correlation energy (eq.2.7.15)

2.7.6. Generalized Random Phase Approximation

The contents in the section are adopted from the work of Jensen.[74]

At the top of the Jacob's ladder classification[100] (shown in Figure 2.7), where the full information of the Kohn-Sham orbitals, both virtual and occupied orbitals, is considered, the formalism is identical to the methods adopted in the Generalized Random Phase Approximation (GRPA). While the inclusion of the virtual orbitals certainly improves a few aspects like van der Waals interactions, etc., very little work is done on these methods. One such development is the class of Optimized Effective Potential (OEP) methods, where mainly the exchange-correlation energy is treated as a functional of the unknown density, but the energy as a function of the orbitals given by the wave function theory to a given order in the

correlation as defined by perturbation expansion, for instance. The density is given by the sum of square of the orbitals, which implicitly defines the energy as a function of the density. The exchange correlation potential is defined by the density derived from a KS calculation using a single determinant wave function that exactly matches the density derived from a correlated wave function. While this method tries to unite two different theories, DFT and WFT (wave function theory), it possesses the disadvantage of slow convergence with respect to basis set size.

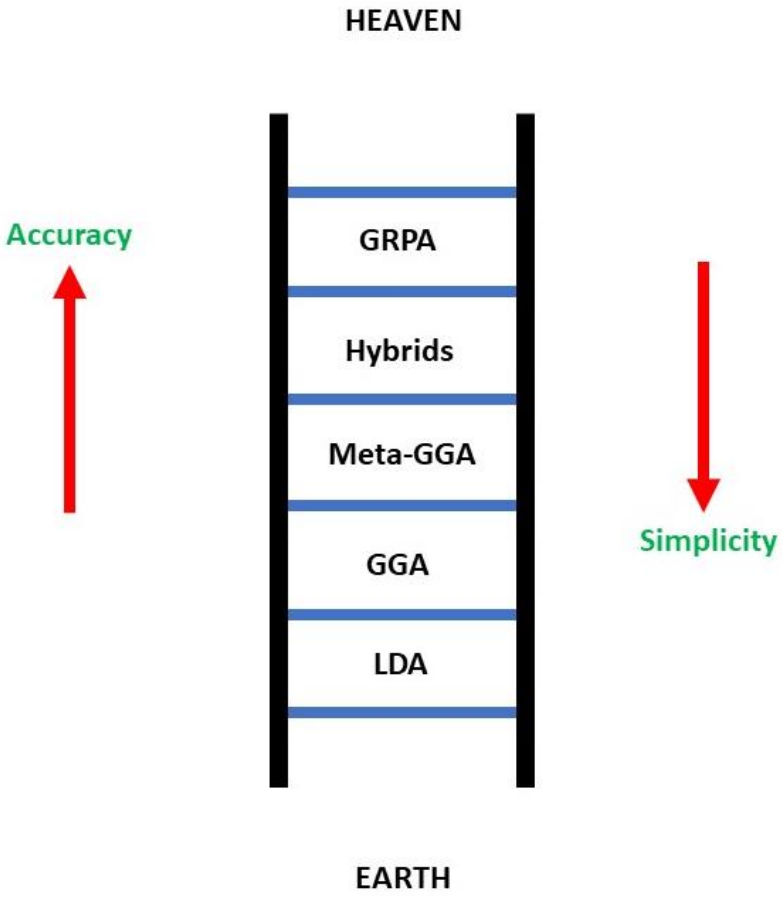

Figure 2.2 Jacob's ladder classification of DFT functionals

2.8. Relativistic Effects

The contents in the section are adopted from the work of Jensen.[74]

Amalgamation of relativistic mechanics and quantum chemistry became necessary to explain certain types of behaviour in elements, for instance colour of gold, mercury occurring in liquid state at room temperature, etc., and their chemistry.[101] The Dirac equation[102] (see eq. 2.8.1);

named after the legendary physicist Paul Dirac, describes the relativistic effects on electronic structure.

$$[c\alpha.p + ßmc^2]\Psi = i\frac{\partial\Psi}{\partial t} \qquad \text{(eq.2.8.1)}$$

Where,

c is the speed of light, p is the momentum, and α and ß are 4 x 4 matrices, and α is given by the three 2 x 2 Pauli spin matrices and ß in terms of a 2x2 unit matrix I

$$\alpha = \begin{bmatrix} 0 & \sigma \\ \sigma & 0 \end{bmatrix}$$

$$\sigma_x = \begin{bmatrix} 0 & 1 \\ 1 & 0 \end{bmatrix} \quad \sigma_y = \begin{bmatrix} 0 & -i \\ i & 0 \end{bmatrix} \quad \sigma_z = \begin{bmatrix} 1 & 0 \\ 0 & -1 \end{bmatrix}$$

$$ß = \begin{bmatrix} I & 0 \\ 0 & I \end{bmatrix}$$

$$\text{where } I = \begin{bmatrix} 1 & 0 \\ 0 & 1 \end{bmatrix}$$

Computationally, solving a full Dirac equation would be very expensive, as well as there is always the risk of variational collapse. To tackle this problem, approximations are made, and one such popular approximation is the Zeroth Order Regular Approximation (ZORA).[103–108] ZORA is one of the best approximations which can help in solving the relativistic effects issue with respect to heavy elements. In the ZORA method, the Dirac equation is solved approximately, via a two component approach. Along with relativistic kinetic energy and potential energy terms, the ZORA method also has a spin-orbit energy term (see eq.2.8.2). Usually, the spin-orbit term can be ignored if the number of free electrons in a given reaction system does not change, as it doesn't really affect the geometry or the relative energy of the system (except for transactinides), and therefore any effects on the reaction energies are assumed to cancel out. If and when the spin-orbit energy term is ignored, it is called the scalar relativistic ZORA method.

$$\left[\frac{c^2p^2}{2mc^2-V} + \frac{2c^2}{(2mc^2-V)^2} + \frac{Z.s.I}{r^3} + V\right]\Psi_L = E\Psi_L \qquad \text{(eq.2.8.2)}$$

Another possible way to handle the relativistic effects problem is by employing Effective Core Potentials (ECPs).[109,110] In ECPs, the inner shell electrons are parametrized by one-electron operator, in a way treating them as a potential, while the valence electrons are considered for the relativistic effects.

The advantage of using ZORA is that it is an all-electron calculation, while ECP is not. Adopting ZORA with small/large frozen core would reduce the computational cost, as the core electrons are calculated only once for to obtain their states, and then it remains that way throughout the rest of the calculation. The frozen core ZORA approach gives us the right balance between the computational cost and the accuracy.

2.9. Solvation Effects

The contents in the section are adopted from the work of Cramer.[73]

It is only logical to adopt solvation effects for calculations that involve the marine world. Solvation effects show a very significant difference in comparison to their gaseous counter parts. For instance, cation and anion interactions in gas phase result in extremely high formation energies, while in aqueous phase, not so.

Solvation effects can be calculated via explicit and implicit/continuum solvation models. Explicit solvation adds a number of solvent molecules around the solute molecule. As the size of the molecule becomes large, computational cost increases due to the addition of solvent molecules, and this addition of solvent molecules makes the search for global minima much more difficult. A continuum model can be defined as a model with a number of the degrees of freedom of the constituent particles that are described in a continuous way, usually by a distribution function. Of the widely used solvation models, two implicit models are Polarized Continuum Model (PCM)[111–114] and Conductor like Screening Model (COSMO)[115,116]. PCM model comes mainly in two flavours, dielectric PCM (D-PCM), where it adopts polarizable continuum, and the second type is conductor like PCM (CPCM), which is basically COSMO in PCM. In COSMO, the surrounding medium is well modelled as a conductor, but lacks the proper modelling of the specific interactions between solute and solvent molecules. This problem can be tackled by modelling the first solvation shell which can contain a number of explicit solvent molecules.[117]

In the implicit solvation models, the interactions between the solute and the solvent are given by the free energy of the solvation ΔG^0_S. For a molecule X, the free energy of the solvation refers to the change in the free energy of the molecule X leaving the gas phase and entering the solvation phase, and it can be determined from the equilibrium constant describing the change in phase from gas to solvation, as shown in the equation 2.9.1.

$$\Delta G_S^0 = lim_{[X]_{sol}\to 0}\left\{-RT\ln\frac{[X]_{sol}}{[X]_{gas}}\Big|_{eq}\right\} \qquad \text{(eq. 2.9.1)}$$

For a solute molecule X, the Hamiltonian is given as a perturbation to the X's Hamiltonian in implicit solvent models, as shown in equation 2.9.2.

$$\hat{H}(X_{total}) = \hat{H}(X_{molecule}) + \hat{V}(X_{molecule+solvent}) \qquad \text{(eq. 2.9.2)}$$

The contributing terms to the Gibbs free energy can be given as shown in equation 2.9.3.

$$G = G_{cavity} + G_{electrostatic} + G_{dispersion} + G_{repulsion} + G_{thermal\ motion} \qquad \text{(eq. 2.9.3)}$$

Equilibrium electrostatic interactions between solvent and solute are always non-positive. They are zero if the solute has no electrical moments (like in case of a noble gas), or negative (meaning an attraction). In continuum models, the solute in a cavity is 'immersed' in a continuous electric field, also called as 'reaction field' because it derives from the reaction of the solvent to the presence of solute. The electric field at a given point in space is the gradient of the electrostatic potential Φ at that point and the required work to create the charge distribution can be derived from the interaction of solute charge density ρ with the electrostatic potential, that which can be obtained from Poisson equation. The polarization energy is given in the equation 2.9.4.

$$G = -\frac{1}{2}\int \rho(r)\Phi(r)\,dr \qquad \text{(eq. 2.9.4)}$$

Where G is the polarization energy

The total entropy of a molecule in solvation has been explained in the literature[73,118,119], and can be given as shown in equation 2.9.5.

$$S_{total} = S_{vibration} + S_{translation} + S_{rotation} + S_{cavity}$$

Where the S_{cavity} can be given as

$$S_{cavity} = \left(\frac{\partial G_{cavity}}{\partial T}\right)$$

In explicit solvation models, the solvent molecules are modelled around the solute to capture the realistic picture. However, these models are computationally expensive because of the size of super-molecule. Besides the computational cost with the size of the super-molecule, one of the major issues of explicit solvation models is the fact that one has to deal with so many potential conformers of the solvation shell, which can be done with the aid of molecular

dynamic studies. But they do pose an advantage over the implicit models as they are capable of capturing the interactions between the solvent and solute molecules.

In our work, we have employed a hybrid model, where the metal is coordinated with water molecules, and then as a whole we have used COSMO and CPCM solvation models. This way we were able to capture the interactions between the solute and solvent.

2.10. Charge Analysis

The contents in the section are adopted from the work of Jensen.[74]

Atomic charge is not a physical observable. But it helps in understanding and analysing the electron density in a molecule. There are various tools to analyse the atomic charges, some popular ones being Mulliken,[120] Mayer Bond analysis,[121] Hirshfeld,[122] Natural Bonding Orbitals (NBO)[123] and Voronoi Deformation Density (VDD)[124].

Mulliken population analysis method assigns an electronic charge to an atom as the sum of overall orbitals belonging to that atom and then the charge is defined as the difference with the number of electrons on the isolated free atom. Mayer bond analysis adopts a technique along the similar lines, by summing up all electron density contribution to the bonds. As both Mulliken and Mayer Bond analytical tools depend on the coefficients of basis functions, ergo, have a basis set dependency, usage of larger basis set would 'ill define' the populations and the charges obtained may tend to give different set of results for different basis sets.

In VDD, the technique is built on the partitioning of space into non-overlapping atomic areas modelled as Voronoi cells and then calculating the deformation density in the interior of those cells. In Hirshfeld charges, the partial charge is defined relative to the deformation density, i.e., difference between the molecular and unrelaxed atomic charge densities. The benefit of adopting Hirshfeld charges is when the molecular deformation density converges to the true solution, the computed net charges will necessarily converge. The NBO analysis adopts a method where the electronic wave functions are interpreted in terms of Lewis-like chemical bonds. The NBO method considers a quantitative interpretation of the electronic structure of a molecular system akin to that of a Lewis structure. NBO analysis, as it is not dependent on the basis set, is a reliable tool.

2.11. Computational methods in this work

Amsterdam Density Functional (ADF)[125–127] software (version 2017.114) with GGA functional BLYP[128,129] and GGA functional with dispersion correction PBE-D3[130,131] with TZ2P[105] basis set, scalar ZORA[103,104,106,107] relativistic approach (with small frozen core), and COSMO (with water) for solvation effects was adopted for two sets of calculations. ORCA[132,133] software (version 4.2.1) with GGA functional BLYP and hybrid functional B3LYP[129,134] with basis set def2-TZVPP (SARC-ZORA-TZVPP for Uranium and Thorium), scalar ZORA relativistic approach, and CPCM (with water) for solvation effects was adopted for two other sets of calculations. Both COSMO[115,116] (in ADF) and CPCM[135] (in ORCA) solvation effects have been used with the respective default settings as given in the respective software applications. Gas phase and solvation phase calculations are performed, where the solvation effects were ignored for the former.

The different levels of theories using two different software applications gives us a validation to the model reactions adopted in this study, as the data suggests (discussed in the following chapter).

CHAPTER-3

Computational studies of the Eudistomin-Metal aqua ion interactions

3.1. Introduction

In an ideal world, tunicates are probably one of the least important things to humans with no use to the hominal community, except for maybe the Chilean, Korean, and Japanese chefs and cooks. But 'reality' often likes to go to a novelty shop, buy a great gift, wrap it in a cheap paper, and deliver it to us on a least expected day. The 'unimportant' tunicates contain compounds of a greater 'importance'. The identification of eudistomins in their biosystem has made them relevant and important to the pharmacological researchers.[27,29–31,45] The identification of the complexation of Eudistomins G, H, and I with iron[47], has sparked interest and made them a prospect in the actinide community. The interactions between $[UO_2]^{2+}$, $[UO_2(H_2O)_5]^{2+}$, and $[UO_2(CO_3)_3]^{4-}$ with the same eudistomins G, H, and I have been explored in a preliminary study.[136] The main goal of this study is to understand if valid interactions are possible between eudistomin ligands and metal aqua ions.

Reiterating the statements from the previous chapters, four simple bidentate eudistomin ligands have been identified from the literature for this study[15,27], viz., Eudistomin-W, Debromoeudistomin-K, Eudistomidin-C, and Eudistomidin-B. Eudistomin-W offers a O-N bidentate structure, while the latter three eudistomins offer a N-N bidentate structure. Debromoeudistomin-K has at least one stereoisomer, while there are no mentioned stereoisomers for the other compounds.[137] Regardless of the isomerism, the structures of the compounds are carefully optimized to avoid any conflict with the structures obtained from the literature.

3.1.1 Eudistomins

Eudistomin-W is found in a group of undescribed colonial ascidians of the family Polycitoridae[138] (Figure 3.1)[139], which are native to Chuuk state of the Federated States of Micronesia. This compound was isolated, and its anti-bacterial and anti-fungal activity was studied in detail.[40] The molecular structure of the compound is given in Figure 3.2 and the computationally optimized geometry is shown in Figure 3.3 (geometry shown is of ADF PBE-D3 level in solvation phase).

Figure.3.1 *Eudistoma sp.* from Polycitoridae family[139] (Image from the reference provided. CC BY-SA 2.0)

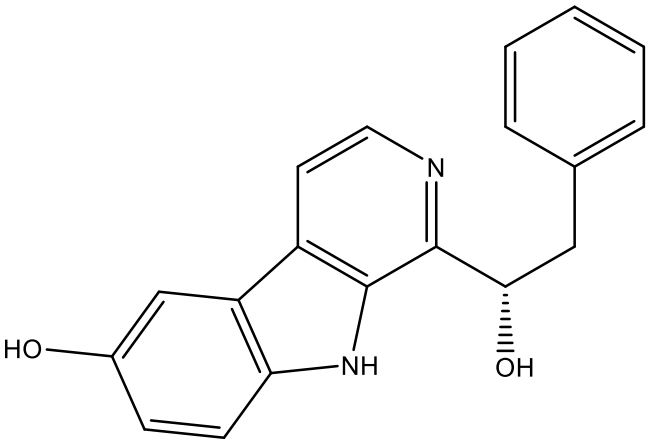

Figure 3.2 Molecular structure of Eudistomin-W

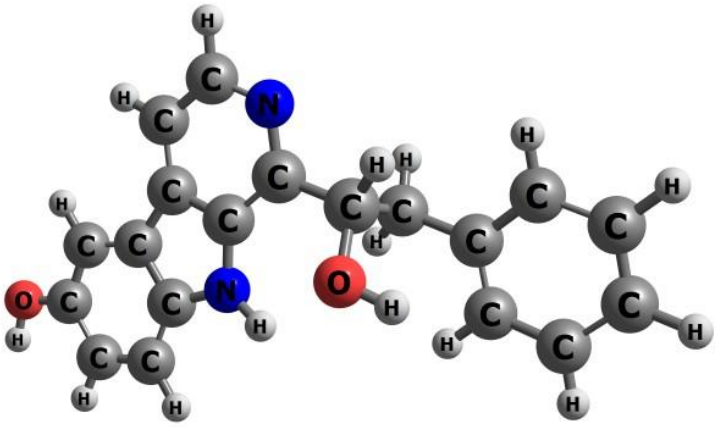

Figure 3.3 Optimized geometry of Eudistomin-W (ADF PBE-D3 solvation phase geometry)

Debromoeudistomin-K was first isolated and reported by Lake *et al*.[26] The presence of this eudistomin is found to be in the ascidian native to New Zealand, *Ritterella sigillinoides* (Figure 3.4). All eudistomins are proven to be tryptophan derivatives, and successful synthetic reports have emphasized the same, with debromoeudistomin-K as one of their target molecules.[140] Ring-closure reactions, i.e., Pictet-Spengler reactions, have shown successful results in synthesizing the eudistomins, including debromoeudistomin-K.[140] Debromoeudistomin-K has analogues, i.e., stereoisomers obtained from the respective synthetic works. However, the ascidians from New Zealand only have debromoeudistomin-K in their bio-systems amongst other eudistomins, not its analogues.[26] This makes debromoeudistomin-K a natural eudistomin, while its analogues are synthetic eudistomins. This was discussed in the literature, and is likely due to the stereoselectivity preference. The molecular structure of the debromoeudistomin-K is given in Figure 3.5, and the optimized geometry obtained from ADF PBE-D3 solvation phase calculation is given in Figure 3.6.

Figure 3.4 Ascidians of the genus *Ritterella* (© Gary McDonald, http://www.inaturalist.org/photos/1394648. CC BY-NC-SA 4.0)

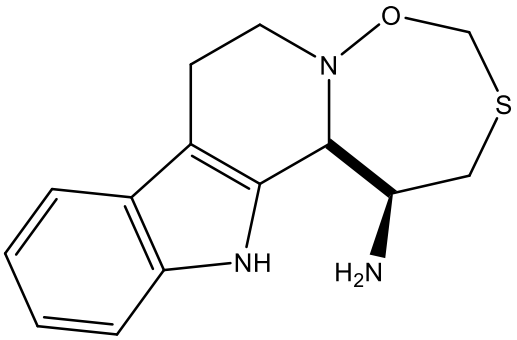

Figure 3.5 Molecular structure of Debromoeudistomin-K

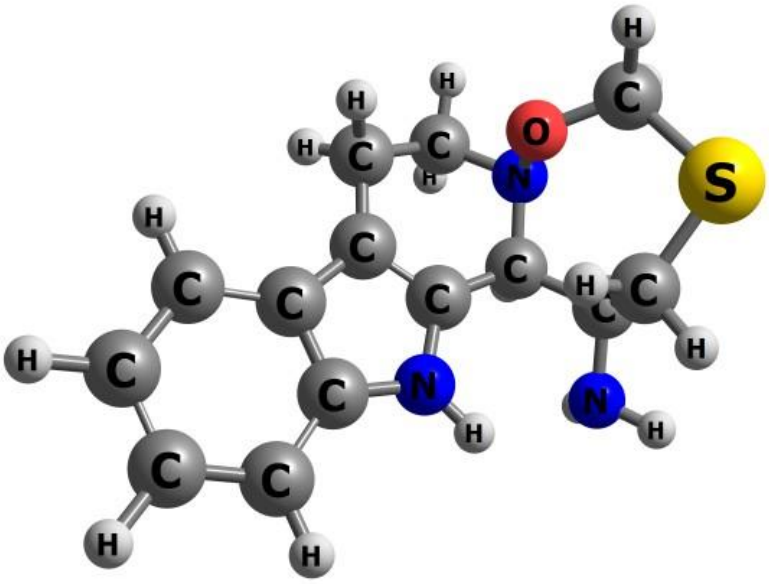

Figure 3.6 Optimized geometry of Debromoeudistomin-K (ADF PBE-D3 solvation phase geometry)

Eudistomidins B and C are identified to be in the biosystem of *Eudistoma glaucus* (Figure 3.7), native to Iejima, Okinawa Island of Japan.[45] This Japanese native is a colonial tunicate, and also plays host to several other eudistomins, including eudistomidin D, and eudistomins D, E, H, and I.[45] The molecular structures of Eudistomidins B and C are given in Figure 3.8 and the optimized geometries (ADF PBE-D3 solvation phase) are given in Figure 3.9.

Figure 3.7 *Eudistoma glaucus*[141] (image obtained from the reference given. Copyright details given in http://chigaku.ed.gifu-u.ac.jp/chigakuhp/html/index.html)

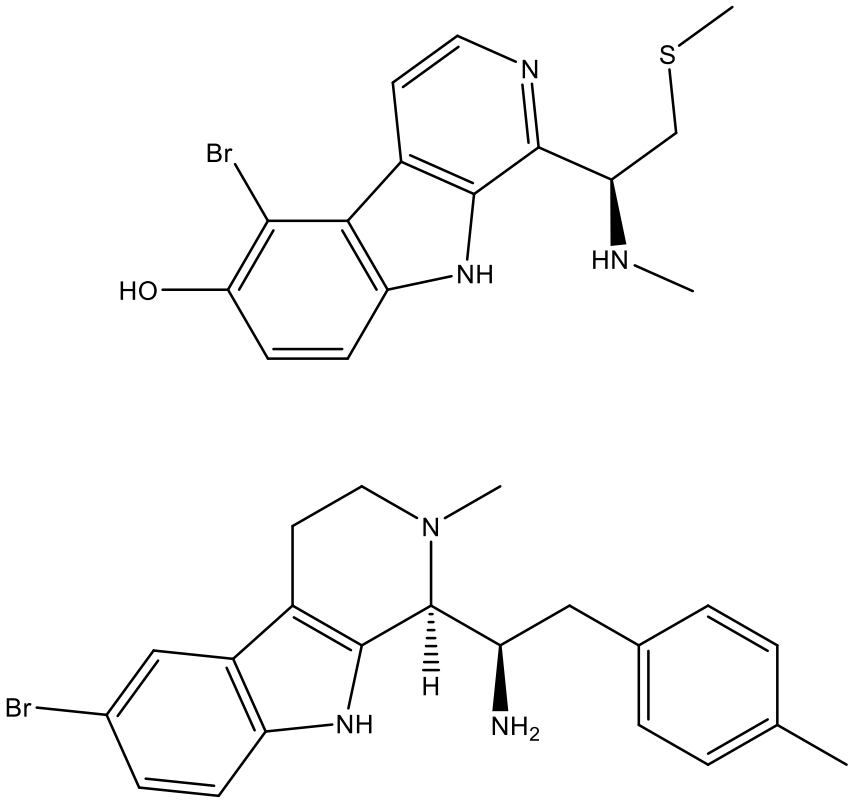

Figure 3.8 Molecular structures of Eudistomidin-C (top) and Eudistomidin-B (bottom)

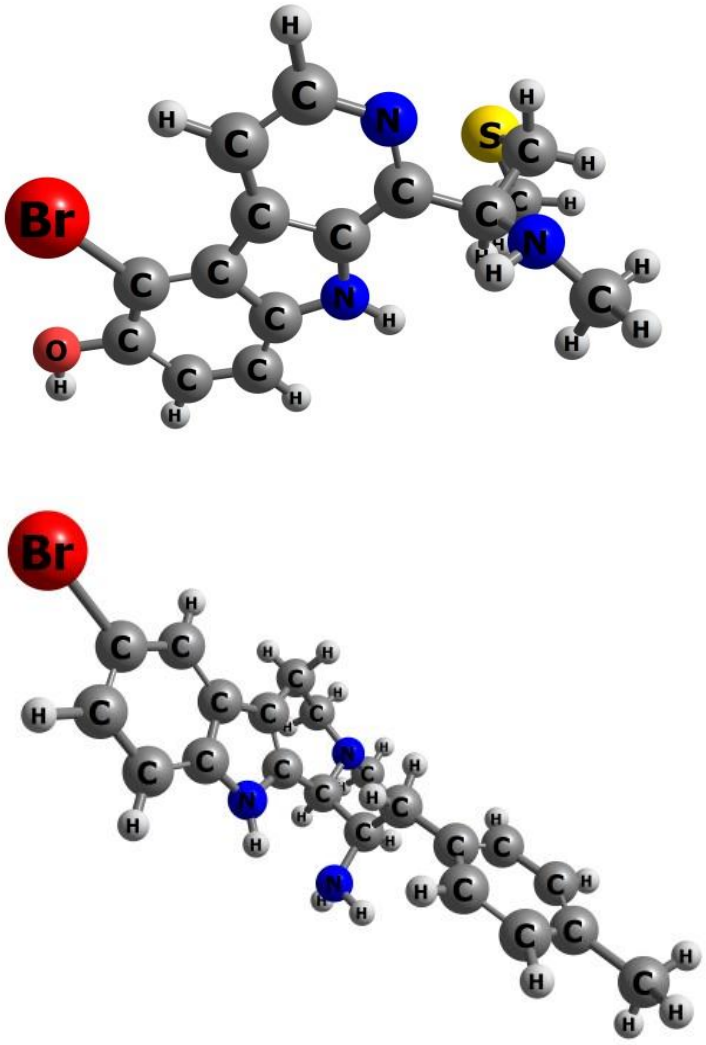

Figure 3.9 Optimized geometries of Eudistomidin-C (top) and Eudistomidin-B (bottom) (ADF PBE-D3 solvation phase geometry)

3.1.2 Metal Aqua Ions

Not one scientist or researcher can talk about ascidians' biochemistry without mentioning vanadium. The presence of vanadium in almost every (if not all) animal belonging to this family made researchers ponder the importance. Haemovanadin, a compound that is believed (in part) to contribute to the green-coloured blood of several species in this family has made scientists wonder if there is any possible oxygen-carrying activity associated with this vanadium-protein.[53] Studies have indicated that it is not the case.[53] A class of vanadium binding proteins known as vanabins are found to be present in ascidians.[142,143] The presence of V^{3+} and VO^{2+} and the related chemistry in ascidians has been studied by various researchers in the past.[144,145] However, no study was made to examine the complexation of vanadium with eudistomins.

In this work, due to the importance of vanadium in the biochemistry of ascidians, VO^{2+} (vanadyl ion) surrounded by four and five water molecules, is one of the subjects. The optimized geometries of the respective ions are given in the Figure 3.10. The six-coordinated vanadyl aqua ion has optimized to a distorted octahedral structure, and the five-coordinated vanadyl aqua ion has optimized to a distorted square pyramid structure. Figure 3.10 (a) and (b) show a five-coordinated vanadium and 3.10 (c) and (d) show a six-coordinated vanadium. The vanadyl ion is usually surrounded by five water molecules in its aqua ion. Tetrahydrate and hexahydrate aqua ions are also possible.[61] In most of the crystal structures, vanadyl ion occurs as a (vanadium-centred) distorted octahedral structure with four water molecules, and the sixth coordination to the ligand (mostly bound as monodentate ligands).[89,146] But di-anionic bidentate ligands can distort the structure to a (vanadium-centred) distorted square pyramidal structure or trigonal bipyramidal structure. For this reason, calculations are performed with vanadyl tetrahydrate ion and vanadyl pentahydrate ion. While there is a noticeable structural difference in the cations, the optimized geometries of the complexes show that in all of the cases, the structures of the complexes have not resulted in (vanadium-centred) distorted octahedral structures. This is discussed in detail in the further parts.

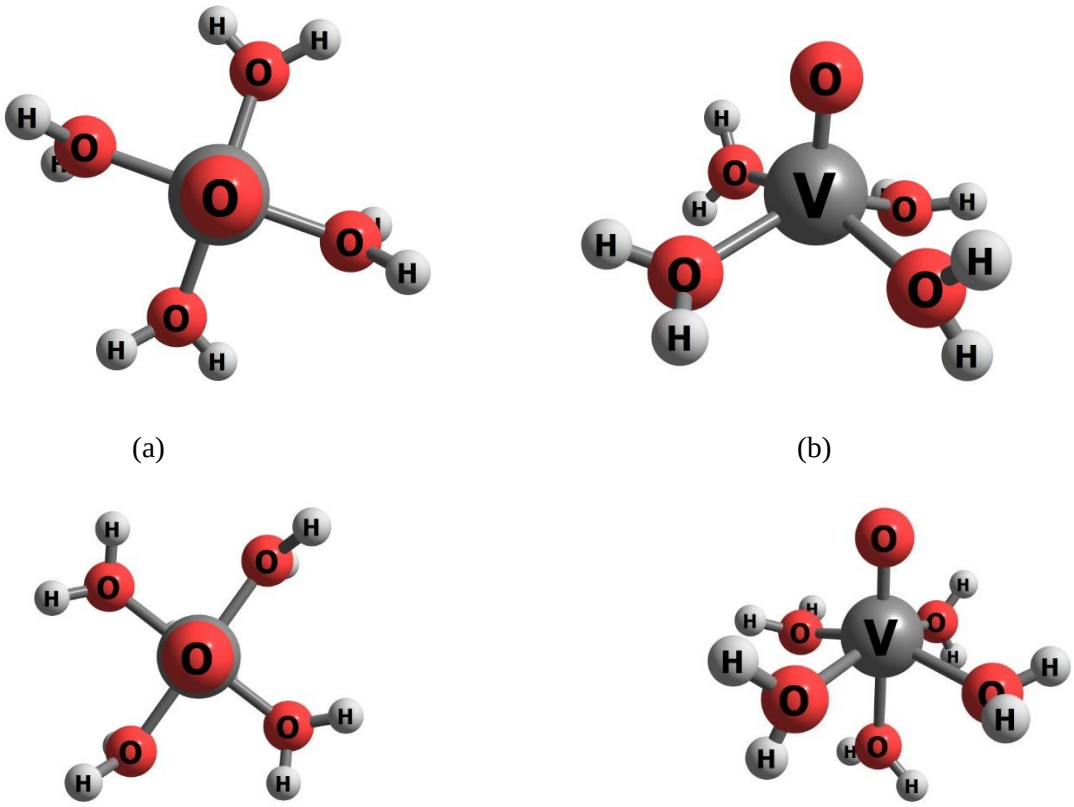

(a) (b)

(c) (d)

Figure 3.10 Optimized geometries of vanadyl aqua ion (ADF PBE-D3 solvation phase geometries)

(a) Top view of $[VO(H_2O)_4]^{2+}$ (b) Side view of $[VO(H_2O)_4]^{2+}$

(c) Top view of $[VO(H_2O)_5]^{2+}$ (d) Side view of $[VO(H_2O)_5]^{2+}$

The octahedral vanadyl ion geometry bond lengths, i.e., the V=O bond lengths from the results obtained (from the calculations performed at the forementioned different levels of theory) are compared to the experimental values. In experimental conditions, the task of obtaining a bond length from a cation is difficult, and therefore the bond lengths obtained are usually of a complex. The V=O bond lengths of the vanadyl (octahedral) aqua ion from the experimental results are around 1.58Å[147,148], and our results are in agreement with the same (shown in Table 3.1). In the work of Krakowiak *et al*, V=O bond length in oxovanadium perchlorate is 1.588Å, and the V=O bond length in pentakis (dmso) oxovanadium is 1.575Å.[148] The V=O bond length from the work of Magnussen *et al*, is 1.577Å, which is of pentaaquaoxovanadium (IV) bis

(trifluoromethanesulfonate).[147] These are crystal data. The data of V=O bond lengths obtained from the work shown in Table 3.1 are of solvation phase geometries. Comparing the results from the different levels of theory, we notice that the hybrid functional (B3LYP) yields a shorter bond length in comparison to the GGA functionals. Also, despite the usage of different sets of BLYP calculations, i.e., using ADF with STO basis functions and ORCA with GTO basis functions, we obtain identical results. These observations conform fully to the expectations from the literature.

Table 3.1 Comparison of V=O bond lengths (Å)

Source	V=O Bond Length
Oxovanadium perchlorate [reference[148]]	1.588
Pentakis (dmso) oxovanadium [reference[148]]	1.575
Pentaaquaoxovanadium (IV) bis (trifluoromethanesulfonate) [reference[147]]	1.577
ADF PBE-D3	1.577
ADF BLYP	1.589
ORCA BLYP	1.590
ORCA B3LYP	1.566

Uranium[149] is probably the 'super-star' in actinide elements due to its wide importance and applications. At least half of the actinide research work is based on uranium, simply because it is abundant, has a 4.5-billion-year half-life, and perfectly satiates the requirements for various actinide based physical and chemical experiments. Given the same reasons, uranium is therefore the 'top-actinide' for various civilian and military applications. Henceforth, it is not an exaggeration or extrapolation to state that it is 'the superstar' of actinide elements.

Uranium has been observed to have bio-chemical interactions. Various species from bacteria like *Geobacter* spp., *Shewanella* spp., species from the genus *Anaeromyxobacter* etc., are all known to reduce uranium using their respective biomechanisms.[150–156] Uranium, restating the lines from previous chapters, is found to be present in the biosystem of ascidians in noticeable quantities.[24] For this reason, UO_2^{2+} (uranyl ion) with five water molecules in the equatorial plane was our choice for the calculations. The optimized structure is given in Figure 3.11. The cation has five water molecules surrounding the O=U=O equatorially. The O=U=O angle is 178.29°, and the U=O bond lengths are 1.766 Å.

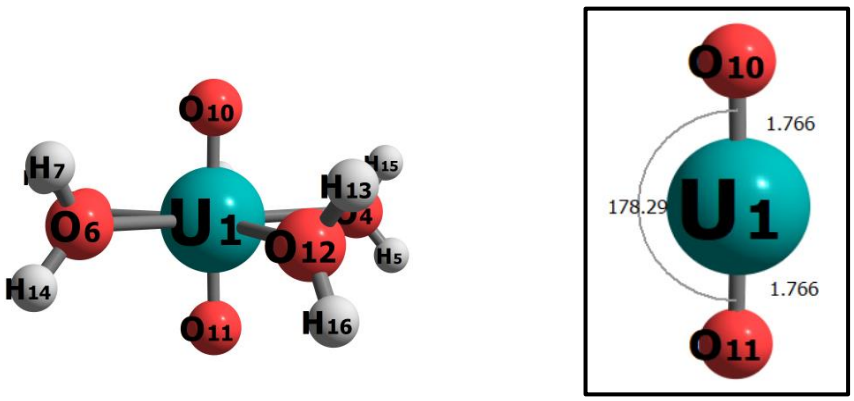

Figure 3.11 Optimized geometry of $[UO_2(H_2O)_5]^{2+}$ (ADF PBE-D3 solvation phase geometries)

The insert shows the uranyl part of the uranyl aqua ion (Bond lengths in Å and bond angle in degrees)

The uranyl bond lengths obtained from the computational calculations (at forementioned levels of theory) are compared with the experimental results given in the literature.[157,158] The uranyl bond lengths, i.e., O=U=O bond lengths are symmetrical and were measured using EXAFS in 0.1 HCl in the work of Vallet *et al*, and is 1.77 Å. In the work of Wahlgren *et al*, the bond lengths are measured using EXAFS in 0.1M of $HCLO_4$, and is 1.78 Å. The results from this work in good agreement with the experimental results. When comparing the bond lengths, we note very similar trends to the ones discussed above for the vanadyl aqua ion. The data is given in the Table 3.2.

Table 3.2 Comparison of U=O bond lengths (Å)

Source	**U=O Bond Length**
UO_2^{2+} in 0.1M $HClO_4$ [reference[158]]	1.78
UO_2^{2+} in 0.1M HCl [reference[157]]	1.77
ADF PBE-D3	1.766
ADF BLYP	1.795
ORCA BLYP	1.791
ORCA B3LYP	1.755

Thorium[149] is the only other naturally occurring actinide other than uranium, and is the most abundant actinide on earth. Thorium based nuclear power applications is an ongoing topic.[159] While there are advantages with thorium, such as abundance, better neutron absorption, etc., there are disadvantages as well, mainly the gamma emitting daughter products and low

efficiency. Currently, significant research is in progress to make thorium a useful resource for nuclear power programmes.[160]

Thorium, in its natural state, can occur as a Th^{4+} ion with nine water molecules[64] in the coordination sphere. The optimized of geometry of Th^{4+} ion is given in Figure 3.12. While there is not a lot of research and/or evidence with respect to Thorium's involvement in bio-chemical aspects of living organisms, there is at least one study which points to the binding of thorium with bio-polymers.[161] A class of microalgae called Bacillariophyceae, also known as Diatoms, are known to produce around 20% to 50% of the total oxygen produced on the planet each year.[162] A species in that class, *Phaeodactylum tricornutum*[163], is found to scavenge for radionuclides which includes thorium and protactinium among others.[161] Given the abundance of thorium, it is logical to suspect the possibility of a eudistomin-thorium interaction. There is one study, on *Ciona intestinalis*, in which the researchers have suggested that the injection of thorium compounds would make the animal treat them as foreign particles, activating the action of lymphocytes.[164] Regardless, the study has resulted in the death of the animal. While this can mean that thorium may not be a preferred element by *Ciona intestinalis*, it wouldn't rule out the possibility of the interactions between eudistomins and thorium from a purely chemistry point of view.

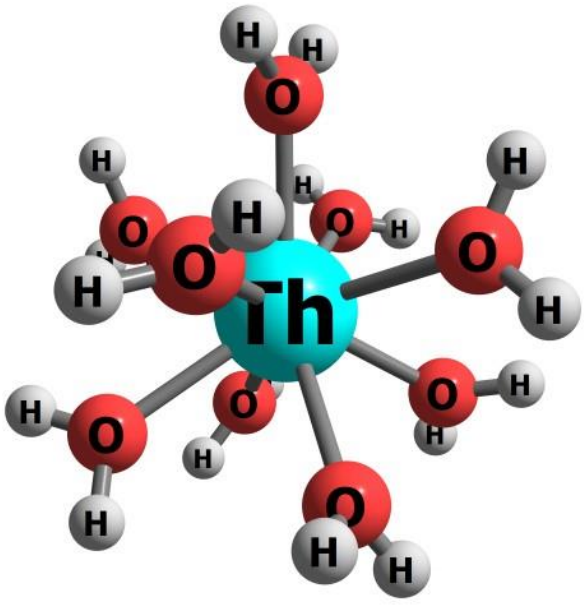

Figure 3.12 Optimized structure of Th^{4+} ion with nine water molecule coordination (ADF PBE-D3 solvation geometry is shown here)

In the subsequent sections, the metal complexes with Eudistomin-W (L1) are given as M1, with Debromoeudistomin-K (L2) are given as M2, with Eudistomidin-C (L3) are given as M3, and with Eudistomidin-B are given as M4; where M=V/U/T.

3.2. Vanadyl-Eudistomin Complexes

Vanadyl-eudistomin complexes were optimized in gas phase and solvation phase with water as solvent using the forementioned software packages (ADF and ORCA) with the level of theory mentioned earlier. The gas phase geometries have served as the input geometries for the solvation phase geometries. The four complexes, when calculated with different forementioned levels of theory, have resulted in identical geometries with insignificant variations in the respective cases.

NOTE: Vanadyl complexes with L(n) are denoted as V(n) for complexes with two water molecules and as V(n)* for complexes with three water molecules. [n=1,2,3,4]

None of the *-complexes (complexes with three water molecules) exhibit a vanadium centric distorted octahedral structure, despite the input geometries being vanadium centric distorted octahedral structures. The ‘extra’ water molecule has moved away from the vanadium atom to the second coordination sphere during the geometry optimization, and is held by the neighbouring water molecules via hydrogen bonds (the differences can be noticed in Figures 3.14 and Figure 3.15). This confirms that the preferred coordination for vanadium is five (including the oxygen atom on the apex of the square pyramid). This phenomenon was also observed in the vanadyl sulphate molecules (Figure 3.13) [ADF PBE-D3 solvation phase geometries are shown here].

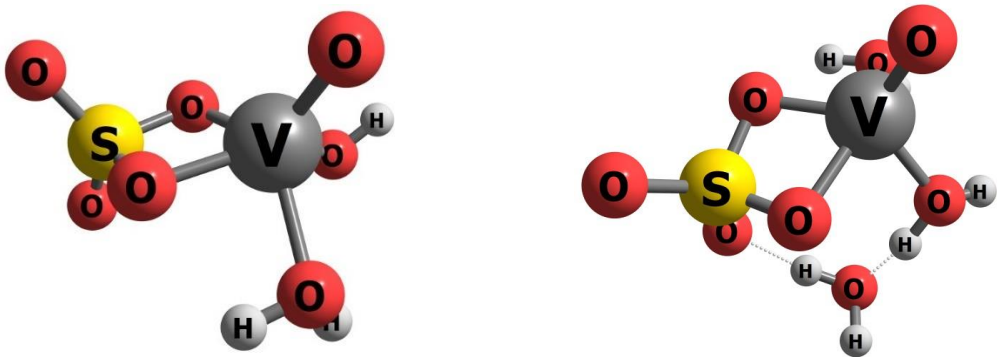

(a) (b)

Figure 3.13 Optimized geometries of vanadyl sulphate (ADF PBE-D3 solvation phase)

a. Optimized geometry of $[VOSO_4.(H_2O)_2]$ b. Optimized geometry of $[VOSO_4.(H_2O)_2.(H_2O)]$

The vanadyl complexes with two water molecules (vanadium-centric distorted square pyramid input geometry) are given in Figure 3.14, and the vanadyl complexes with three water molecules (vanadium-centric distorted octahedral input geometry) are given in Figure 3.15. [ADF PBE-D3 solvation phase geometries are shown here].

Examining the optimized geometries, all of the complexes exhibit similar metal-nitrogen bond lengths in most cases, meaning most eudistomins might exhibit similar bonding behaviour. The metal-nitrogen bond lengths with respect to the five-membered ring's nitrogen are close to 2.0Å. The bond lengths showing the metal's binding with the ligands are shown in Figure 3.14 and Figure 3.15, and are also given in the Tables 3.3 and 3.4. The bond lengths obtained from the V(n) complexes and V(n)* complexes are comparable to each other and are in agreement with each other. To examine the influence of the equatorial bonding, we have also compared the V=O bond lengths of the V(n)* metal-eudistomin complexes with the V=O bond length in the vanadyl cation and the experimental values (only ADF PBE-D3 solvation phase geometries are compared) in Table 3.5. The V=O bond lengths in the complexes are around 1.62Å, significantly elongated from the naked vanadyl ion and the vanadyl sulphate, signifying the strengthening of equatorial binding.

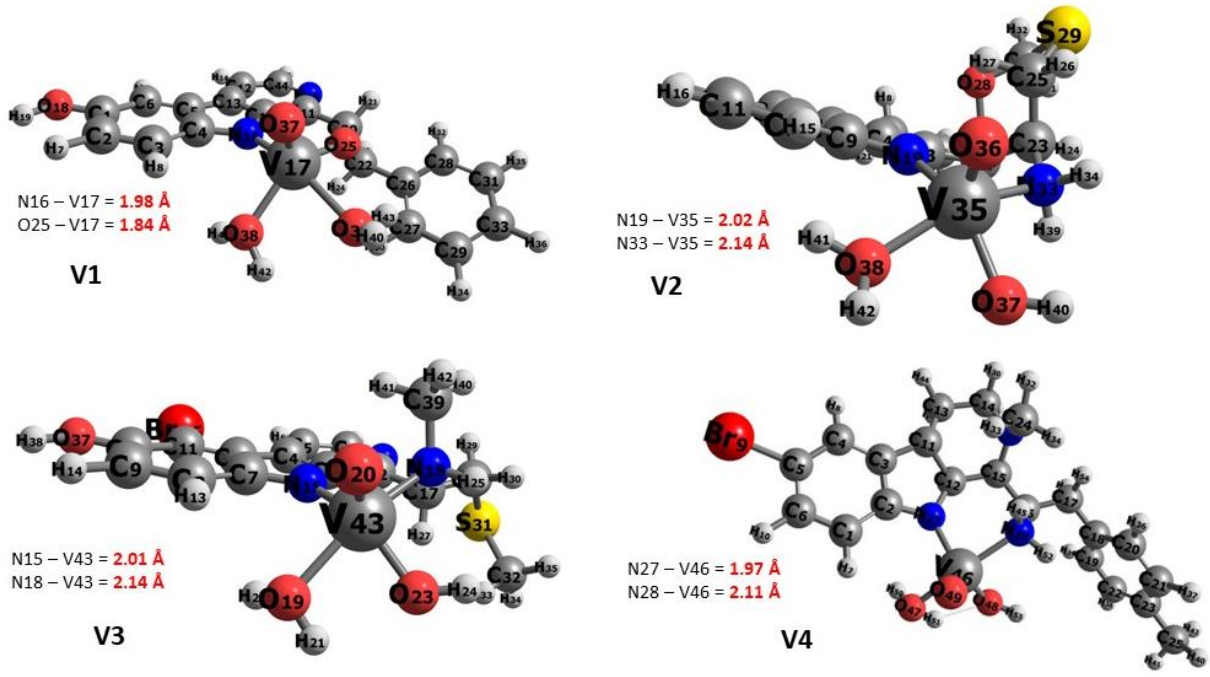

Figure 3.14 Optimized geometries of $[VO(H_2O)_2]$ eudistomin ligand complexes

Table 3.3 Bond lengths between the metal-eudistomin binding atoms in V(n) complexes

Complex	Binding atoms	Bond length (Å)
V1	N16-V17	1.980
	O25-V17	1.836
V2	N19-V35	2.025
	N33-V35	2.139
V3	N15-V43	2.016
	N18-V43	2.136
V4	N27-V48	1.966
	N28-V48	2.113

(coloured cells are of the five-membered ring's nitrogen and metal bond lengths)

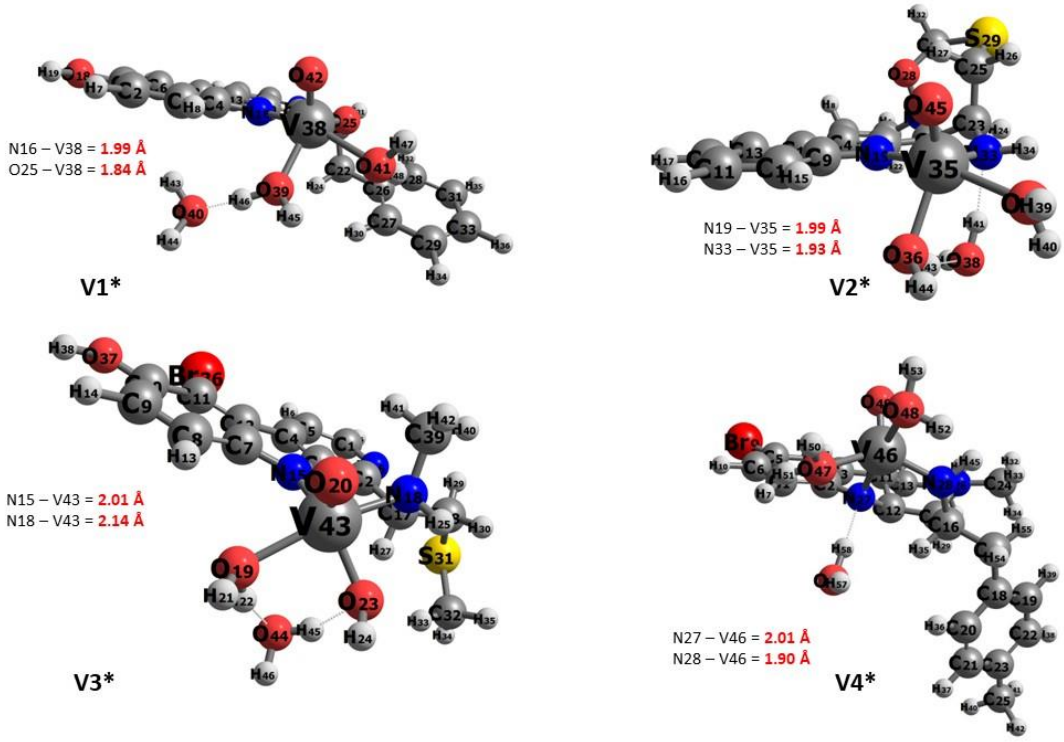

Figure 3.15 Optimized geometries of $[VO(H_2O)_2(H_2O)]$ eudistomin ligand complexes

Table 3.4 Bond lengths between the metal-eudistomin binding atoms in V(n)* complexes

Complex	Binding atoms	Bond length (Å)
V1*	N16-V38	1.993
	O25-V38	1.845
V2*	N19-V35	1.986
	N33-V35	1.929
V3*	N15-V43	2.010
	N18-V43	2.136
V4*	N27-V48	2.014
	N28-V48	1.898

(coloured cells are of the five-membered ring's nitrogen and metal bond lengths)

Table 3.5 Comparison of V=O bond lengths in V(n)* complexes (Å)

Source	V=O Bond Length
Oxovanadium perchlorate [reference[148]]	1.588
Pentakis (dmso) oxovanadium [reference[148]]	1.575
Pentaaquaoxovanadium (IV) bis (trifluoromethanesulfonate) [reference[147]]	1.577
VO^{2+}	1.577
$VOSO_4$	1.596
V1*	1.620
V2*	1.620
V3*	1.606
V4*	1.625

As detailed in the Chapter 1 (section 1.5), with the vanadyl complexes with two water molecules, i.e., V(n) complexes, the following equations were considered as model reactions.

1. $L^{2-} + [VO(H_2O)_4]^{2+} \Leftrightarrow [VO.L\ (H_2O)_2] + 2H_2O$
2. $H_2L + [VO(H_2O)_4]^{2+} \Leftrightarrow [VO.L\ (H_2O)_2] + 2H_3O^+$
3. $H_2L + [VOSO_4.\ (H_2O)_2] \Leftrightarrow [VO.L\ (H_2O)_2] + H_2SO_4$
4. $VOSO_4\ (H_2O)_2 + L^{2-} \Leftrightarrow VOL\ (H_2O)_2 + SO_4^{2-}$
5. $H_2SO_4 + VOSO_4\ (H_2O)_2 + L^{2-} \Leftrightarrow VOL\ (H_2O)_2 + 2HSO_4^-$

*where H_2L is the neutral ligand

The model reactions have been tested in gas phase and in solvation phase using (overall) four different input settings (i.e., solvation model, DFT functional, GTO in ORCA vs STO in ADF, etc.). Despite the differences in the methodologies, the formation energy values, i.e., ΔG values have shown similar results with respect to the different model reactions. These results are shown in Table 3.6 through Table 3.10. The gas phase ΔG and the solvation phase (water) ΔG are given.

Table 3.6 ΔG values of model reaction 1 [for Vanadyl complexes with L(n)] (kcal/mol)

L	PBE-D3 (ADF)	BLYP (ADF)	BLYP (ORCA)	B3LYP (ORCA)	PBE-D3 (ADF)	BLYP (ADF)	BLYP (ORCA)	B3LYP (ORCA)
L1	-437.11	-432.72	-429.96	-432.22	-83.39	-81.13	-80.51	-80.13
L2	-474.45	-468.05	-466.04	-468.55	-113.32	-111.51	-109.44	-109.87
L3	-456.44	-448.22	-446.21	-449.85	-107.74	-103.04	-100.90	-101.91
L4	-461.34	-454.37	-450.98	-454.37	-121.17	-116.90	-113.14	-116.53

(Orange columns are of gas phase and the blue columns are of solvation phase)

Table 3.7 ΔG values of model reaction 2 [for Vanadyl complexes with L(n)] (kcal/mol)

L	PBE-D3 (ADF)	BLYP (ADF)	BLYP (ORCA)	B3LYP (ORCA)	PBE-D3 (ADF)	BLYP (ADF)	BLYP (ORCA)	B3LYP (ORCA)
L1	4.70	11.23	11.30	16.69	31.44	47.94	49.51	38.84
L2	-1.44	5.71	6.15	10.98	27.11	66.33	68.02	35.83
L3	-9.35	0.00	0.69	4.83	22.59	61.12	62.87	33.25
L4	6.90	15.56	15.94	21.46	38.53	71.60	73.54	45.61

(Orange columns are of gas phase and the blue columns are of solvation phase)

Table 3.8 ΔG values of model reaction 3 [for Vanadyl complexes with L(n)] (kcal/mol)

L	PBE-D3 (ADF)	BLYP (ADF)	BLYP (ORCA)	B3LYP (ORCA)	PBE-D3 (ADF)	BLYP (ADF)	BLYP (ORCA)	B3LYP (ORCA)
L1	8.22	10.10	4.52	12.80	20.08	24.66	9.73	25.03
L2	2.07	4.58	-0.63	7.09	15.75	20.46	7.03	22.02
L3	-5.83	-1.13	-6.08	0.94	11.23	19.45	4.64	19.45
L4	10.42	14.43	9.16	17.57	27.17	29.74	17.38	31.81

(Orange columns are of gas phase and the blue columns are of solvation phase)

Table 3.9 ΔG values of model reaction 4 [for Vandyl complexes with L(n)] (kcal/mol)

L	PBE-D3 (ADF)	BLYP (ADF)	BLYP (ORCA)	B3LYP (ORCA)	PBE-D3 (ADF)	BLYP (ADF)	BLYP (ORCA)	B3LYP (ORCA)
L1	3.64	4.33	1.63	3.76	-50.58	-46.94	-57.60	-47.12
L2	-33.70	-31.00	-34.45	-32.57	-80.51	-77.31	-86.22	-76.87
L3	-15.69	-11.17	-14.62	-13.86	-74.92	-68.84	-78.00	-68.90
L4	-20.58	-17.32	-19.39	-18.38	-88.35	-82.70	-90.23	-83.52

(Orange columns are of gas phase and the blue columns are of solvation phase)

Table 3.10 ΔG values of model reaction 5 [for Vanadyl complexes with L(n)] (kcal/mol)

L	PBE-D3 (ADF)	BLYP (ADF)	BLYP (ORCA)	B3LYP (ORCA)	PBE-D3 (ADF)	BLYP (ADF)	BLYP (ORCA)	B3LYP (ORCA)
L1	-138.68	-137.30	-145.33	-138.55	-71.53	-67.14	-81.01	-69.71
L2	-176.01	-172.63	-181.41	-174.88	-101.47	-97.51	-109.94	-99.46
L3	-158.00	-152.80	-161.58	-156.18	-95.88	-89.04	-101.40	-91.49
L4	-162.90	-158.95	-166.35	-160.70	-109.31	-102.91	-113.64	-106.11

(Orange columns are of gas phase and the blue columns are of solvation phase)

With the vanadyl complexes with three water molecules, i.e., V(n)* complexes, the following equations were considered as model reactions.

1. $L^{2-} + [VO(H_2O)_5]^{2+} \Leftrightarrow [VO.L\ (H_2O)_3] + 2H_2O$
2. $H_2L + [VO(H_2O)_5]^{2+} \Leftrightarrow [VO.L\ (H_2O)_3] + 2H_3O^+$
3. $H_2L + [VOSO_4.\ (H_2O)_3] \Leftrightarrow [VO.L\ (H_2O)_3] + H_2SO_4$
4. $VOSO_4\ (H_2O)_3 + L^{2-} \Leftrightarrow VOL\ (H_2O)_3 + SO_4^{2-}$
5. $H_2SO_4 + VOSO_4\ (H_2O)_3 + L^{2-} \Leftrightarrow VOL\ (H_2O)_3 + 2HSO_4^-$

*where H_2L is the neutral ligand

The model reactions have been tested in gas phase and in solvation phase using the forementioned levels of theory. The ΔG values obtained from the model reactions are shown in table 3.11 through table 3.15. The formation energy values, i.e., ΔG values are comparable to the V(n) complexes, although there are noticeable differences because of the extra water molecule. For instance, the ΔG values of the model reaction 1 for L1 with ADF PBE-D3 method of the vanadyl complex is -437.11 kcal/mol and for vanadyl* complex is -459.02 kcal/mol. The difference is ~22 kcal/mol, which is due to the 'third' water molecule. Given

that the 'third' water molecule has moved away from the vanadium atom in the optimized geometries, we are inclined to believe that vanadyl complexes may serve as better models in comparison to the vanadyl* complexes.

Table 3.11 ΔG values of model reaction 1 [for Vanadyl *-complexes with L(n)] (kcal/mol)

L	PBE-D3 (ADF)	BLYP (ADF)	BLYP (ORCA)	B3LYP (ORCA)	PBE-D3 (ADF)	BLYP (ADF)	BLYP (ORCA)	B3LYP (ORCA)
L1	-459.02	-414.21	-409.19	-416.47	-99.21	-79.44	-75.24	-73.92
L2	-443.83	-431.28	-425.69	-431.28	-89.36	-92.49	-88.29	-86.67
L3	-467.11	-430.34	-429.02	-430.34	-130.64	-102.09	-93.69	-96.70
L4	-457.51	-409.88	-431.28	-435.73	-110.44	-86.85	-109.81	-109.94

(Orange columns are of gas phase and the blue columns are of solvation phase)

Table 3.12 ΔG values of model reaction 2 [for Vanadyl *-complexes with L(n)] (kcal/mol)

L	PBE-D3 (ADF)	BLYP (ADF)	BLYP (ORCA)	B3LYP (ORCA)	PBE-D3 (ADF)	BLYP (ADF)	BLYP (ORCA)	B3LYP (ORCA)
L1	21.84	29.74	32.06	32.44	41.22	37.46	40.72	45.05
L2	-3.01	42.48	46.50	48.25	25.48	50.58	53.90	56.03
L3	11.29	17.88	17.88	24.35	29.05	31.50	37.59	38.46
L4	3.07	60.05	35.64	40.10	19.89	70.91	46.44	52.21

(Orange columns are of gas phase and the blue columns are of solvation phase)

Table 3.13 ΔG values of model reaction 3 [for Vanadyl *-complexes with L(n)] (kcal/mol)

L	PBE-D3 (ADF)	BLYP (ADF)	BLYP (ORCA)	B3LYP (ORCA)	PBE-D3 (ADF)	BLYP (ADF)	BLYP (ORCA)	B3LYP (ORCA)
L1	30.87	15.06	17.95	12.99	34.45	16.63	16.00	19.83
L2	14.87	27.8	32.38	28.80	18.70	29.74	29.18	30.81
L3	18.01	3.20	3.77	4.89	22.28	10.67	12.86	13.24
L4	6.46	45.37	21.52	20.64	13.11	50.07	21.71	26.98

(Orange columns are of gas phase and the blue columns are of solvation phase)

Table 3.14 ΔG values of model reaction 4 [for Vanadyl *-complexes with L(n)] (kcal/mol)

L	PBE-D3 (ADF)	BLYP (ADF)	BLYP (ORCA)	B3LYP (ORCA)	PBE-D3 (ADF)	BLYP (ADF)	BLYP (ORCA)	B3LYP (ORCA)
L1	12.17	9.29	15.06	3.95	-53.46	-54.97	-51.33	-52.33
L2	-3.01	-7.79	-1.44	-10.85	-63.31	-68.02	-64.38	-68.08
L3	-1.51	-6.84	-4.77	-9.91	-74.55	-77.62	-69.78	-75.11
L4	-12.30	13.62	-7.03	-15.31	-63.88	-62.37	-85.90	-88.35

(Orange columns are of gas phase and the blue columns are of solvation phase)

Table 3.15 ΔG values of model reaction 5 [for Vanadyl *-complexes with L(n)] (kcal/mol)

L	PBE-D3 (ADF)	BLYP (ADF)	BLYP (ORCA)	B3LYP (ORCA)	PBE-D3 (ADF)	BLYP (ADF)	BLYP (ORCA)	B3LYP (ORCA)
L1	-130.14	-132.34	-131.9	-138.36	-74.42	-75.17	-74.73	-74.92
L2	-145.33	-149.41	-148.40	-153.17	-84.27	-88.23	-87.79	-90.67
L3	-143.82	-148.47	-151.73	-152.23	-95.51	-97.83	-93.18	-97.70
L4	-154.55	-128.01	-154.00	-157.63	-84.84	-82.58	-109.31	-110.94

(Orange columns are of gas phase and the blue columns are of solvation phase)

From the formation energy values, for vanadyl complexes in solvation phase, model 1, 4, and 5 show positive interactions, i.e., negative ΔG. As model 4 and 5 are designed to resemble what might be the realistic scenario, and given the similarity of the values despite different levels of theory, i.e., the basis sets, solvation model, etc., this would suggest the vanadium binding with eudistomins. Both two-water complexes and three-water complexes exhibit similar results, the differences in the numbers being due to the one extra-water molecule. We are inclined to think that the two-water complexes may be the better model, as the third water molecule in the three-water complexes was observed to settle in the second solvation sphere, leading to a potentially unbalanced description of the solvation of these complexes.

3.3. Uranyl-Eudistomin Complexes

Uranyl-eudistomin complexes were optimized using the forementioned software packages (ADF and ORCA) with the levels of theory mentioned earlier, in gas phase and solvation phase with water as solvent. In all of the cases the gas phase geometries have served as the input geometries for the solvation phase geometries. The complexes have resulted in similar

geometries, i.e., the geometrical parameters had insignificant differences in the respective cases.

From the optimized geometries, we can confirm that the binding is very much similar in all of the cases as the nitrogen-uranium bond distances are very similar (shown in Figure 3.17). The bond lengths between the binding atoms, i.e., the atoms of ligand and uranium, are also given in Table 3.16 (ADF PBE-D3 solvation phase geometries). Additionally, we were interested to see the geometrical changes in the uranyl part of the complex. In actinide chemistry, a significant uranyl angle bending, i.e., a very large deviation of the O=U=O bond angle from 180° means that the equatorial binding might be influencing the reactivity on the oxygen atoms. Our complexes, however, do not deviate much from the 180°, and are closer to the deviation that was observed in the uranyl sulphate molecule which is at 173.10° (shown in Figure 3.16). The deviation of the O=U=O angles in the U(n) complexes is compared with the UO_2^{2+} cation and is tabulated in Table 3.17. Also, the bond lengths of O=U=O bonds are compared in the same Table 3.17. As expected, we see slightly longer uranyl bond lengths in the eudistomin complexes compared to the naked uranyl or the sulphate complex. Moreover, the uranyl bond lengths are very similar for the four eudistomin complexes. In the O-N bidentate ligand complex of uranyl aqua ion, i.e., complex U1, there is no effect on the five-ligand coordination in the equatorial plane of the uranium atom. However, the N-N bidentate ligands, i.e., U2, U3, and U4, in the equatorial plane, one of the water molecules is not directly coordinated to the uranium atom, but is bound with the complex via hydrogen bonding. The uranium atom exhibits six coordination sites, with a distorted octahedral geometry. This could be due to repulsions between the lone pairs and/or proton attractions, of (from) the neighbouring atoms, and/or due to steric effects.

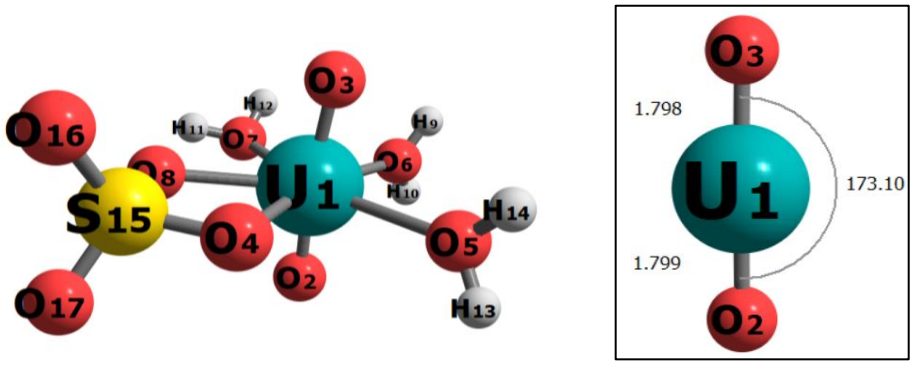

Figure 3.16 Optimized geometry of uranyl sulphate [ADF PBE-D3 solvation phase geometry] The insert shows the uranyl part of the uranyl sulphate (angle in degrees, bond lengths in Å)

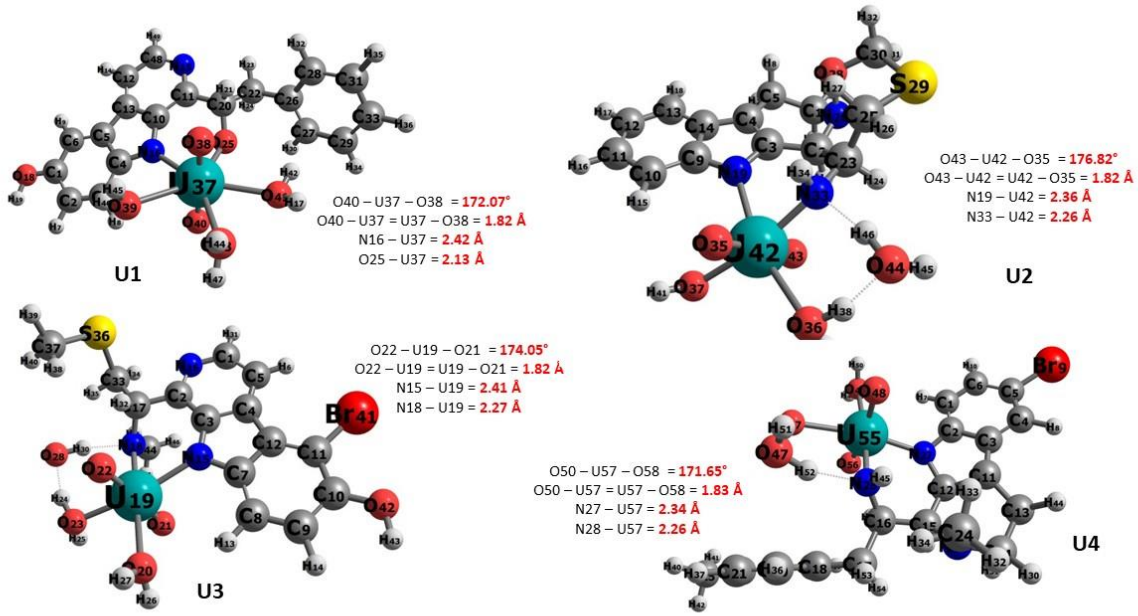

Figure 3.17 Optimized geometries of uranyl eudistomin ligand aqua complexes [ADF PBE-D3 solvation phase geometries]

Table 3.16 Bond lengths between the metal-eudistomin binding atoms in U(n) complexes

Complex	Binding atoms	Bond length (Å)
U1	N16-U37	2.426
	O25-U37	2.130
U2	N19-U42	2.363
	N33-U42	2.260
U3	N15-U19	2.411
	N18-U19	2.269
U4	N27-U57	2.338
	N28-U57	2.257

(coloured cells are of the five-membered ring's nitrogen and metal bond lengths)

Table 3.17 Comparison of U=O bond lengths and angles in U(n) complexes

Source	O=U=O angle (degrees)	U=O Bond Length (Å)
UO_2^{2+} in 0.1M $HClO_4$ [reference[158]]	-	1.78
UO_2^{2+} in 0.1M HCl [reference[157]]	-	1.77
UO_2^{2+}	178.29	1.766
UO_2SO_4	173.10	1.798
U1	172.07	1.823
U2	176.82	1.821
U3	174.05	1.819
U4	171.65	1.830

The following model reactions are considered for our calculations with respect to uranyl complexes.

1. $L^{2-} + [UO_2\ 5H_2O]^{2+} \Leftrightarrow [UO_2.L.\ 3H_2O] + 2H_2O$
2. $H_2L + [UO_2\ 5H_2O]^{2+} \Leftrightarrow [UO_2.L.\ 3H_2O] + 2H_3O^+$
3. $H_2L + [UO_2SO_4.\ 3H_2O] \Leftrightarrow [UO_2.L.\ 3H_2O] + H_2SO_4$
4. $UO_2SO_4\ (H_2O)_3 + L^{2-} \Leftrightarrow UO_2L\ (H_2O)_3 + SO_4^{2-}$
5. $H_2SO_4 + UO_2SO_4(H2O)_3 + L^{2-} \Leftrightarrow UO_2L(H2O)_3 + 2HSO_4^-$

*where H_2L is the neutral ligand

Using the forementioned levels of theory, we have calculated the formation energies of the model reactions, and as in the case of vanadyl complexes, the formation energy values have resulted in similar numbers with respect to the respective model reactions. These results are shown in Table 3.18 through Table 3.22.

Table 3.18 ΔG values of model reaction 1 [for Uranyl complexes with L(n)] (kcal/mol)

L	PBE-D3 (ADF)	BLYP (ADF)	BLYP (ORCA)	B3LYP (ORCA)	PBE-D3 (ADF)	BLYP (ADF)	BLYP (ORCA)	B3LYP (ORCA)
L1	-401.03	-393.69	-389.93	-388.36	-73.35	-68.96	-66.45	-61.49
L2	-410.19	-402.16	-399.72	-397.65	-82.39	-76.74	-74.17	-69.59
L3	-396.01	-384.34	-381.39	-379.32	-78.31	-72.47	-68.4	-63.06
L4	-402.54	-393.44	-389.68	-386.73	-89.35	-86.15	-82.70	-77.12

(Orange columns are of gas phase and the blue columns are of solvation phase)

Table 3.19 ΔG values of model reaction 2 [for Uranyl complexes with L(n)] (kcal/mol)

L	PBE-D3 (ADF)	BLYP (ADF)	BLYP (ORCA)	B3LYP (ORCA)	PBE-D3 (ADF)	BLYP (ADF)	BLYP (ORCA)	B3LYP (ORCA)
L1	40.79	50.26	51.33	60.55	41.48	47.94	49.51	57.48
L2	62.81	71.6	72.48	81.89	58.04	66.33	68.02	76.11
L3	51.08	63.88	65.51	75.36	52.02	61.12	62.87	72.1
L4	69.53	76.49	77.24	89.1	70.34	71.6	73.54	85.03

(Orange columns are of gas phase and the blue columns are of solvation phase)

Table 3.20 ΔG values of model reaction 3 [for Uranyl complexes with L(n)] (kcal/mol)

L	PBE-D3 (ADF)	BLYP (ADF)	BLYP (ORCA)	B3LYP (ORCA)	PBE-D3 (ADF)	BLYP (ADF)	BLYP (ORCA)	B3LYP (ORCA)
L1	8.66	15.75	15.94	14.74	24.28	32.57	31.37	31.0
L2	30.68	37.08	37.08	36.08	40.85	50.95	49.88	49.63
L3	18.95	29.37	30.12	29.55	34.87	45.74	44.74	45.62
L4	37.40	41.98	41.85	43.3	53.15	56.22	55.41	58.54

(Orange columns are of gas phase and the blue columns are of solvation phase)

Table 3.21 ΔG values of model reaction 4 [for Uranyl complexes with L(n)] (kcal/mol)

L	PBE-D3 (ADF)	BLYP (ADF)	BLYP (ORCA)	B3LYP (ORCA)	PBE-D3 (ADF)	BLYP (ADF)	BLYP (ORCA)	B3LYP (ORCA)
L1	4.08	9.98	13.05	5.71	-46.37	-39.03	-35.96	-41.16
L2	-5.08	1.51	3.27	-3.58	-55.41	-46.81	-43.67	-49.26
L3	9.10	19.33	21.59	14.74	-51.33	-42.54	-37.90	-42.73
L4	6.40	10.23	13.3	7.34	-62.37	-56.22	-52.21	-56.79

(Orange columns are of gas phase and the blue columns are of solvation phase)

Table 3.22 ΔG values of model reaction 5 [for Uranyl complexes with L(n)] (kcal/mol)

L	PBE-D3 (ADF)	BLYP (ADF)	BLYP (ORCA)	B3LYP (ORCA)	PBE-D3 (ADF)	BLYP (ADF)	BLYP (ORCA)	B3LYP (ORCA)
L1	-138.24	-131.65	-133.91	-136.61	-67.33	-59.24	-59.36	-63.75
L2	-147.40	-140.12	-143.7	-145.89	-76.37	-67.02	-67.08	-71.85
L3	-133.22	-122.3	-125.38	-127.57	-72.29	-62.75	-61.31	-65.32
L4	-135.92	-131.4	-133.66	-134.97	-83.33	-76.43	-75.61	-79.38

(Orange columns are of gas phase and the blue columns are of solvation phase)

From the values obtained from solvation phase model reactions 1, 4, and 5, we believe that akin to vanadium, even uranium is capable of binding to the eudistomin ligands. The formation energies of the complexes are in closer proximity, with the differences in the energy values being ~20 kcal/mol. This could mean that, regardless of the eudistomin ligand, uranyl ion may form similar type of interactions, and exhibit similar type of bonding behaviour. However, the minute differences could determine to which eudistomin might the uranyl ion bind strongly.

We have also examined the bonding orbitals of the uranyl complexes, as actinide chemists are interested in the contribution of 5f and 6d orbitals of uranium. From the occupied bonding orbitals of the complexes, we have selected the ones which show an overlap between the uranium atom and the binding atoms of the ligand. As the binding atoms are mostly nitrogen (except in one case (U1), which is oxygen), they can contribute p_x or p_y or p_z orbitals. But with respect to uranium, there are 7 flavours of 5f orbitals and 5 flavours of 6d orbitals. All but one such selected bonding orbitals contribute majorly via 5f, while the odd case (U4) exhibits 6d contribution (Figure 3.18). The contributions are from the uranium atom towards the occupied bonding orbitals which exhibit an overlap between the ligand's atoms and uranium atom. The z^3 orbital was observed to contribute the most in U2 and U3 complexes, while the contributions from other f orbitals x^3, z^2x, y^3, z^2y, and xyz are also observed in U(n) complexes. Only in U4, a small 6d contribution from x^2-y^2 orbital is observed.

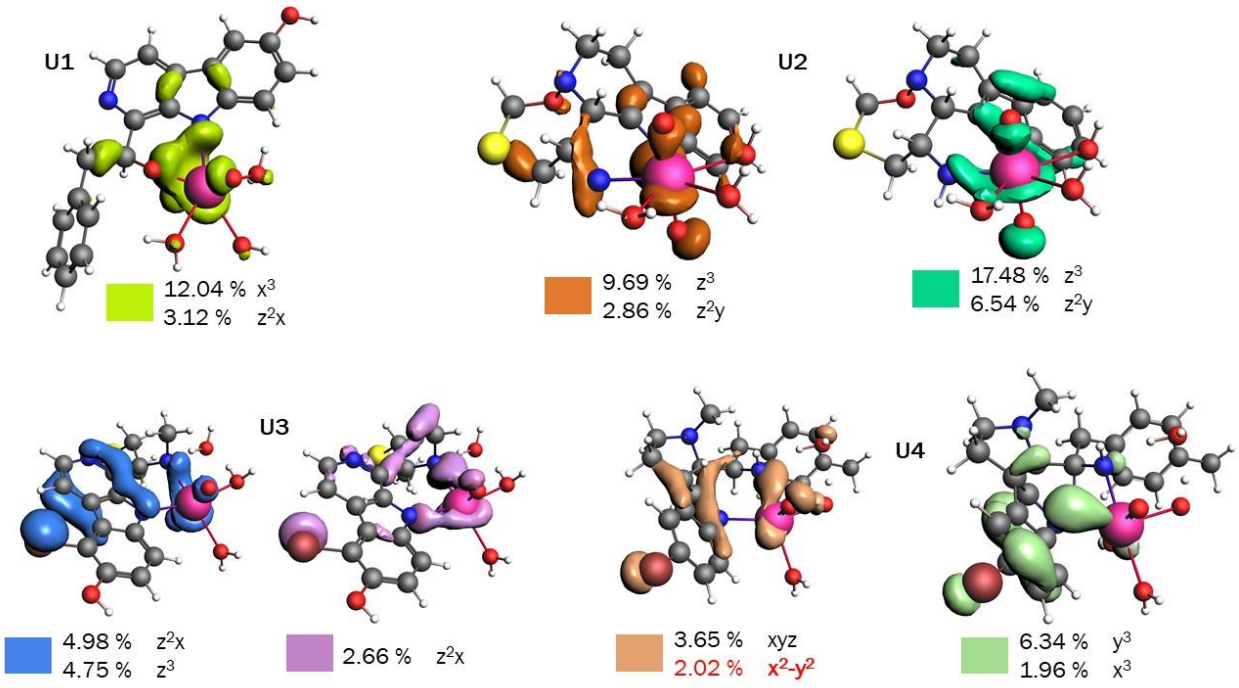

Figure 3.18 Orbital contributions from uranium towards uranyl complexes (black font = 5f orbitals; red font = 6d orbitals)

3.4. Thorium-Eudistomin Complexes

Thorium-eudistomin complexes were optimized in gas phase and solvation phase with water as solvent. The levels of theory are the same as mentioned before. The optimized geometries of the respective complexes have resulted in similar geometries, i.e., with essentially identical geometrical parameters in the respective cases. As thorium is a tetra-positive cation, we have modelled our complexes as 1:1 (Th:L) complexes and 1:2 (Th:L) complexes [where L is ligand].

Note:

- The 1:2 (Th:L) complexes are given in the format T(n)[a]
- The 1:1 (Th:L) complexes with +2 charge are given in the format T(n)[b]
- The 1:1 (Th:L) complexes with neutral charge are given in the format T(n)[s]

From the optimized structures, in all four cases of 1:2 (Th:L) bonding (shown in Figure 3.19), the bond lengths of the binding atoms from the ligand and the thorium atom are completely different, i.e., they do not exhibit a proximity unlike the V(n) or V(n)* or U(n) complexes (shown in Figure 3.19). The bond lengths between the thorium atom and the binding atoms of

the ligands are given in Table 3.23. In case of 1:1 (Th:L) complexes, one set of the complexes were +2 charged (shown in Figure 3.20), and the other set of the complexes were neutral with the sulphate anion countering the charge (shown in Figure 3.21). In all of the complexes, thorium exhibits a 7-coordination. The bond lengths between the binding atoms of the ligand and the thorium atom of the 1:1 (Th:L) complexes, i.e., the $T(n)^b$ and $T(n)^s$ complexes are given in Table 3.24. Comparing the bond lengths in $T(n)^b$ complexes to $T(n)^s$ complexes, the bond lengths in the +2 charged complexes, i.e., the $T(n)^b$ complexes are slightly shorter than the $T(n)^s$ complexes. As the bonding is mainly ionic in these cases, smaller charge could have led to slightly weaker bonds, henceforth the slight differences in the bond lengths.

In case of the sulphate-ligand-metal complexes, the sulphate ion seems to show a mono-dentate structure in the Figure 3.21, because the O-Th bonds are uneven. The unevenness is simply because of the heavy crowding of atoms around the Th atom. There actually exists a bonding between Th and the oxygen atoms from the sulphate, but in the Figure 3.21, the complexes seem to appear as mono-dentate because of this reason. Also, the Figure 3.21 depicts the hydrogen bonding between the oxygen atom of the sulphate ion with the neighbouring water molecules. This could mean that the sulphate ion is stabilized via hydrogen bonding. The Th-O bonds pertaining to the sulphate ion are given in Table 3.25.

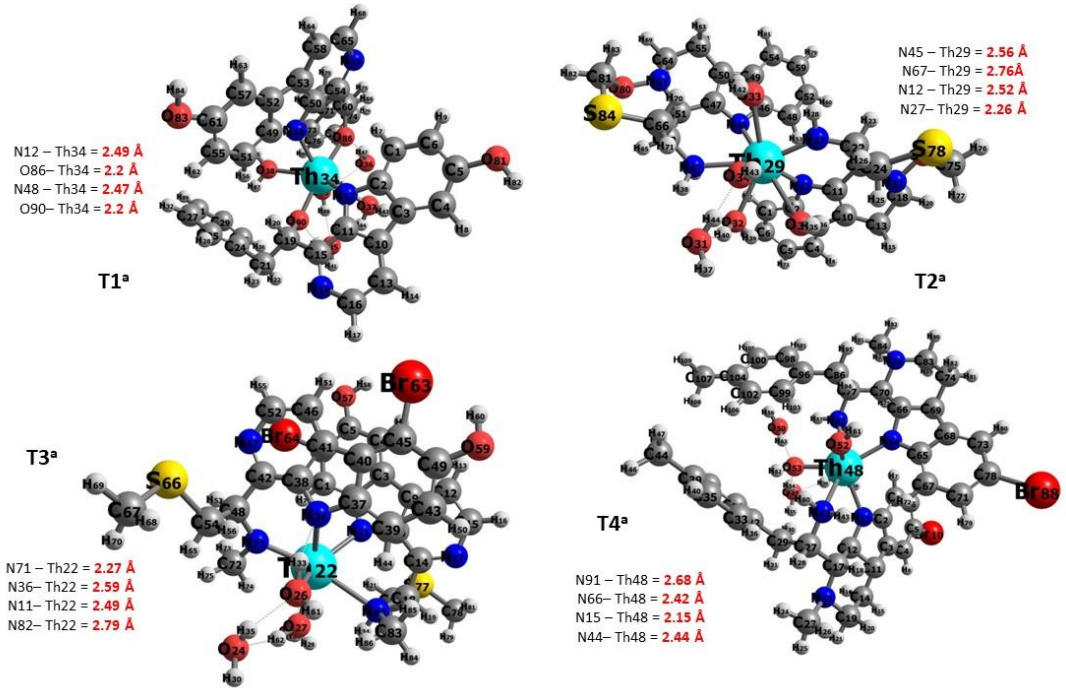

Figure 3.19 Optimized geometries of 1:2 (Th:L) thorium-eudistomin ligand complexes [ADF PBE-D3 solvation phase geometries are shown here]

Table 3.23 Bond lengths between the metal-eudistomin binding atoms in T(n)ª complexes

Complex	Binding atoms	Bond length (Å)
T1ª	N12-Th34	2.490
	O90-Th34	2.202
	N48-Th34	2.468
	O86-Th34	2.199
T2ª	N45-Th29	2.563
	N67-Th29	2.764
	N12-Th29	2.525
	N27-Th29	2.265
T3ª	N36-Th22	2.596
	N71-Th22	2.269
	N11-Th22	2.490
	N82-Th22	2.793
T4ª	N66-Th50	2.424
	N91-Th50	2.679
	N15-Th50	2.468
	N44-Th50	2.687

(coloured cells are of the five-membered ring's nitrogen and metal bond lengths)

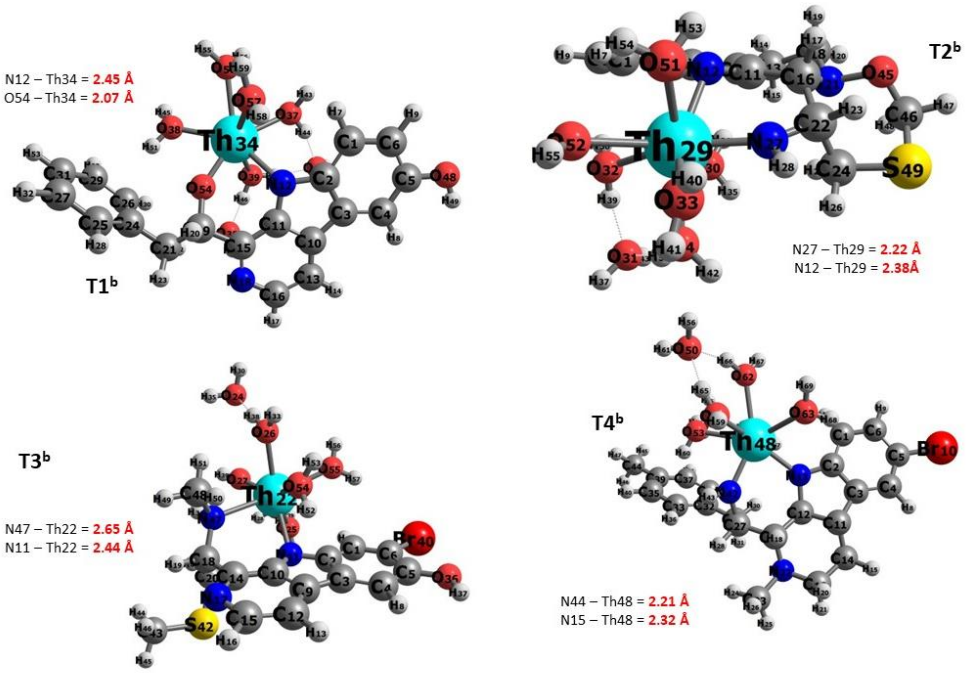

Figure 3.20 Optimized geometries of 1:1 (Th:L) thorium-eudistomin ligand +2 charged complexes [ADF PBE-D3 solvation phase geometries are shown here]

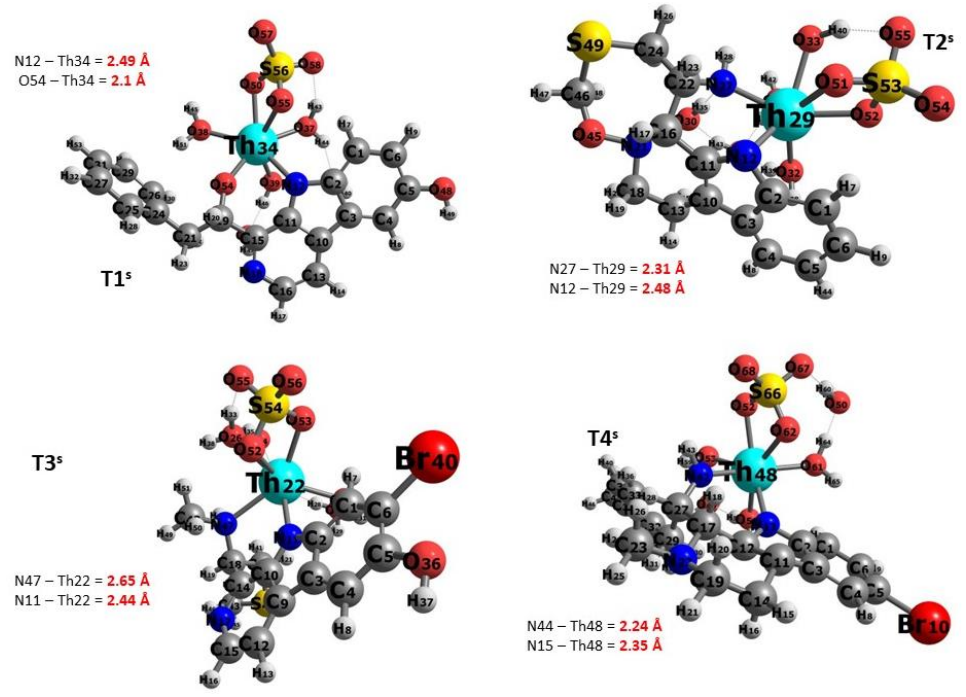

Figure 3.21 Optimized geometries of 1:1 (Th:L) thorium-eudistomin ligand neutral complexes [ADF PBE-D3 solvation phase geometries are shown here]

Table 3.24 Bond lengths between the metal-eudistomin binding atoms in $T(n)^b$ and $T(n)^s$ complexes

Complex	Binding atoms	Bond length (Å)
$T1^b$	N12-Th34	2.457
	O54-Th34	2.077
$T1^s$	N12-Th34	2.493
	O54-Th34	2.108
$T2^b$	N12-Th29	2.387
	N27-Th29	2.222
$T2^s$	N12-Th29	2.479
	N27-Th29	2.312
$T3^b$	N11-Th22	2.440
	N47-Th22	2.647
$T3^s$	N11-Th22	2.436
	N47-Th22	2.649
$T4^b$	N15-Th50	2.321
	N44-Th50	2.216
$T4^s$	N15-Th50	2.349
	N44-Th50	2.238

(coloured cells are of the five-membered ring's nitrogen and metal bond lengths)

Table 3.25 Bond lengths between the Thorium-Oxygen in $T(n)^s$ complexes

Complex	Binding atoms	Bond length (Å)
$T1^s$	O55-Th34	2.411
	O50-Th34	2.495
$T2^s$	O51-Th29	2.394
	O52-Th29	2.443
$T3^s$	O53-Th22	2.383
	O52-Th22	2.457
$T4^s$	O64-Th50	2.457
	O54-Th50	2.458

(the coloured cells show bonding in the Figure 3.21)

The following model reactions were considered for the thorium complexes (1Th:2L). The formation energy values of these reactions are given in the Tables 3.26 to 3.30. In these model reactions, as Th is tetra-positive cation, two units of ligand are made to interact with the thorium atom. The model reactions reflect the similar mould as described in Chapter 1 (section 1.5).

1. $2L^{2-} + [Th\ 9H_2O]^{4+} \Leftrightarrow [Th.L_2.\ 5H_2O] + 4H_2O$
2. $2H_2L + [Th\ 9H_2O]^{4+} \Leftrightarrow [Th.L_2.\ 5H_2O] + 4H_3O^{+}$
3. $2H_2L + [Th(SO_4)_2.\ 5H_2O] \Leftrightarrow [Th.L_2.\ 5H_2O] + 2H_2SO_4$
4. $Th(SO_4)_2\ (H_2O)_5 + 2L^{2-} \Leftrightarrow Th.L_2\ (H_2O)_5 + 2(SO_4^{2-})$
5. $2H_2SO_4 + Th(SO_4)_2(H2O)_5 + 2L^{2-} \Leftrightarrow Th.L_2.\ (H_2O)_5 + 4HSO_4^{-}$

*where H_2L is the neutral ligand

Table 3.26 ΔG values of model reaction 1 [for Thorium 1:2 (Th:L) complexes with L(n)] (kcal/mol)

L	PBE-D3 (ADF)	BLYP (ADF)	BLYP (ORCA)	B3LYP (ORCA)	PBE-D3 (ADF)	BLYP (ADF)	BLYP (ORCA)	B3LYP (ORCA)
L1	-1103.52	-1081.31	-1073.53	-1082.00	-160.14	-159.13	-133.28	-132.21
L2	-1133.96	-1109.48	-1103.40	-1115.19	-175.87	-144.26	-149.28	-150.91
L3	-1095.43	-1063.86	-1056.71	-1068.00	-169.80	-152.79	-138.48	-139.68
L4	-1157.11	-1131.95	-1122.47	-1135.9	-242.29	-221.95	-208.77	-213.66

(Orange columns are of gas phase and the blue columns are of solvation phase)

Table 3.27 ΔG values of model reaction 2 [for Thorium 1:2 (Th:L)complexes with L(n)] (kcal/mol)

L	PBE-D3 (ADF)	BLYP (ADF)	BLYP (ORCA)	B3LYP (ORCA)	PBE-D3 (ADF)	BLYP (ADF)	BLYP (ORCA)	B3LYP (ORCA)
L1	-221.88	-193.40	-191.01	-184.17	69.53	89.54	98.64	105.73
L2	-189.94	-161.96	-159.00	-156.12	105.04	127.00	135.10	140.50
L3	-203.25	-167.42	-162.90	-158.63	90.86	114.39	124.12	130.65
L4	-222.64	-192.08	-188.63	-184.23	77.12	93.56	103.72	110.63

(Orange columns are of gas phase and the blue columns are of solvation phase)

Table 3.28 ΔG values of model reaction 3 [for Thorium1:2 (Th:L) complexes with L(n)] (kcal/mol)

L	PBE-D3 (ADF)	BLYP (ADF)	BLYP (ORCA)	B3LYP (ORCA)	PBE-D3 (ADF)	BLYP (ADF)	BLYP (ORCA)	B3LYP (ORCA)
L1	43.17	60.93	66.89	67.39	54.72	71.10	72.60	79.00
L2	75.11	92.37	98.89	95.44	90.23	108.56	109.06	113.76
L3	61.81	86.91	95.00	92.93	76.05	95.94	98.08	103.91
L4	42.42	62.25	69.28	67.33	62.31	75.11	77.68	83.90

(Orange columns are of gas phase and the blue columns are of solvation phase)

Table 3.29 ΔG values of model reaction 4 [for Thorium 1:2 (Th:L)complexes with L(n)] (kcal/mol)

L	PBE-D3 (ADF)	BLYP (ADF)	BLYP (ORCA)	B3LYP (ORCA)	PBE-D3 (ADF)	BLYP (ADF)	BLYP (ORCA)	B3LYP (ORCA)
L1	34.51	49.38	61.12	49.32	-86.59	-72.10	-62.06	-65.32
L2	4.08	21.21	31.25	16.12	-102.28	-86.97	-78.06	-84.02
L3	42.61	66.83	77.93	63.31	-96.26	-80.63	-67.20	-72.79
L4	-19.08	-1.25	12.17	-4.58	-168.73	-149.78	-137.55	-146.77

(Orange columns are of gas phase and the blue columns are of solvation phase)

Table 3.30 ΔG values of model reaction 5 [for Thorium 1:2 (Th:L)complexes with L(n)] (kcal/mol)

L	PBE-D3 (ADF)	BLYP (ADF)	BLYP (ORCA)	B3LYP (ORCA)	PBE-D3 (ADF)	BLYP (ADF)	BLYP (ORCA)	B3LYP (ORCA)
L1	-250.62	-233.87	-232.80	-235.31	-128.51	-112.51	-108.87	-110.50
L2	-281.06	-262.04	-262.67	-268.51	-144.20	-127.38	-124.87	-129.20
L3	-242.53	-216.42	-215.99	-221.32	-138.18	-121.05	-114.02	-117.97
L4	-304.21	-284.51	-281.75	-289.21	-210.65	-190.20	-184.36	-191.95

(Orange columns are of gas phase and the blue columns are of solvation phase)

The following model reactions were considered for the 1:1 thorium complexes (1Th:1L). The formation energy values are given in the tables 3.31 to 3.35. In these model reactions, one ligand is made to interact with the Th^{+4} cation. In model reactions 1 and 2, the formed complexes are +2 charged, while in the model reactions 3, 4, and 5, the formed complexes are

neutral and have a sulphate anion countering the charge, i.e., in the model reactions 3, 4, and 5, the complexes are in a $Th(SO_4)(L)$ mould.

1. $L^{2-} + [Th\ 9H_2O]^{4+} \Leftrightarrow [Th.L.\ 7H_2O]^{2+} + 2H_2O$
2. $H_2L + [Th\ 9H_2O]^{4+} \Leftrightarrow [Th.L.\ 7H_2O]^{2+} + 2H_3O^{+}$
3. $H_2L + [Th(SO_4)_2.\ 5H_2O] \Leftrightarrow [Th(SO_4)L.\ 5H_2O] + H_2SO_4$
4. $Th(SO_4)_2\ (H_2O)_5 + L^{2-} \Leftrightarrow Th(SO_4)L.\ (H2O)_5 + (SO_4^{2-})$
5. $H_2SO_4 + Th(SO_4)_2(H2O)_5 + L^{2-} \Leftrightarrow Th(SO_4)L.\ (H2O)_5 + 2HSO_4^{-}$

*where H_2L is the neutral ligand

Table 3.31 ΔG values of model reaction 1 [for Thorium 1:1 (Th:L) complexes with L(n)] (kcal/mol)

L	PBE-D3 (ADF)	BLYP (ADF)	BLYP (ORCA)	B3LYP (ORCA)	PBE-D3 (ADF)	BLYP (ADF)	BLYP (ORCA)	B3LYP (ORCA)
L1	-740.76	-730.97	-726.08	-728.72	-89.67	-85.15	-75.11	-72.35
L2	-743.09	-730.28	-727.77	-732.04	-91.80	-86.15	-79.75	-79.38
L3	-748.04	-737.06	-732.92	-738.63	-101.84	-100.46	-90.42	-88.54
L4	-756.08	-744.72	-739.57	-744.90	-114.08	-110.56	-100.84	-100.90

(Orange columns are of gas phase and the blue columns are of solvation phase)

Table 3.32 ΔG values of model reaction 2 [for Thorium 1:1 (Th:L) complexes with L(n)] (kcal/mol)

L	PBE-D3 (ADF)	BLYP (ADF)	BLYP (ORCA)	B3LYP (ORCA)	PBE-D3 (ADF)	BLYP (ADF)	BLYP (ORCA)	B3LYP (ORCA)
L1	-299.95	-287.02	-284.82	-279.80	25.16	31.75	40.85	46.62
L2	-271.08	-256.52	-255.58	-252.51	48.63	56.91	62.44	66.32
L3	-301.95	-288.84	-286.01	-283.95	28.49	33.13	40.85	46.62
L4	-288.84	-274.78	-272.65	-269.07	45.62	47.19	55.41	61.24

(Orange columns are of gas phase and the blue columns are of solvation phase)

Table 3.33 ΔG values of model reaction 3 [for Thorium 1:1 (Th:L) complexes with L(n)] (kcal/mol)

L	PBE-D3 (ADF)	BLYP (ADF)	BLYP (ORCA)	B3LYP (ORCA)	PBE-D3 (ADF)	BLYP (ADF)	BLYP (ORCA)	B3LYP (ORCA)
L1	23.22	31.63	33.94	34.13	28.99	32.63	34.20	39.22
L2	45.43	58.11	61.12	55.85	53.34	62.69	64.26	68.96
L3	26.10	31.75	36.33	32.06	32.13	33.32	38.40	43.36
L4	45.12	48.07	51.33	53.40	51.58	50.45	51.27	56.16

(Orange columns are of gas phase and the blue columns are of solvation phase)

Table 3.34 ΔG values of model reaction 4 [for Thorium 1:1 (Th:L) complexes with L(n)] (kcal/mol)

L	PBE-D3 (ADF)	BLYP (ADF)	BLYP (ORCA)	B3LYP (ORCA)	PBE-D3 (ADF)	BLYP (ADF)	BLYP (ORCA)	B3LYP (ORCA)
L1	18.89	25.85	31.06	25.10	-41.67	-38.97	-33.13	-32.94
L2	9.91	22.53	27.30	16.19	-42.92	-35.07	-29.30	-29.93
L3	16.50	21.71	27.80	17.25	-54.03	-54.97	-44.24	-44.99
L4	14.37	16.31	22.78	17.44	-63.94	-62.00	-56.35	-59.17

(Orange columns are of gas phase and the blue columns are of solvation phase)

Table 3.35 ΔG values of model reaction 5 [for Thorium 1:1 (Th:L) complexes with L(n)] (kcal/mol)

L	PBE-D3 (ADF)	BLYP (ADF)	BLYP (ORCA)	B3LYP (ORCA)	PBE-D3 (ADF)	BLYP (ADF)	BLYP (ORCA)	B3LYP (ORCA)
L1	-123.68	-115.77	-115.90	-117.22	-62.62	-59.17	-56.54	-55.53
L2	-132.65	-119.10	-119.66	-126.13	-63.88	-55.28	-52.71	-52.52
L3	-126.07	-119.92	-119.16	-125.06	-74.99	-75.17	-67.64	-67.58
L4	-128.20	-125.31	-124.18	-124.87	-84.90	-82.20	-79.75	-81.76

(Orange columns are of gas phase and the blue columns are of solvation phase)

The formation energy values of model reactions 1, 4, and 5 in solvation phase suggest that the interactions between eudistomins and thorium tetrapositive cation are possible. The values of the model reactions of 1:2 (Th:L) complexes, in most cases are close to double the values obtained from the model reactions of the 1:1 (Th:L) complexes.

3.5. Discussion

The results show that there are possible interactions between eudistomin ligands and metal aqua ions. The model reactions 1, 4, and 5, where the ligand anion is made to interact with the metal aqua ion/metal sulphate, have resulted in exothermic formation energies. The model reactions 2 and 3, which involve a H-N bond breaking (deprotonation), have resulted in endothermic formation energies, owing to the broken bonds. We are inclined to think that model reactions 4 and 5 may provide a better result as they are modelled to resemble the, what could be, real-time scenario. The fact that both these models have resulted in exothermic formation energies makes us believe that the metal aqua ions may form decent interactions with the eudistomin ligands.

The vanadyl complexes with three water molecules (i.e., the vanadium-centric distorted octahedral input geometry), i.e., V(n)* complexes have all resulted in geometrical structures with the third water molecule pushed away into the second solvation sphere (the water molecule opposite to the oxygen atom in the V=O bond). The size of ligands may have influenced this and could have allowed the extra-water molecule to get away from the vanadium atom.

Uranium has a ground state electronic configuration of [Rn] 7s2 6d1 5f3.[61] The near-degeneracy of 5f and 6d orbitals is an interesting aspect for physicists and chemists as well. The degeneracy driven covalency is a very interesting region for the "explorers". [165] Actinide-ligand bonding might exhibit covalency due to the near-degeneracy, especially in the middle actinides like americium. However, these types of systems may not be as stable as their "ionic-bond" counter-parts, i.e., when the stability of the molecules with covalent behaviour and ionic behaviour are compared, ionic compounds have shown a better stability than the covalent molecules.[166] We, as actinide chemists, were interested to take a note of which orbital binds to our ligands, and see if there was any such phenomenon. Unsurprisingly, our complexes are "electrostatics-driven", and in all but one case there was a 5f-domination the exception being the 6d contribution (in case of U4 complex, as shown in Figure 3.18).

With thorium tetrapositive cation we have explored two possible flavours of complexes, i.e., 1:2 (Th:L) and 1:1 (Th:L) complexes. The 1:2 (Th:L) complexes, in most of the cases, have formation energy values close to two times the values obtained from the 1:1 (Th:L) complexes. The formation of 1:1 (Th:L) complexes or 1:2 (Th:L) complexes would be a question of the concentrations and we are inclined to think that they are low enough to result in 1:1 (Th:L)

complexes. So, possibly it may be the right way to examine the interactions with the eudistomins.

In total, we have performed 800 calculations (4 ligands x 4 methods x 2 phases x 5 model reactions x 5 types of metal-ligand complexes). As we have used 4 different computational methods in gas and solvation phases (ADF PBE-D3/ ADF BLYP/ ORCA BLYP/ ORCA B3LYP), it makes 200 of the cases unique. Despite this fact, we've seen the formation energy values, i.e., the ΔG values to be similar in almost all of the cases, some of the numbers being very much identical to each other. There are some noticeable differences in some cases, and they pertain to the PBE-D3 method of ADF. This is because PBE-D3 includes an empirical dispersion correction. Our complexes have hydrogen bonds, and this makes us believe PBE-D3 method more than the results of the other three methods due to its efficiency and accuracy, despite the congruent formation energy values obtained from other levels of theory.[167,168] This is also the reason why this thesis shows the ADF PBE-D3 geometries, despite the more or less identical geometries obtained from the other computational methods. For systems with such hydrogen bonding type geometries, the addition of dispersion correction always yields better results.

Now the question is, which of the three metals bind better? Vanadium, Uranium, or Thorium? For to answer this question, we have picked just one metal-ligand (L1, i.e., Eudistomin-W) complex with ADF PBE-D3 solvation phase, and have examined the formation energy values. (This is to highlight our point.) The vanadyl complex with two water molecules and Thorium complex with 1:1 (Th:L) ratio are considered here because of the forementioned reasons. The respective model reactions are considered here.

Table 3.36 ΔG values Vanadyl, Uranyl, and Thorium complexes with Eudistomin-W (L1) (units in kcal/mol)

Complex	Vanadyl-L1	Uranyl-L1	Thorium-L1
Model reaction 1	-83.39	-73.35	-89.67
Model reaction 2	31.44	41.48	25.16
Model reaction 3	20.08	24.28	28.99
Model reaction 4	-50.58	-46.37	-41.67
Model reaction 5	-71.53	-67.33	-62.62

From Table 3.36, we can see that the formation energy values are distinguishable, but are within the range of ~20kcal/mol in most cases, especially the model reactions involving sulphuric acid, sulphate ion, and bisulphate ion. This takes us back to the question, do ascidians need metals, or do they need the sulphate part of the metal-sulphate? From these results we are inclined to assume that the metal-sulphate is what ascidians tend to sequester, not the metals alone. Also, the closeness of the values in all of the cases adds to our assumption that the over-presence of vanadium in ascidians in comparison to uranium or thorium might have a relation with the abundance of vanadium in sea-waters, not with the preference of ascidians. Vanadium is the second most-abundant d-block element in the ocean waters, and VO^{2+} is the most stable oxy-cation. On the other hand, uranium and thorium (also other metals which are observed to be sequestered by ascidians) are not that abundant in comparison to vanadium. Whether this could have a role to play? It is debatable.

In conclusion to this chapter, it can be stated that our study has confirmed the possible interactions between the eudistomin ligands and metals as per the respective model reactions 1, 4, and 5. There is not a lot to distinguish as all three metals have formation energy close to each other (~10 kcal/mol) when compared, which prompts the idea that any metal can bind to eudistomins. However, the minor differences might play a role when we apply this philosophy to nuclear reprocessing.

CHAPTER-4

Conclusions and Future work

4.1. Conclusions

Nuclear reprocessing is an essential procedure to recovering useful uranium and other actinides.[169] This procedure requires ligands which can bind with the actinides. Ascidians are marine animals which contain eudistomins, compounds of pharmacological importance. In this work, we have started with an agenda to identify the potential of eudistomins as possible biogenic ligands for nuclear reprocessing. In that process, we have investigated the possible interactions between metal aqua ions and eudistomins. Five model reactions were designed to explore the possible interactions and calculations were done in accordance. The simplest possible eudistomins which could provide a bidentate structure were selected from the literature. Three metal aqua ions, viz., vanadyl, uranyl, and thorium ions were adopted for our study. Our study suggests that eudistomins are capable of forming exothermic interactions with metals while in anionic form, as per the designed respective model reactions 1, 4, and 5. The cells which contain the vanadium also contain sulphate ion/sulphuric acid, and have a pH range of 1.8 to 2.0. At this range, sulphuric acid can occur as HSO_4^- ion. Model reactions 4 and 5 were designed to resemble the possible conditions in the ascidians, i.e., have a SO_4^{2-} ion (in model reaction 4) and HSO_4^- ion (in model reaction 5) on the product side, along with the eudistomin-metal complex. We conclude this study by stating that model reactions 4 and 5 may provide a better picture in comparison to the rest. The conclusions derived from this study can be given as follows.

1. Eudistomins, when in anionic form as in (respective) model reactions 1, 4, and 5 show exothermic interactions with the metal ions/sulphates. All of the interactions in these respective model reactions are electrostatic in nature.
2. We are inclined to think that ascidians may not have preference to a specific metal, but could be more interested towards the ‘sulphate’ part of the metal-sulphates.
3. Vanadium, when bound to a bidentate structure, is likely to prefer five coordination over six coordination (including the oxygen in V=O).
4. Uranium in the uranyl complexes of our study has shown interactions dominated by 5f-orbitals.

5. Thorium as it is a tetrapositive cation, was subject to studies of 1:2 (Th:L) and 1:1 (Th:L) complexes. In most of the cases, the 1:2 (Th:L) complexes exhibit formation energy values close to being double those of the 1:1 (Th:L) complexes, prompting that the 1:1 (Th:L) complexes may provide a better picture than the 1:2 (Th:L) complexes. [L is ligand].
6. We have used two different codes (ADF and ORCA), two different phases of calculations (gas and solvation), two different solvation methods (COSMO and CPCM), and three different functionals (PBE-D3, BLYP, and B3LYP) for our calculations. Despite this, we were able to observe similar trends and identical ΔG values, confirming that our approach can stand the test of different methodologies.
7. We can conclude that eudistomins could be used as biogenic ligands for nuclear reprocessing.

4.2. Future Work

A wise man once said, “What makes us human? An eternally burning desire to always want more.”

As humans, we want more, and adopting the philosophy learnt from Dr. Georg Schreckenbach, there are three axis that can be explored in this work, as shown in Figure 4.1. At the given moment we can say that the ‘Eudistomins’ axis is partly under control as we have seen that all the eudistomins we have studied are capable of interacting with the metal ion/sulphates.

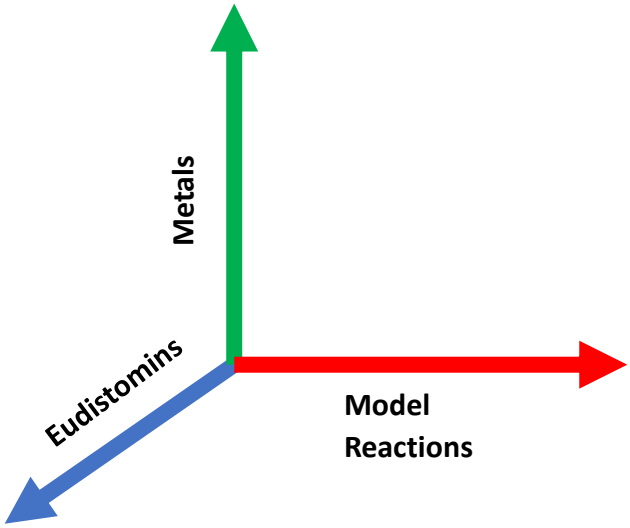

Figure 4.1 Future work axes

In the dimension of the model reactions, we move towards exploring novel model reactions, with which we aim to improve the existing model reactions. The reason for this is, the model reactions which we develop are close to the real-scenario, but are never exact. So, we would want to better existing model reactions. In this study, we have designed model reactions to form neutral complexes and in our next step we are developing model reactions where we have charged complexes. The motivation behind this is to explore the possibility of the formation of charged complexes as well. The complexes in this work are neutrally charged and we believe that there are other ways to explore the interactions, one being the formation of charged complexes, i.e., interactions with protonated versions of the ligands. A set of data for uranyl complexes is given in Table 4.1. The calculations were done in accordance with the model reaction 6 (given below). In this model reaction, instead of di-anionic ligands, we have considered mono-anionic structures. The bidentate complex structures are still intact via the lone pair interactions. These sets of calculations were performed in solvation phase using ORCA with DFT method BLYP, ZORA for relativistic approximation, with basis sets def2-TZVPP (SARC-ZORA-TZVPP for Uranium and Thorium), and CPCM for solvation effects.

Model reaction 6 for uranyl complexes:

$$[UO_2\,(H_2O)_5]^{2+} + HL^{-1} \rightarrow [UO_2\,(HL)\,(H_2O)_3]^{1+} + 2H_2O$$

Table 4.1 ΔG values for model reaction 6 for uranyl complexes (kcal/mol)

Ligand	**L1**	**L2**	**L3**	**L4**
ΔG value	-18.38	-28.05	-18.70	-39.78

Where L1 is Eudistomin-W, L2 is Debromoeudistomin-K, L3 is Eudistomidin-C, and L4 is Eudistomidin-B

The other dimension of the development is the metals. We have studied vanadyl, uranyl, and thorium ions in this work. The real challenge in a nuclear reprocessing unit is the separation of trivalent lanthanides and actinides. We are currently adopting our philosophy and methodology to trivalent americium and europium to understand the possible interactions and the differences between them.

In the end, we would like to conclude that we have successfully completed step-one in our work of exploring the possibility of using biogenic ligands for nuclear reprocessing.

REFERENCES

1. Nuclear Power in the World Today. https://www.world-nuclear.org/information-library/current-and-future-generation/nuclear-power-in-the-world-today.aspx.
2. Ağbulut, Ü. Turkey's electricity generation problem and nuclear energy policy. *Energy Sources, Part A Recover. Util. Environ. Eff.* **41**, 2281–2298 (2019).
3. Emsley, J. *Nature's building blocks : an A-Z guide to the elements*. (Oxford University Press, 2003).
4. Ewing, R. C. Nuclear waste forms for actinides. *Proc. Natl. Acad. Sci.* **96**, 3432–3439 (1999).
5. Anderson, H. H. & Asprey, L. B. Solvent Extraction Process for Plutonium. (1960).
6. Nuclear Reprocessing. https://en.wikipedia.org/wiki/Nuclear_reprocessing.
7. United States Government Accountability Office. *Nuclear Fuel Cycle Options (Report to Congressional Requesters)*. (2011).
8. Panak, P. J. & Geist, A. Complexation and Extraction of Trivalent Actinides and Lanthanides by Triazinylpyridine N -Donor Ligands. *Chem. Rev.* **113**, 1199–1236 (2013).
9. Geist, A. & Panak, P. J. Recent Progress in Trivalent Actinide and Lanthanide Solvent Extraction and Coordination Chemistry with Triazinylpyridine N Donor Ligands. *Solvent Extr. Ion Exch.* **39**, 128–151 (2021).
10. Afsar, A., Distler, P., Harwood, L. M., John, J. & Westwood, J. Synthesis and Screening of Modified 6,6′-Bis(5,5,8,8-tetramethyl-5,6,7,8-tetrahydrobenzo[e][1,2,4]triazin-3-yl)-2,2′-bipyridine Ligands for Actinide and Lanthanide Separation in Nuclear Waste Treatment. *J. Org. Chem.* **81**, 10517–10520 (2016).
11. Sittel, T., Trumm, M., Adam, C., Geist, A. & Panak, P. J. Impact of Solvent Polarity on the Ligand Configuration in Tetravalent Thorium N-Donor Complexes. *Inorg. Chem.* **60**, 1092–1098 (2021).
12. Lewis, F. W. *et al.* Synthesis and Evaluation of Lipophilic BTBP Ligands for An/Ln Separation in Nuclear Waste Treatment: The Effect of Alkyl Substitution on Extraction Properties and Implications for Ligand Design. *European J. Org. Chem.*

2012, 1509–1519 (2012).

13. Xia, M., Yang, X., Chai, Z. & Wang, D. Stronger Hydration of Eu(III) Impedes Its Competition against Am(III) in Binding with N-donor Extractants. *Inorg. Chem.* **59**, 6267–6278 (2020).

14. Ekberg, C. *et al.* An overview and historical look back at the solvent extraction using nitrogen donor ligands to extract and separate An(III) from Ln(III). *Radiochim. Acta* **96**, (2008).

15. Menna, M., Fattorusso, E. & Imperatore, C. Alkaloids from Marine Ascidians. *Molecules* **16**, 8694–8732 (2011).

16. Aniszewski, T. *Alkaloids — Secrets of Life*. (Elsevier, 2007).

17. Shenkar, N. & Swalla, B. J. Global Diversity of Ascidiacea. *PLoS One* **6**, e20657 (2011).

18. Chen, J.-Y. *et al.* The first tunicate from the Early Cambrian of South China. *Proc. Natl. Acad. Sci.* **100**, 8314–8318 (2003).

19. Porter, S. M. Calcite and aragonite seas and the de novo acquisition of carbonate skeletons. *Geobiology* **8**, 256–277 (2010).

20. Varol, O. & Houghton, S. D. A review and classification of fossil didemnid ascidian spicules. *J. Micropalaeontology* **15**, 135–149 (1996).

21. Buge, E. & Monniot, F. Nouveaux Spicules D'Ascidiesde L'Ypresien du Bassin de Paris et du Toarcien des Deux-Sevres. *Geobios* **5**, 83–90 (1972).

22. Fedonkin, M. A., Vickers-Rich, P., Swalla, B. J., Trusler, P. & Hall, M. A new metazoan from the Vendian of the White Sea, Russia, with possible affinities to the ascidians. *Paleontol. J.* **46**, 1–11 (2012).

23. Odate, S. & Pawlik, J. R. The Role of Vanadium in the Chemical Defense of the Solitary Tunicate, Phallusia nigra. *J. Chem. Ecol.* **33**, 643–654 (2007).

24. Bromley, L. C. The Chemistry of Aloga Bay Ascidians. (Rhodes University, SA, 2015).

25. Davis, A. R. Alkaloids and ascidian chemical defense: Evidence for the ecological role of natural products fromEudistoma olivaceum. *Mar. Biol.* **111**, 375–379 (1991).

26. Lake, R., Blunt, J. & Munro, M. Eudistomins From the New Zealand Ascidian Ritterella sigillinoides. *Aust. J. Chem.* **42**, 1201 (1989).

27. Cao, R., Peng, W., Wang, Z. & Xu, A. ß-Carboline Alkaloids: Biochemical and Pharmacological Functions. *Curr. Med. Chem.* **14**, 479–500 (2007).

28. Kobayashi, J., Harbour, G. C., Gilmore, J. & Rinehart, K. L. Eudistomins A, D, G, H, I, J, M, N, O, P, and Q, bromo, hydroxy, pyrrolyl and iminoazepino .beta.-carbolines from the antiviral Caribbean tunicate Eudistoma olivaceum. *J. Am. Chem. Soc.* **106**, 1526–1528 (1984).

29. Buaban, K., Phutdhawong, W., Taechowisan, T. & Phutdhawong, W. S. Synthesis and Investigation of Tetrahydro-β-carboline Derivatives as Inhibitors of Plant Pathogenic Fungi. *Molecules* **26**, 207 (2021).

30. Bracegirdle, J. & Keyzers, R. A. Marine-derived Polyaromatic Butenolides - Isolation, Synthesis and Biological Evaluations. *Curr. Pharm. Des.* **26**, 4351–4361 (2020).

31. Casertano, M., Menna, M. & Imperatore, C. The Ascidian-Derived Metabolites with Antimicrobial Properties. *Antibiotics* **9**, 510 (2020).

32. Silva, K. L. & Trigo, J. R. Structure–Activity Relationships of Pyrrolizidine Alkaloids in Insect Chemical Defense Against the Orb-Weaving Spider Nephila clavipes. *J. Chem. Ecol.* **28**, 657–688 (2002).

33. Bennet, R. N. & Wallsgrove, R. M. Secondary metabolites in plant defence mechanisms. *New Phytol.* **127**, 617–633 (1994).

34. Bell, M. V. *et al.* Contents of Vanadium and Sulphur in the Blood Cells of Ascidia Mentula and Ascidiella Aspersa. *J. Mar. Biol. Assoc. United Kingdom* **62**, 709–716 (1982).

35. Michibata, H., Iwata, Y. & Hirata, J. Isolation of highly acidic and vanadium-containing blood cells from among several types of blood cell from ascidiidae species by density-gradient centrifugation. *J. Exp. Zool.* **257**, 306–313 (1991).

36. Frank, P., Hedman, B. & Hodgson, K. O. Sulfur Allocation and Vanadium−Sulfate Interactions in Whole Blood Cells from the Tunicate Ascidia ceratodes , Investigated Using X-ray Absorption Spectroscopy. *Inorg. Chem.* **38**, 260–270 (1999).

37. Pisut, D. P. & Pawlik, J. R. Anti-predatory chemical defenses of ascidians: secondary metabolites or inorganic acids? *J. Exp. Mar. Bio. Ecol.* **270**, 203–214 (2002).

38. Mackenzie, F. T., Byrne, Howard, R., Duxbury & Alyn, C. Seawater. Encylopedia Britannica. https://www.britannica.com/science/seawater (2020).

39. Kinzer, K. F. & Cardellina, J. H. Three new β-carbolines from the bermudian tunicate Eudistoma olivaceum. *Tetrahedron Lett.* **28**, 925–926 (1987).

40. Schupp, P. *et al.* Eudistomins W and X, Two New β-Carbolines from the Micronesian Tunicate Eudistoma sp. *J. Nat. Prod.* **66**, 272–275 (2003).

41. Davis, R. A., Carroll, A. R. & Quinn, R. J. Eudistomin V, a New β-Carboline from the Australian Ascidian Pseudodistoma aureum. *J. Nat. Prod.* **61**, 959–960 (1998).

42. Schumacher, R. W. & Davidson, B. S. Didemnolines A-D, new N9-substituted β-carbolines from the marine ascidian Didemnum sp. *Tetrahedron* **51**, 10125–10130 (1995).

43. Ravinder, K. *et al.* Isolation and synthesis of a novel β-carboline guanidine derivative tiruchanduramine from the Indian ascidian Synoicum macroglossum. *Tetrahedron Lett.* **46**, 5475–5478 (2005).

44. Badre, A. *et al.* Eudistomin U and Isoeudistomin U, New Alkaloids from the Carribean Ascidian Lissoclinum fragile. *J. Nat. Prod.* **57**, 528–533 (1994).

45. Kobayashi, J. *et al.* Eudistomidins B, C, and D: novel antileukemic alkaloids from the Okinawan marine tunicate Eudistoma glaucus. *J. Org. Chem.* **55**, 3666–3670 (1990).

46. Shen, G. Q. & Baker, B. J. Biosynthetic studies of the eudistomins in the tunicate eudistoma olivaceum. *Tetrahedron Lett.* **35**, 1141–1144 (1994).

47. Wright, S. H. *et al.* Marine metabolites and metal ion chelation: Intact recovery and identification of an iron(II) complex in the extract of the ascidian Eudistoma gilboviride. *Angew. Chemie - Int. Ed.* **47**, 8090–8092 (2008).

48. Kalk, M. Absorption of vanadium by tunicates. *Nature* **198**, 1010–1011 (1963).

49. Macara, I. G., Mcleod, G. . & Kustin, K. Vanadium in tunicates: Oxygen-binding studies. *Comp. Biochem. Physiol. Part A Physiol.* **62**, 821–826 (1979).

50. Swinehart, J. H., Biggs, W. R., Halko, D. J. & Schroeder, N. C. The vanadium and

selected metal contents of some ascidians. *BIOL.BULL.* **146**, 302–312 (1974).

51. Frank, P., Carlson, E. J., Carlson, R. M. K., Hedman, B. & Hodgson, K. O. The uptake and fate of vanadyl ion in ascidian blood cells and a detailed hypothesis for the mechanism and location of biological vanadium reduction. A visible and X-ray absorption spectroscopic study. *J. Inorg. Biochem.* **102**, 809–823 (2008).

52. Fox, D. L. *Biochromy: Natural Coloration of Living Things.* (University of California Press, 1979).

53. Boeri, E. The determination of hemovanadin and its oxidation potential. *Arch. Biochem. Biophys.* **37**, 449–456 (1952).

54. Henze, M. Untersuchungen über das Blut der Ascidien. I. Mitteilung. Die Vanadiumverbindung der Blutkörperchen. *Hoppe-Seyler´s Zeitschrift für Physiol. Chemie* **72**, 494–501 (1911).

55. Michibata, H., Uyama, T., Ueki, T. & Kanamori, K. Vanadocytes, cells hold the key to resolving the highly selective accumulation and reduction of vanadium in ascidians. *Microsc. Res. Tech.* **56**, 421–434 (2002).

56. Ueki, T., Yamaguchi, N. & Michibata, H. Chloride channel in vanadocytes of a vanadium-rich ascidian Ascidia sydneiensis samea. *Comp. Biochem. Physiol. Part B Biochem. Mol. Biol.* **136**, 91–98 (2003).

57. Hamada, T. *et al.* Solution structure of vanabin2, a vanadium(IV)-binding protein from the vanadium-rich ascidian Ascidia sydneiensis samea. *J. Am. Chem. Soc.* **127**, 4216–4222 (2005).

58. Schreckenbach, G. & Shamov, G. A. Theoretical Actinide Molecular Science. *Acc. Chem. Res.* **43**, 19–29 (2010).

59. Hay, P. J., Martin, R. L. & Schreckenbach, G. Theoretical Studies of the Properties and Solution Chemistry of AnO 2 2+ and AnO 2 + Aquo Complexes for An = U, Np, and Pu. *J. Phys. Chem. A* **104**, 6259–6270 (2000).

60. Mason, M. M., Smith, C., Vasiliu, M., Carrick, J. D. & Dixon, D. A. Prediction of An(III)/Ln(III) Separation by 1,2,4-Triazinylpyridine Derivatives. *J. Phys. Chem. A* **125**, 6529–6542 (2021).

61. Greenwood. *Chemistry of the Elements*. (Elsevier Science & Technology Books, 1996).

62. Ballhausen, C. J. & Gray, H. B. The Electronic Structure of the Vanadyl Ion. *Inorg. Chem.* **1**, 111–122 (1962).

63. Evans, H. T. Uranyl Ion Coordination. *Science (80-.).* **141**, 154–158 (1963).

64. Tutson, C. D. & Gorden, A. E. V. Thorium coordination: A comprehensive review based on coordination number. *Coord. Chem. Rev.* **333**, 27–43 (2017).

65. Frank, P., Carlson, R. M. K., Carlson, E. J., Hedman, B. & Hodgson, K. O. Biological sulfur in the blood cells of Ascidia ceratodes: XAS spectroscopy and a cellular-enzymatic hypothesis for vanadium reduction in the ascidians. *J. Inorg. Biochem.* **205**, 110991 (2020).

66. Boys, S. F., Cook, G. B., Reeves, C. M. & Shavitt, I. Automatic Fundamental Calculations of Molecular Structure. *Nature* **178**, 1207–1209 (1956).

67. Preuss, H. DasSCF-MO-P(LCGO)-Verfahren und seine Varianten. *Int. J. Quantum Chem.* **2**, 651–662 (1968).

68. Allinger, N. L. Conformational analysis. 130. MM2. A hydrocarbon force field utilizing V1 and V2 torsional terms. *J. Am. Chem. Soc.* **99**, 8127–8134 (1977).

69. Buenker, R. J. & Peyerimhoff, S. D. Ab initio SCF calculations for azulene and naphthalene. *Chem. Phys. Lett.* **3**, 37–42 (1969).

70. Nobel Prize in Chemistry, 1998. https://www.nobelprize.org/prizes/chemistry/1998/summary/.

71. Nobel Prize in Chemistry, 2013. https://www.nobelprize.org/prizes/chemistry/2013/press-release/.

72. Schrödinger, E. An Undulatory Theory of the Mechanics of Atoms and Molecules. *Phys. Rev.* **28**, 1049–1070 (1926).

73. Cramer, C. J. *Essentials of Computational Chemistry: Theories and Models*. (Wiley, 2004).

74. Jensen, F. *Introduction to Computational Chemistry*. (John Wiley & Sons, Ltd, 2007).

75. Gordon, A. & Avron, J. E. Born-Oppenheimer Approximation near Level Crossing. *Phys. Rev. Lett.* **85**, 34–37 (2000).

76. Waschewsky, G. C. G., Kash, P. W., Myers, T. L., Kitchen, D. C. & Butler, L. J. What Woodward and Hoffmann didn't tell us: the failure of the Born–Oppenheimer approximation in competing reaction pathways. *J. Chem. Soc., Faraday Trans.* **90**, 1581–1598 (1994).

77. Born, M. & Oppenheimer, R. Zur Quantentheorie der Molekeln. *Ann. Phys.* **389**, 457–484 (1927).

78. Sommerfeld, T. Lorentz Trial Function for the Hydrogen Atom: A Simple, Elegant Exercise. *J. Chem. Educ.* **88**, 1521–1524 (2011).

79. Slater, J. C. Atomic Shielding Constants. *Phys. Rev.* **36**, 57–64 (1930).

80. Boys, S. F. Electronic wave functions - I. A general method of calculation for the stationary states of any molecular system. *Proc. R. Soc. London. Ser. A. Math. Phys. Sci.* **200**, 542–554 (1950).

81. Hartree, D. R. The Wave Mechanics of an Atom with a Non-Coulomb Central Field. Part II. Some Results and Discussion. *Math. Proc. Cambridge Philos. Soc.* **24**, 111–132 (1928).

82. Slater, J. C. The Self Consistent Field and the Structure of Atoms. *Phys. Rev.* **32**, 339–348 (1928).

83. Gaunt, J. A. A Theory of Hartree's Atomic Fields. *Math. Proc. Cambridge Philos. Soc.* **24**, 328–342 (1928).

84. Roothaan, C. C. J. New Developments in Molecular Orbital Theory. *Rev. Mod. Phys.* **23**, 69–89 (1951).

85. Hall, G. . The molecular orbital theory of chemical valency VIII. A method of calculating ionization potentials. *Proc. R. Soc. London. Ser. A. Math. Phys. Sci.* **205**, 541–552 (1951).

86. Fock, V. Näherungsmethode zur Lösung des quantenmechanischen Mehrkörperproblems. *Zeitschrift für Phys.* **61**, 126–148 (1930).

87. Koch, W. & Holthausen, M. C. *A Chemist's Guide to Density Functional Theory*.

(Wiley-VCH, 2000).

88. Brás, N. F., Perez, M. A. S., Fernandes, P. A., Silva, P. J. & Ramos, M. J. Accuracy of Density Functionals in the Prediction of Electronic Proton Affinities of Amino Acid Side Chains. *J. Chem. Theory Comput.* **7**, 3898–3908 (2011).

89. Holthausen, M. C. Benchmarking approximate density functional theory. I.s/d excitation energies in 3d transition metal cations. *J. Comput. Chem.* **26**, 1505–1518 (2005).

90. Neumann, R., Nobes, R. H. & Handy, N. C. Exchange functionals and potentials. *Mol. Phys.* **87**, 1–36 (1996).

91. Wellendorff, J. *et al.* A benchmark database for adsorption bond energies to transition metal surfaces and comparison to selected DFT functionals. *Surf. Sci.* **640**, 36–44 (2015).

92. Quintal, M. M., Karton, A., Iron, M. A., Boese, A. D. & Martin, J. M. L. Benchmark Study of DFT Functionals for Late-Transition-Metal Reactions †. *J. Phys. Chem. A* **110**, 709–716 (2006).

93. Hohenberg, P. & Kohn, W. Inhomogeneous Electron Gas. *Phys. Rev.* **136**, B864–B871 (1964).

94. Kohn, W. & Sham, L. J. Self-Consistent Equations Including Exchange and Correlation Effects. *Phys. Rev.* **140**, A1133–A1138 (1965).

95. Jaoul, A., Nocton, G. & Clavaguéra, C. Assessment of Density Functionals for Computing Thermodynamic Properties of Lanthanide Complexes. *ChemPhysChem* **18**, 2688–2696 (2017).

96. Nazarian, D., Ganesh, P. & Sholl, D. S. Benchmarking density functional theory predictions of framework structures and properties in a chemically diverse test set of metal–organic frameworks. *J. Mater. Chem. A* **3**, 22432–22440 (2015).

97. Fan, J.-Y., Zheng, Z.-Y., Su, Y. & Zhao, J.-J. Assessment of dispersion correction methods within density functional theory for energetic materials. *Mol. Simul.* **43**, 568–574 (2017).

98. Grimme, S., Antony, J., Ehrlich, S. & Krieg, H. A consistent and accurate ab initio

parametrization of density functional dispersion correction (DFT-D) for the 94 elements H-Pu. *J. Chem. Phys.* **132**, 154104 (2010).

99. Perdew, J. P. *et al.* Rationale for mixing exact exchange with density functional approximations Rationale for mixing exact exchange with density functional approximations. **9982**, 9982–9985 (2010).

100. Perdew, J. P. & Schmidt, K. Jacob's ladder of density functional approximations for the exchange-correlation energy. in *AIP Conference Proceedings* vol. 577 1–20 (AIP, 2001).

101. Pyykkö, P. Relativistic Effects in Chemistry: More Common Than You Thought. *Annu. Rev. Phys. Chem.* **63**, 45–64 (2012).

102. Dirac, P. A. M. The quantum theory of the electron. *Proc. R. Soc. London. Ser. A, Contain. Pap. a Math. Phys. Character* **117**, 610–624 (1928).

103. Van Lenthe, E., Baerends, E. J. & Snijders, J. G. Relativistic total energy using regular approximations. *J. Chem. Phys.* **101**, 9783–9792 (1994).

104. Van Lenthe, E. Geometry optimizations in the zero order regular approximation for relativistic effects. *J. Chem. Phys.* **110**, 8943–8953 (1999).

105. Van Lenthe, E. & Baerends, E. J. Optimized Slater-type basis sets for the elements 1-118. *J. Comput. Chem.* **24**, 1142–1156 (2003).

106. Visscher, L. & Van Lenthe, E. On the distinction between scalar and spin-orbit relativistic effects. *Chem. Phys. Lett.* **306**, 357–365 (1999).

107. Van Lenthe, E., Snijders, J. G. & Baerends, E. J. The zero-order regular approximation for relativistic effects: The effect of spin-orbit coupling in closed shell molecules. *J. Chem. Phys.* **105**, 6505–6516 (1996).

108. Van Lenthe, E., Baerends, E. J. & Snijders, J. G. Relativistic regular two-component Hamiltonians. *J. Chem. Phys.* **99**, 4597–4610 (1993).

109. Yin, M. T. & Cohen, M. L. Theory of ab initio pseudopotential calculations. *Phys. Rev. B* **25**, 7403–7412 (1982).

110. Vanderbilt, D. Soft self-consistent pseudopotentials in a generalized eigenvalue formalism. *Phys. Rev. B* **41**, 7892–7895 (1990).

111. Tomasi, J. & Persico, M. Molecular Interactions in Solution: An Overview of Methods Based on Continuous Distributions of the Solvent. *Chem. Rev.* **94**, 2027–2094 (1994).

112. Miertuš, S., Scrocco, E. & Tomasi, J. Electrostatic interaction of a solute with a continuum. A direct utilizaion of AB initio molecular potentials for the prevision of solvent effects. *Chem. Phys.* **55**, 117–129 (1981).

113. Cammi, R. & Tomasi, J. Remarks on the use of the apparent surface charges (ASC) methods in solvation problems: Iterative versus matrix-inversion procedures and the renormalization of the apparent charges. *J. Comput. Chem.* **16**, 1449–1458 (1995).

114. Cossi, M., Barone, V., Cammi, R. & Tomasi, J. Ab initio study of solvated molecules: a new implementation of the polarizable continuum model. *Chem. Phys. Lett.* **255**, 327–335 (1996).

115. Klamt, A., Moya, C. & Palomar, J. A Comprehensive Comparison of the IEFPCM and SS(V)PE Continuum Solvation Methods with the COSMO Approach. *J. Chem. Theory Comput.* **11**, 4220–4225 (2015).

116. Klamt, A. Conductor-like Screening Model for Real Solvents: A New Approach to the Quantitative Calculation of Solvation Phenomena. *J. Phys. Chem.* **99**, 2224–2235 (1995).

117. Cramer, C. J. & Truhlar, D. G. Implicit Solvation Models: Equilibria, Structure, Spectra, and Dynamics. *Chem. Rev.* **99**, 2161–2200 (1999).

118. Leung, B. O., Reid, D. L., Armstrong, D. A. & Rauk, A. Entropies in Solution from Entropies in the Gas Phase. *J. Phys. Chem. A* **108**, 2720–2725 (2004).

119. Garza, A. J. Solvation Entropy Made Simple. *J. Chem. Theory Comput.* **15**, 3204–3214 (2019).

120. Mulliken, R. S. Electronic Population Analysis on LCAO–MO Molecular Wave Functions. I. *J. Chem. Phys.* **23**, 1833–1840 (1955).

121. Mayer, I. Bond order and valence indices: A personal account. *J. Comput. Chem.* **28**, 204–221 (2007).

122. Hirshfeld, F. L. Bonded-atom fragments for describing molecular charge densities. *Theor. Chim. Acta* **44**, 129–138 (1977).

123. Reed, A. E., Weinstock, R. B. & Weinhold, F. Natural population analysis. *J. Chem. Phys.* **83**, 735–746 (1985).

124. Fonseca Guerra, C., Handgraaf, J.-W., Baerends, E. J. & Bickelhaupt, F. M. Voronoi deformation density (VDD) charges: Assessment of the Mulliken, Bader, Hirshfeld, Weinhold, and VDD methods for charge analysis. *J. Comput. Chem.* **25**, 189–210 (2004).

125. te Velde, G. *et al.* Chemistry with ADF. *J. Comput. Chem.* **22**, 931–967 (2001).

126. Fonseca Guerra, C., Snijders, J. G., te Velde, G. & Baerends, E. J. Towards an order-N DFT method. *Theor. Chem. Accounts Theory, Comput. Model. (Theoretica Chim. Acta)* **99**, 391–403 (1998).

127. ADF, SCM, Theoretical Chemistry, Vrije Universiteit, . ADF. (2017).

128. Becke, A. D. Density-functional exchange-energy approximation with correct asymptotic behavior. *Phys. Rev. A* **38**, 3098–3100 (1988).

129. Lee, C., Yang, W. & Parr, R. G. Development of the Colle-Salvetti correlation-energy formula into a functional of the electron density. *Phys. Rev. B* **37**, 785–789 (1988).

130. Perdew, J. P., Burke, K. & Ernzerhof, M. Generalized Gradient Approximation Made Simple. *Phys. Rev. Lett.* **77**, 3865–3868 (1996).

131. Burke, K., Ernzerhof, M. & Perdew, J. P. The adiabatic connection method: a non-empirical hybrid. *Chem. Phys. Lett.* **265**, 115–120 (1997).

132. Neese, F. The ORCA program system. *WIREs Comput. Mol. Sci.* **2**, 73–78 (2012).

133. Neese, F. Software update: the ORCA program system, version 4.0. *WIREs Comput. Mol. Sci.* **8**, (2018).

134. Becke, A. D. A new mixing of Hartree–Fock and local density-functional theories. *J. Chem. Phys.* **98**, 1372–1377 (1993).

135. Barone, V. & Cossi, M. Quantum Calculation of Molecular Energies and Energy Gradients in Solution by a Conductor Solvent Model. *J. Phys. Chem. A* **102**, 1995–2001 (1998).

136. Santos, R. Application of Density Functional Theory to the Interaction of Uranium with Eudistomins. (University of Manitoba, 2019).

137. SpectraBase. *John Wiley & Sons, Inc. SpectraBase* https://spectrabase.com/.

138. Polycitoridae. https://www.gbif.org/species/7349.

139. Dupont, B. Colonial Ascidian Eudistoma sp. https://www.flickr.com/photos/berniedup/8502008103/.

140. Nakagawa, M., Liu, J. J. & Hino, T. Total synthesis of (-)-eudistomin L and (-)-debromoeudistomin L. *J. Am. Chem. Soc.* **111**, 2721–2722 (1989).

141. Toru. Midori Kaimen Boya. http://www.ha.shotoku.ac.jp/~kawa/KYO/SEIBUTSU/DOUBUTSU/sango/okinawa/sekisakudoubutsumon/midorikaimen/01.html.

142. Hamada, T. *et al.* Solution Structure of Vanabin2, a Vanadium(IV)-Binding Protein from the Vanadium-Rich Ascidian Ascidia s ydneiensis samea. *J. Am. Chem. Soc.* **127**, 4216–4222 (2005).

143. Kawakami, N., Ueki, T., Matsuo, K., Gekko, K. & Michibata, H. Selective metal binding by Vanabin2 from the vanadium-rich ascidian, Ascidia sydneiensis samea. *Biochim. Biophys. Acta - Gen. Subj.* **1760**, 1096–1101 (2006).

144. Frank, P., Carlson, E. J., Carlson, R. M. K., Hedman, B. & Hodgson, K. O. The uptake and fate of vanadyl ion in ascidian blood cells and a detailed hypothesis for the mechanism and location of biological vanadium reduction. A visible and X-ray absorption spectroscopic study. *J. Inorg. Biochem.* **102**, 809–823 (2008).

145. Frank, P., Robinson, W. E., Kustin, K. & Hodgson, K. O. Unprecedented forms of vanadium observed within the blood cells of Phallusia nigra using K-edge X-ray absorption spectroscopy. *J. Inorg. Biochem.* **86**, 635–648 (2001).

146. Tachez, M. & Théobald, F. Structure du sulfate de vanadyle pentahydraté VO(H 2 O) 5 SO 4 β (variété orthorhombique). *Acta Crystallogr. Sect. B Struct. Crystallogr. Cryst. Chem.* **36**, 1757–1761 (1980).

147. Magnussen, M., Brock-Nannestad, T. & Bendix, J. Pentaaquaoxovanadium(IV) bis(trifluoromethanesulfonate). *Acta Crystallogr. Sect. C Cryst. Struct. Commun.* **63**, m51–m53 (2007).

148. Krakowiak, J., Lundberg, D. & Persson, I. A Coordination Chemistry Study of

Hydrated and Solvated Cationic Vanadium Ions in Oxidation States +III, +IV, and +V in Solution and Solid State. *Inorg. Chem.* **51**, 9598–9609 (2012).

149. *The Chemistry of the Actinide and Transactinide Elements*. (Springer Netherlands, 2006). doi:10.1007/1-4020-3598-5.

150. Rui, X. *et al.* Bioreduction of hydrogen uranyl phosphate: Mechanisms and U(IV) products. *Environ. Sci. Technol.* **47**, 5668–5678 (2013).

151. Koribanics, N. M. *et al.* Spatial distribution of an uranium-respiring betaproteobacterium at the Rifle, CO field research site. *PLoS One* **10**, (2015).

152. Vettese, G. F. *et al.* Multiple Lines of Evidence Identify U(V) as a Key Intermediate during U(VI) Reduction by Shewanella oneidensis MR1. *Environ. Sci. Technol.* **54**, 2268–2276 (2020).

153. Wu, Q., Sanford, R. A. & Löffler, F. E. Uranium(VI) reduction by Anaeromyxobacter dehalogenans strain 2CP-C. *Appl. Environ. Microbiol.* **72**, 3608–3614 (2006).

154. Khijniak, T. V. *et al.* Reduction of uranium(VI) phosphate during growth of the thermophilic bacterium Thermoterrabacterium ferrireducens. *Appl. Environ. Microbiol.* **71**, 6423–6426 (2005).

155. Lovley, D. R., Phillips, E. J. P., Gorby, Y. A. & Landa, E. R. Microbial reduction of uranium. *Nature* **350**, 413–416 (1991).

156. Lovley, D. R. & Phillips, E. J. P. Reduction of uranium by Desulfovibrio desulfuricans. *Appl. Environ. Microbiol.* **58**, 850–856 (1992).

157. Vallet, V. *et al.* Solvent Effects on Uranium(VI) Fluoride and Hydroxide Complexes Studied by EXAFS and Quantum Chemistry. *Inorg. Chem.* **40**, 3516–3525 (2001).

158. Wahlgren, U. *et al.* Structure of Uranium(VI) in Strong Alkaline Solutions. A Combined Theoretical and Experimental Investigation. *J. Phys. Chem. A* **103**, 8257–8264 (1999).

159. Cooper, N., Minakata, D., Begovic, M. & Crittenden, J. Should We Consider Using Liquid Fluoride Thorium Reactors for Power Generation? *Environ. Sci. Technol.* **45**, 6237–6238 (2011).

160. World Nuclear Association ‘Thorium’. https://www.world-nuclear.org/information-

library/current-and-future-generation/thorium.aspx#References (2020).

161. Chuang, C.-Y. *et al.* Important role of biomolecules from diatoms in the scavenging of particle-reactive radionuclides of thorium, protactinium, lead, polonium, and beryllium in the ocean: A case study with Phaeodactylum tricornutum. *Limnol. Oceanogr.* **59**, 1256–1266 (2014).

162. Alverson, A. The Air You're Breathing? A Diatom Made That. https://www.livescience.com/46250-teasing-apart-the-diatom-genome.html (2014).

163. Martino, A. De, Meichenin, A., Shi, J., Pan, K. & Bowler, C. Genetic and phenotypic characterization of Phaeodactylum tricornutum (Bacillariophyceae) accessions 1. *J. Phycol.* **43**, 992–1009 (2007).

164. Brown, A. C. & Davies, A. B. The fate of thorium dioxide introduced into the body cavity of Ciona intestinalis (Tunicata). *J. Invertebr. Pathol.* **18**, 276–279 (1971).

165. Cooper, S. & Kaltsoyannis, N. Covalency in AnCl 3 (An = Th–No). *Dalt. Trans.* **50**, 1478–1485 (2021).

166. Sadhu, B. & Dolg, M. Enhancing Actinide(III) over Lanthanide(III) Selectivity through Hard-by-Soft Donor Substitution: Exploitation and Implication of Near-Degeneracy-Driven Covalency. *Inorg. Chem.* **58**, 9738–9748 (2019).

167. Grimme, S., Huenerbein, R. & Ehrlich, S. On the Importance of the Dispersion Energy for the Thermodynamic Stability of Molecules. *ChemPhysChem* **12**, 1258–1261 (2011).

168. Grimme, S., Hansen, A., Brandenburg, J. G. & Bannwarth, C. Dispersion-Corrected Mean-Field Electronic Structure Methods. *Chem. Rev.* **116**, 5105–5154 (2016).

169. Taylor, R. *Reprocessing and Recycling of Spent Nuclear Fuel 1st Edition*. (Woodhead Publishing, Elsevier Ltd., 2015).